To the Graduate Council:

I am submitting herewith a thesis written by Reid L. Kress entitled "A Valve Cap Coal Feeder for Fluidized Beds." I have examined the final copy of this thesis for form and content and recommend that it be accepted in partial fulfillment of the requirements for the degree of Master of Science, with a major in Mechanical Engineering.

H. J. Wilkerson

H. J. Wilkerson, Major Professor

We have read this thesis and recommend its acceptance:

M Milligan

H. J. Edmondson

W S Johnson

Accepted for the Council:

L Evans Roth

Vice Chancellor
Graduate Studies and Research

A

A VALVE CAP COAL FEEDER
FOR FLUIDIZED BEDS

A Thesis
Presented for the
Master of Science
Degree
The University of Tennessee, Knoxville

Reid L. Kress

June 1982

ACKNOWLEDGEMENTS

The author would like to thank the Tennessee Valley Authority for their support through continued funding of this project. The Tennessee Valley Authority, Division of Energy Demonstrations and Technology, and Dr. Arnold Manaker also deserve thanks for their inputs to the project.

The author extends his gratitude to Dr. H. J. Wilkerson for his encouragement, assistance and guidance. The author would also like to thank his two assistants, Richard Fontana and William Hemphill.

Finally, he wishes to thank his wife for her persistence and help during the course of this research.

ABSTRACT

This thesis covers the design of a valve cap coal feed system for an atmospheric fluidized bed combustion unit. The system is a flat cap within a cage which operates as a check valve, allowing coal to be injected into the bed, but preventing bed material from draining down into the feed line. The cap was required to remain fully open with an air volumetric flow rate of 97.3 cubic feet per minute at 80^{o}F and 14.3 psia which corresponds to the requirements of the Tennessee Valley Authority (TVA) 20MW pilot plant located in Paducah, Kentucky. An additional requirement was for the cap to be thick enough to have a reasonable life expectancy when subjected to the abrasive conditions of coal feed operation.

The design was effected by conceiving candidate valve cap systems, testing them in an ambient temperature, atmospheric pressure fluidized bed and iterating the design using the experimental results. The valve cap systems were subjected to numerous air only and air plus solids tests in order to cover their full spectrum of operating modes.

The result of the design and test steps was a valve cap system which operated according to the design specifications and a sufficient base of data to allow a valve cap to be designed for similar, but slightly different conditions. The cap developed has added potential for wear prevention as a consequence of its unique recessed design.

Three additional feeder designs and a limited amount of experimental data are presented in the appendices. These designs include two below-bed feeders: a flat plate and a sphere cap. The third feeder, the four-arm cross, is a combination coal feed system and fluidization system.

TABLE OF CONTENTS

CHAPTER PAGE

CHAPTER PAGE

LIST OF TABLES

TABLE PAGE

LIST OF FIGURES

FIGURE PAGE

LIST OF SYMBOLS

A	-	Area (in^2)
c	-	Speed of Sound (ft/sec)
C	-	Operating Clearance, Four-Bar Cage (in)
C'	-	Operating Clearance, Three-Bar Cage (in)
C*	-	Corrected Coal to Total Mass Comparison Percent Ratio
CH	-	Cap Height (in) [Reference 10]
d	-	Diameter (in)
$d\bar{A}$	-	Differential Area Vector
dr	-	Differential Radius
d(Vol)	-	Differential Volume
$d\theta$	-	Differential Angle
E	-	Percent Bed Expansion
f	-	Friction Factor
F	-	Force (lbf)
g	-	Acceleration Due to Gravity, 32.2 ft/sec^2
g_c	-	Dimensional Constant, 32.2 $lbm\text{-}ft/lbf\text{-}sec^2$
Gap	-	Cap Free Travel (in)
h	-	Height (in)
h_f	-	Head Loss Created by Viscous Effects (Pressure Units)
h_L	-	General Head Loss (Pressure Units)
h_{LB}	-	Bend Head Loss (Pressure Units)
h_{LC}	-	Contraction Head Loss (Pressure Units)
h_{Le}	-	Entrance Head Loss (Pressure Units)

h_{LE}	-	Exit Head Loss (Pressure Units)
h_{L1}	-	Head Loss in Pipe #1 (Pressure Units)
h_{L2}	-	Head Loss in Pipe #2 (Pressure Units)
h_s	-	Slumped Height (in)
Δh	-	Change in Head (in H_2O)
j	-	Length (in)
J	-	Solids Mass Flux to Air Mass Flux Ratio
k	-	Specific Heat Ratio (c_p/c_v)
K	-	Momentum Correction Factor
K_c	-	Contraction Loss Coefficient
k_D	-	Orifice Discharge Coefficient
K_e	-	Entrance Loss Coefficient
K_E	-	Exit Loss Coefficient
L	-	Length (in)
$\dot{m}$	-	Mass (grams)
m	-	Mass Flux (lbm/min)
Ma	-	Mach Number
n	-	Number of Variables
P_{AB}	-	Above Bed Pressure (in H_2O)
P_{ATM}	-	Atmospheric Pressure (lbf/in^2)
P_B'	-	Bed Pressure for Flat Cap Tests (in H_2O)
P_o	-	Penetration Depth (in)
ΔP	-	Pressure Drop (in H_2O)
Q	-	Flow Rate (ft^3/min)
r	-	Radius (in)

r^2	-	Coefficient of Determination
r_c	-	Cap Radius (in)
r_o	-	Pipe Outside Radius (in)
r_s	-	Cage Supports Inside Radius, Four-Bar Cage (in)
r_s'	-	Cage Supports Inside Radius, Three-Bar Cage (in)
R	-	Radius (in)
R^*	-	Corrected Coal Mass to Total Mass Ratio
$\bar{R}^*$	-	Average Corrected Coal Mass to Total Mass Ratio
R_A	-	Gas Constant for Air, 1,716 ft-lbf/slug-^oR
R_H	-	Hydraulic Radius (in)
Re	-	Reynolds Number
ΔS	-	Manometer Deflection (in H_2O)
S	-	Coal Velocity to Air Velocity, Slip Ratio
t	-	Time
T	-	Temperature (^oF)
T_{AVG}	-	Average Temperature (^oF)
U	-	Uncertainty in Calculated Result
V	-	Speed (ft/sec)
$\bar{V}$	-	Velocity Vector (ft/sec)
V_S	-	Superficial Velocity (ft/sec)
W	-	Weight (lbf)
W_u	-	Uncertainty in U
x	-	Length (in)
x'	-	Length (in)
X_n	-	Variable
z	-	Coordinate Direction

Greek Symbols

α	-	Angle (Degrees)
α'	-	Angle (Degrees)
γ	-	Specific Weight (lbf/ft^3)
δ	-	Length (in)
Δ	-	Change in Quantity
θ	-	Angle (Radians)
$\dot{\theta}$	-	Angular Speed (rad/sec)
μ	-	Coefficient of Friction
ν	-	Kinematic Viscosity (ft^2/sec)
ρ	-	Density (lbm/ft^3)
σ	-	Standard Deviation
Σ	-	Summation

Special Subscripts

A	-	Inlet
AB	-	Above Bed
B	-	Bed
C	-	Coal
CC	-	Corrected Coal
F	-	Fluidization
FA	-	Fluidization Air
g	-	Gage
H_2O	-	Water
L	-	Loss
LS	-	Limestone

O	-	Orifice
P	-	Pipe
S	-	Superficial
TA	-	Transport Air
z	-	z - Direction

Special Superscripts

$\bar{A}$	-	Average of A
*	-	Quantity Pertaining to Coal Feed Test Data

CHAPTER 1

INTRODUCTION

Background

There is an imperative to decrease our dependence on foreign oil supplies by employing nationally available fuels. The United States has one of the largest reserves of coal in the world (Table 1.1). The United States is also the second largest producer of coal in the world [1, p. 5-2]. Clearly, coal is a likely choice for an alternate fuel. Coal accounted for 58 percent of the fuels used in utility steam plants in 1974 [1, p. 5-5]. Since this percentage has been increasing from prior years and because coal is the likely choice to replace oil in the utility industry, a clean, environmentally acceptable, inexpensive method of burning coal needs to be developed.

Several methods for burning coal for electrical production are potentially available that will meet the current Federal Environmental Protection Agency's (EPA) emissions standards. From a report by D. J. Walker [2, p. 1] these are:

1. Burning low sulfur coal.
2. Stoker firing of coal with Flue Gas Desulfurization (FGD).
3. Burning Pulverized Coal (PC) with FGD.
4. Using synthetic gas from a coal gasification plant.
5. Firing solvent refined coal.
6. Coal fired in a fluidized bed combustor.

TABLE 1.1

WORLD COAL PRODUCTION

Solid Fossil Fuel Resources by Continents and Nations with Major Resources, 1974 (Million metric tons)

Country or Continent	Economic Reserves Recoverable	Economic Reserves Total	Total Resources
U.S.S.R.	136,600	273,200	5,713,600
China, P.R. of	80,000	300,000	1,000,000
Rest of Asia	17,549	40,479	108,053
United States	181,781	363,562	2,924,503
Canada	5,537	9,034	108,777
Latin America	2,803	9,201	32,928
Europe	126,775	319,807	607,521
Africa	15,628	30,291	58,844
Oceania	24,518	74,699	199,654
Total	591,191	1,402,274	10,753,880

Source, World Energy Conference, Survey of Energy Sources, 1974.

The supply of low sulfur coal is becoming depleted; or the cost of transportation prohibitive, consequently, the burning of high sulfur coal appears unavoidable. Stoker and PC firing with FGD are expensive and create excessive waste. Synthetic gas firing or solvent refined coal are not presently available. Thus, fluidized bed combustion of coal appears to be the most attractive near term alternative for commercial power generation.

As described in a presentation by Shelton Ehrlich [3, pp. 15-20], a fluidized bed used for combustion was first patented in 1928 by Fritz Winkler. However, the first coal fired fluidized bed boiler was not patented until 1944 by the Standard Oil Company. Investigation into fluidized bed boilers stagnated until the early 1960s when research efforts were renewed by the Central Electricity Generating Board (CEGB) and the British Coal Utilization Research Association (BCURA)in England. Pope, Evans, and Robbins of the United States had a small fluidized pot working by 1965. These efforts have grown to present day conceptual design for the Tennessee Valley Authority (TVA) by the Fluidized Combustion Company [4], Babcock and Wilcox [5], and Combustion Engineering [6], for a 150 to 250 megawatt (MW) demonstration plant. TVA is presently constructing a 20MW pilot plant to demonstrate the applicability of fluidized bed technology to commercial power production.

The interest in fluidized bed combustion of coal exists because of several advantages. These include:

1. Nitrous oxide (NO_x) emissions that will meet current Federal EPA limits.

2. Reduced emissions of sulfur dioxide (SO_2).

3. Dry and easily transported waste.

4. Waste that has possible uses in construction and agriculture.

5. Reduction or elimination of fouling and slagging problems.

6. A reduction of the required heat transfer area.

7. Ability to utilize poor quality, (high ash, high sulfur), coal. (Sources: Walker [2] and Fluidized Combustion Company [4]).

Although fluidized bed combustion offers these advantages, it also has some engineering problems associated with its basic design and operation. The major problems are:

1. Carryover of carbon particles from the bed, termed elutriation.

2. Load following for utility operation.

3. Waste disposal.

4. Development of a reliable and effective coal feeding system.

According to Wilkerson [7, p. 1] the most critical of these problems is the development of an acceptable coal feeder. This problem will be addressed in detail by this thesis; however, the basics of coal feeding as it relates to fluidized bed combustion must be understood before specific coal feeders are discussed.

Coal Feeding and Fluidized Bed Combustion in General

In a fluidized bed combustion unit, limestone or dolomite is placed into the bed in order to reduce sulfur dioxide emissions. This is effected through the following reactions.

For limestone: $CaCO_3 + Heat \gtrless CaO + CO_2$ (1.1)

$CaO + SO_2 + \frac{1}{2} O_2 \gtrless CaSO_4.$ (1.2)

For dolomite: $CaCO_3\ MgCO_3 + Heat \gtrless CaO\ MgO + 2CO_2$ (1.3)

$CaO\ MgO + 2SO_2 + O_2 \gtrless CaSO_4\ MgSO_4.$ (1.4)

The CaO in equation 1.1 and the CaO MgO in equation 1.3 are referred to as calcined limestone or lime and calcined dolomite respectively. The limestone or dolomite in the bed is fluidized by the passage of combustion air through the bed. The term fluidized is employed to describe the pseudofluid behavior of the air and limestone. As a result of friction and pressure gradients, the limestone bed is expanded above its slumped or nonfluidized depth. Figures 1.1 and 1.2 show this phenomena in a cold model fluidized bed. The term cold refers to noncombustion. The air that is required to expand and fluidize the slumped bed is termed fluidization air.

Fluidized bed coal feeders can be classified into three major divisions. These are explained in the following section.

Types of Coal Feeders

The three major types of coal feed systems for a fluidized bed are over-bed feeders, in-bed feeders, and below-bed feeders.

Over-bed feeders would employ a rotary type device such as an over-bed stoker to spread coal upon the top of the limestone bed.

In-bed feeders would utilize feed pipes extending into the limestone bed. These pipes could be placed in almost any configuration, but they must be short enough to avoid becoming too hot which results

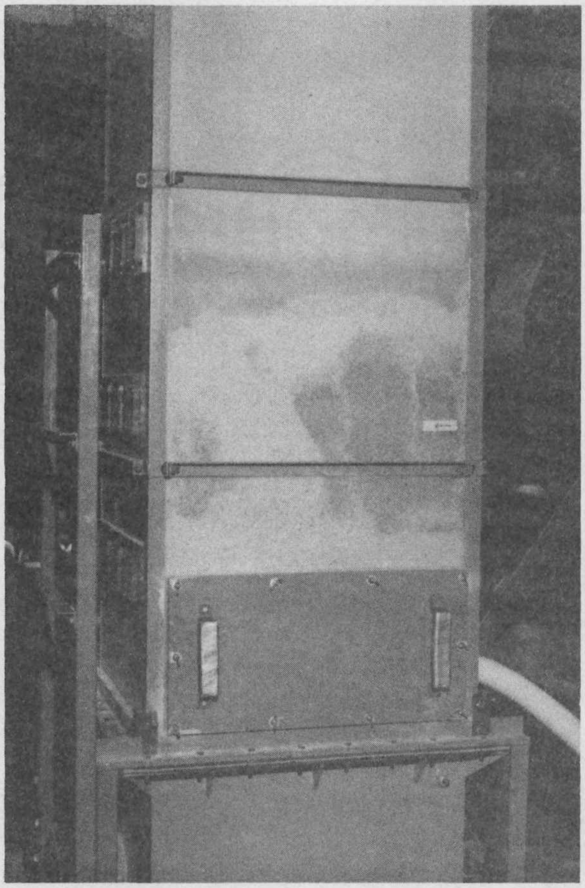

Figure 1.1. Slumped Bed of Limestone.

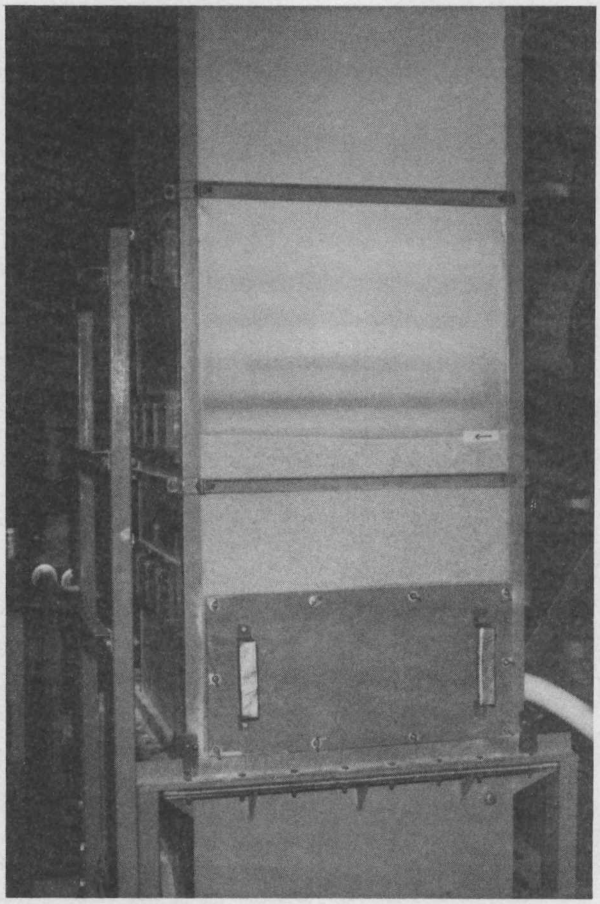

Figure 1.2. Fluidized Bed of Limestone.

in the coal agglomerating and clogging the line. This happened with the needles coal feed system at the fluidized bed test facility at Rivesville, West Virginia.

Below-bed feeders enter the bed through the fluidization grid plate located at the base of the bed. These feeders can be made in various configurations, but they must be designed to distribute coal uniformly and to prevent the fluidized bed from draining back into the feed system.

This thesis covers the design of a valve cap below-bed feed system that operates according to specifications set forth by the TVA. These specifications and a general statement of the problem are presented in Chapter 3.

CHAPTER 2

BELOW-BED COAL FEEDING DESIGN PHILOSOPHIES

Introduction

The primary function of any coal feed system, whether in-bed, below-bed, or over-bed, is to distribute coal uniformly to all sections of the fluidized bed of limestone. Non-uniform distribution will create cool bed sections, uneven temperatures, poor heat transfer characteristics, or oxidizing and reducing zones, and could lead to poor sulfur capture or excessive carbon monoxide emissions.

Another function, applying only to below-bed coal feed systems is the prevention of bed drainback. Bed drainback occurs when the limestone in the bed drains down a feedline that is not being used for feeding. This could occur during bed startup, shutdown or slumping.

Coal Feeding

Coal feeding is most enhanced by having several openings in different directions. Ultimately, a vertical pipe whose exit flow impinges upon a horizontal flat surface and produces a radial coal distribution would be an ideal feed system.

Coal feeding can also be improved through the use of a small opening or large air flow rates to increase jet escape velocity. Higher exit velocity will contribute to deeper bed penetration of the coal particles. This phenomenon was investigated by F. A. Zenz [8].

Naturally, the feeder exit opening should be somewhat larger than the largest expected coal particle. It is typically made three times larger than the maximum particle size.

Drainback

Bed drainback can be prevented with several designs. One method shields the feedline from the limestone bed by employing the concept of angle of repose. Angle of repose is defined as the angle measured with respect to horizontal that a substance makes when placed in a free pile [9, p. 91]. If a vertical entrance pipe is guarded by a surface such that the angle from the top of the pipe to the end of the surface is at all points less than the angle of repose, no limestone should drain back during slumped bed conditions. In theory this works well, and in a single feed point bed, this works in practice, however, in an actual utility fluidized bed boiler, slumped portions of the bed will be adjacent to and in contact with non-slumped (or fluidized) sections. Vibration and interface friction plus some leakage and cross compartment flow from the fluidized section of the bed to the non-fluidized section may cause drainback. This can be counteracted by passing a purge flow of air through the system under these conditions. This is a workable solution, but it is not ideal since it requires operational control.

Drainback can also be effectively prevented by the use of an active closing device. Most simple of these would be a floating cap [10]. These devices are very effective for coal distribution, produce good fluidization and prevent bed drainback. Their only drawback is potential cap hangup in either a closed or an open position because of the bed particles lodging between the cap and its enclosure.

Drainback could also be combatted by the use of an externally controlled valving device, however, when one considers the number of feed points in a typical utility size fluidized bed (on the order of 1000 [5, p. 3-7]), the operation and construction of such a system seems very prohibitive.

Closure

The brief discussion in this chapter presents some of the basic ideas available for use in designing a below-bed feeder. The remainder of this thesis will present the design, fabrication and testing of one particular below-bed feed system. This is the valve cap coal feed system.

The next chapter states the exact design specifications as outlined by the TVA. Chapter 4 discusses the experimental system and test formats.

CHAPTER 3

STATEMENT OF THE PROBLEM

This thesis covered the conceptual design, development and testing of a valve cap below-bed feed system that could distribute coal uniformly to all sections of a fluidized bed and prevent bed drainback. This system was to operate at 97.3 cubic feet per minute at $80^{\circ}F$ and 14.3 psia. The coal feed rate was to be approximately 1500 pounds per hour. The feeder was to be designed to feed nine square feet of bed area. Because of blower limitations, the actual bed area used in this study was four square feet.

The conditions chosen correspond to requirements selected for the TVA 20MW pilot plant located in Paducah, Kentucky.

The valve cap design was based upon a 2.0 inch diameter schedule 40 coal feed pipe with a disk shaped cap enclosed in a four-bar cage. The cage was made adjustable so that its diameter and height could be changed.

CHAPTER 4

FLUIDIZED BED TEST FACILITY

Introduction

The basic fluidized bed test facility, illustrated in Figure 4.1, was designed by Mr. Rod L. Henry [10] and Mr. G. D. Knox [11]. The design specifications, operational procedures and tests are described in their theses accompanied by a description of the testing of two different feeders. Mr. Knox tested an in-bed feeder. It consisted of horizontal pipes with vertically placed holes. Mr. Henry examined a below-bed feed system. It consisted of parallel operating valve caps. The systems tested by Henry and Knox were combined systems meaning that the air required to fluidize the bed and the air required to transport the coal were combined into one system. The performance of the feeders tested in this thesis will be compared to each of these systems.

Experimental System

The experimental apparatus can be divided into ten systems as described below.

First is the limestone feed system. It is used to place limestone into the bed before a test is conducted. This system involves the lower storage bin, a ball valve to meter the limestone into a three inch diameter feed line, and a regulated pressure compressed air supply to pneumatically convey the limestone to the top of the fluidized bed.

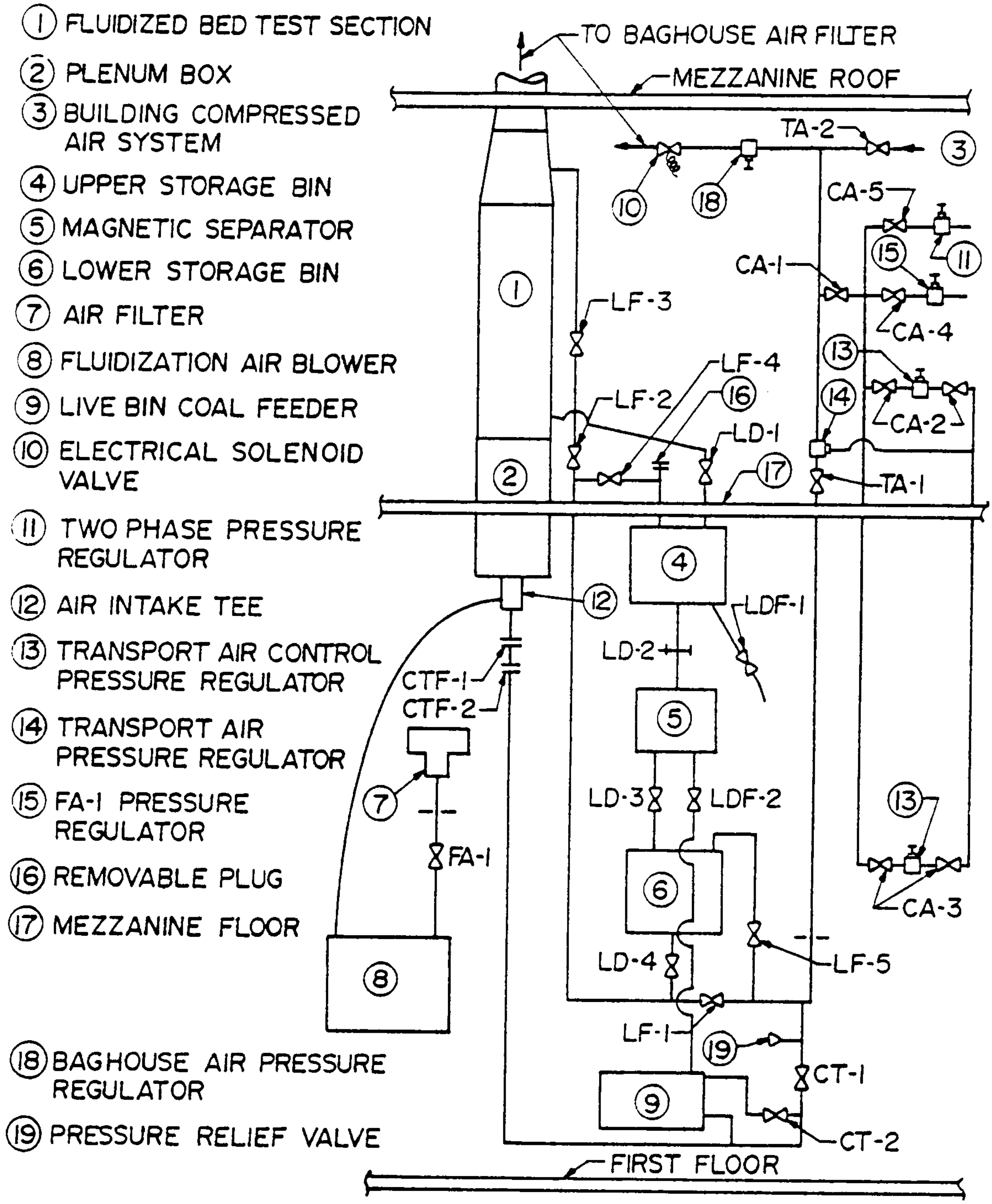

Figure 4.1. Fluidized Bed Test Facility.

Second is the coal feed system. Actual coal is not used in this experiment because it cannot be easily removed from limestone once a coal feed test has been performed. As a result of this, G. D. Knox [11] developed an imitation coal which has the same color, density, shape and size as does real coal. The imitation coal is a polyester resin impregnated with iron powder which makes the imitation coal magnetic. This allows the coal to be conveniently separated from the limestone after a test. The imitation coal is ground to $\frac{1}{4}$ x 0 as specified in representative systems [12, p. 4-7]. The iron impregnation makes the coal an excellent tracer and also allows the same limestone and coal to be used repeatedly. For a complete discussion on the imitation coal, see Knox [11] Chapter 3. For the remainder of the thesis, the imitation coal will simply be referred to as coal. The coal feed system is designed to meter and convey a preset mass flow rate of coal to the particular feed device under investigation. Its components include a vibrascrew metering machine and a three inch line to allow for pneumatic conveyance of the coal to the plenum box. The coal feed system varies depending upon the particular feeder being studied.

Third is the drain system which allows the bed material, typically limestone mixed with coal, to be drained following a test. It incorporates the upper storage bin, a 2.25 inch diameter flexible drain line, a ball valve and a vacuum cleaner (not shown) to facilitate draining. The vacuum is used to create a vacuum in the upper storage bin thus allowing the bed to be drained quickly.

Fourth is the separation system. This system separates coal from the limestone after a coal feeding test. It contains the upper and lower storage bins, a magnetic separator, a three inch recirculation line between the two bins and a regulated pressure compressed air supply for pneumatic conveying. The limestone and coal mixture is directed through the magnetic separator from the upper bin to the lower bin. After all of the limestone and coal have flowed into the lower bin, it is replaced into the top bin through pneumatic conveying and the separation repeated. Four such separations are required to reduce the background coal concentration below 0.40 percent.

Fifth is the fluidization air system. This system supplies air to fluidize the limestone. In an actual bed, this would be the combustion air. This system encompasses the blower and its associated control equipment and a large diameter flexible hose connecting the blower outlet with the plenum box.

Sixth is the transport air system. This system uses compressed air from the building compressor for transporting coal or limestone in the coal feed, limestone feed, or separation systems. It requires a regulated pressure compressed air supply and various control valves.

Seventh is the bed. Fluidization and coal mixing take place within the bed. It is constructed of plexiglass, for observational purposes, and its dimensions are approximately 2 x 2 feet base area and 6.5 feet tall. Holes are cut in one wall for insertion of sample probes for taking samples of the operating bed. Two rectangular sections and a small port were made removable for ease of access to the feeders.

Eighth is the adaptable plenum box. The plenum box is where coal and air mix for a combined feeder and where air is distributed for a below-bed feeder. This piece has the capability of being detached from the bed, coal feed line and fluidization air line so that it can be lowered and a new feeder installed or an existing feeder altered.

Ninth is the grid plate, a steel plate which separates the plenum box from the bed area. This component holds the feeder in place and is an integral part of the coal distribution and fluidization systems. It also supports simulated heat transfer tubes.

Tenth is the dust handling system. It includes the exit ductwork and the baghouse filter. This system filters the air before it exits to the atmosphere.

For complete details on the design, layout, construction and operation of this experimental system, refer to the theses by Henry [10] and Knox [11].

The limestone used in the experimental tests was a nominal 0.125 inch top size double screened limestone. The sieve size was stated as 6 by 16, i.e., all material retained on a number 6 sieve or passing a number 16 sieve was removed. The limestone had an experimentally determined average bulk density of 92 lbm/ft^3.

The imitation coal used was ground in a hammermill crusher containing a 0.25 inch screen. The largest particles were 0.25 inch and the minimum were fines. The imitation coal had an experimentally determined average bulk density of 47 lbm/ft^3. For further information, see Knox [11].

CHAPTER 5

FLUIDIZED BED TEST FORMAT

Introduction

This study involved a detailed experimental investigation of the below-bed valve cap coal feed system. Evaluation was performed with four basic tests. The formats of these tests will be described next as well as the equipment required to perform the tests.

Air Test

The first type of test is the air test. For this test, various air flow rates are passed through the feeder and the resulting pressure drops are measured. Pressure fluctuation and frequency of fluctuation are also recorded. Flow characteristics are observed by the use of tufts placed within the bed as is common practice in fluid dynamics experiments [13, p. 213-214, 14, p. 151]. Two air flow tests are required: one for the fluidization air system and one for the transport air system.

Limestone Test

The second type of test is the limestone test. As with the air tests, different air flow rates are passed through the feeder which will fluidize the limestone bed. This will allow the quality of fluidization to be evaluated through observation. Pressure drop across the feed system is measured in addition to pressure fluctuation and frequency of fluctuation. Bed pressure drop is also recorded. The bed height at each flow rate is measured as well as the slumped or no fluidization depth. These bed depths were measured to allow the degree of fluidization to be determined by calculation of the bed expansion.

Coal Test

A coal test is done exactly as an air test except coal is introduced into the feed system. In this way, the feeder performance with solids and air can be observed and quantified. The same data that are taken for the air test are recorded for the coal test.

Coal Feed Test

The coal feed test models the way in which the feed system would operate under actual combustion conditions.

Coal is fed into the fluidized bed of limestone at specified mass flow rates and air flow conditions. Bed samples are taken at a specific time by sample probes placed in four of the twelve bed entry ports. Three rows of four entry ports are located at levels one foot, two feet and three feet above the grid plate. The sample probes are shown in Figure 5.1 and were designed by G. D. Knox [11, Chapter 3].

Data Summary

The various parameters that were monitored during the experiment are summarized in Table 5.1. They are separated by their particular system.

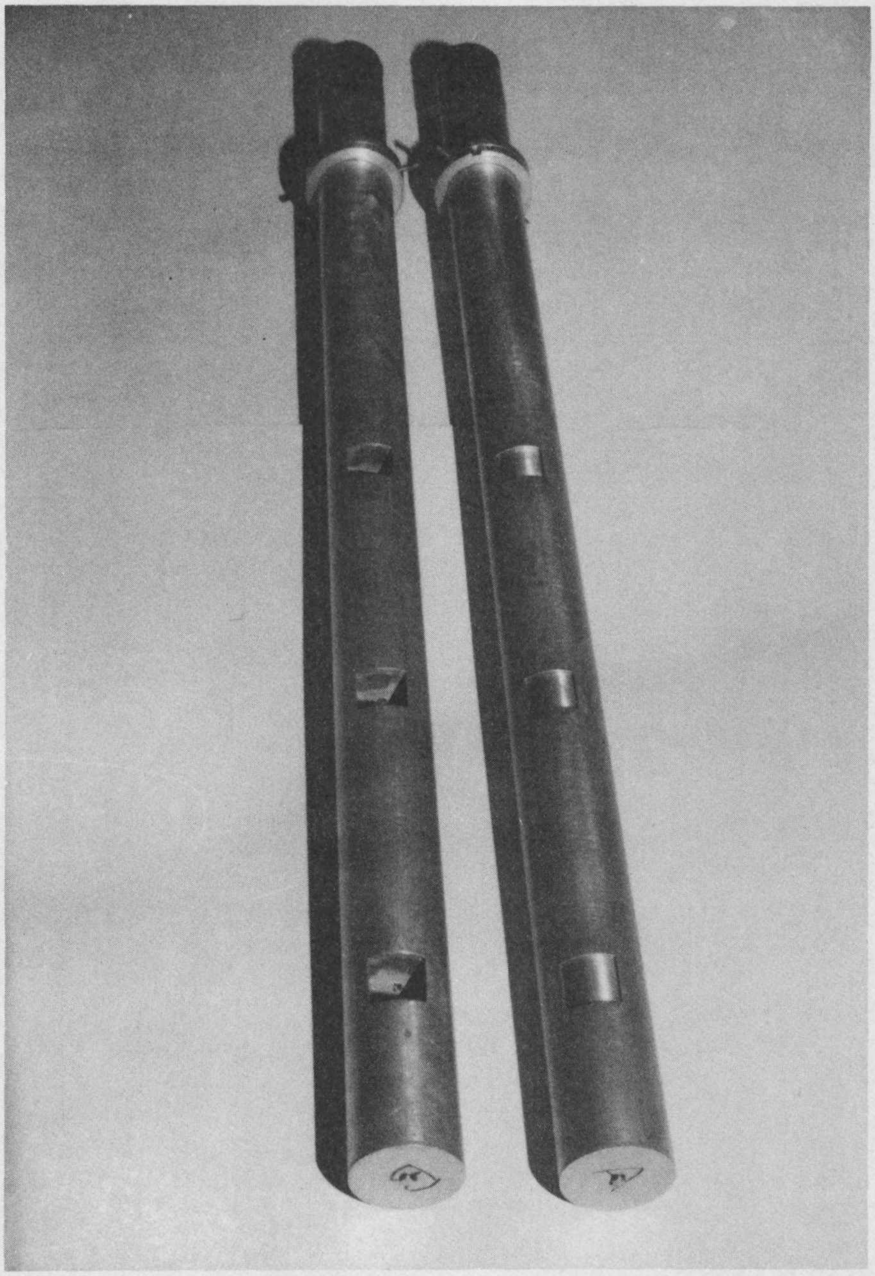

Figure 5.1. Coal Sample Probes.

TABLE 5.1

EXPERIMENTAL FLUIDIZED BED DATA

System	Data
Fluidization Air	Air Flow Rate, Air Inlet Temperature and Pressure, Plenum Pressure, Bed Pressure, Above Bed Temperature and Pressure
Transport Air	Air Flow Rate, Air Inlet Temperature and Pressure, Air Exit Pressure Directly Below the Valve Cap, Bed Pressure, Above Bed Temperature and Pressure
Coal Feed	Coal Mass Flow Rate
Safety	Bed Wall Temperature, Blower Outlet Temperature, Baghouse Pressure Drop

For complete details on measuring and recording data with this system, refer to the theses by Knox [11] and Henry [10].

Feeder Evaluation and Data Reduction

The valve cap feed system was evaluated both qualitatively and quantitatively. Qualitatively, the operating flow regime, the characteristic fluidization and bed drainback were observed. Quantitatively, pressure losses, pressure fluctuation and frequency of fluctuation, bed height and coal distribution were obtained.

To determine the operating flow regime, direct observation during testing and videotapes were used. Possible flow regimes are illustrated in Figure 5.2. The same type of observations were done for determination of the characteristic fluidization except that additional observation of particular bed sections were made after draining. Drainback was checked by simply slumping the bed to see if any material would drain into the feed pipe.

Pressure measurements were taken at three locations: the plenum box, the bed directly above the grid plate, and in the top of the bed. Bed material was kept out of the pressure taps by a nine cubic feet per hour (at room temperature and atmospheric pressure) purge flow. The flow was kept constant by the use of a nozzle (needle valve) with sonic conditions at the throat [10]. This small flow created a constant, but small magnitude error in the pressure readings which was accounted for when a differential pressure was calculated. Frequency and fluctuation of pressure were recorded on a strip chart recorder.

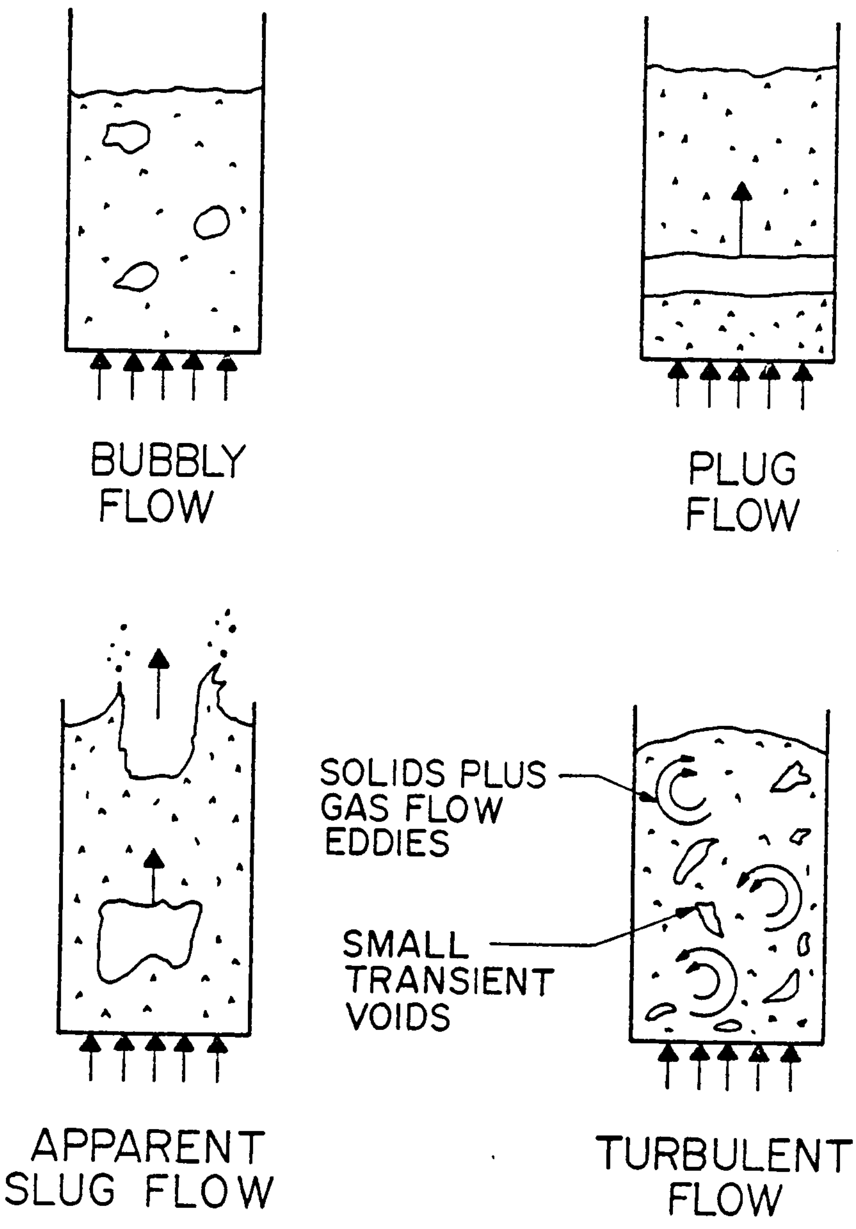

Figure 5.2. Flow Regimes.

Bed expansion was determined by measuring the bed depth with a tape measure attached to the bed wall. This measurement was highly subjective because the upper surface of the fluidized bed moved as much as ten inches. The depth was corrected for the volume lost by covering simulated heat transfer tubes and for the volume occupied by the feeder itself.

Coal distribution was determined by taking samples with the coal sample probes. Twelve locations were sampled during each test: three positions on each of four probes. The coal to limestone mass ratio for each position was determined by separating the coal from the limestone with a hand held magnet. The mass ratios for all of the compartments were averaged and then each mass ratio was compared to this average. This method of reducing the coal sample data determined where coal lean and coal rich regions were located in the bed. For a properly operating feeder, these regions should be randomly mixed. Also, there should be no regions that vary significantly from the average. If there existed such a region, it would show that the feed system was feeding improperly.

The next chapters will discuss the results of the tests performed with the valve cap feed system.

CHAPTER 6

VALVE CAP BELOW-BED FEED SYSTEM

Introduction

This chapter presents the results of tests performed with the fluidized bed test facility on the valve cap below-bed feed system. This system was thoroughly studied, altered and reinvestigated. This chapter presents the initial designs, initial tests, redesigns and latter tests. In Chapter 7, the best system is chosen and recommendations for future tests are presented.

Bubble Cap Fluidization System

Description

The bubble cap fluidization system was selected by the TVA for use in the 20MW pilot plant. Fluidization air passed from the plenum box through the grid plate via twenty-four bubble caps. A bubble cap is shown in Figure 6.1. Each cap has sixteen 0.128 inch diameter exit holes. These bubble caps were supplied by the Babcock and Wilcox Company and were actually used in the Electric Power Research Institute's (EPRI) 6x6 foot test facility.

In an actual bed, the caps would be screwed into the grid plate and the nut placed on the bottom and tack welded. Castable refractory would be poured around the caps up to the level of the neck of the upper section. In the cold model test facility, the neck of the upper section was placed flush with the grid plate, sealed with silicon glue and a wooden false bottom was placed at the base of the caps. The

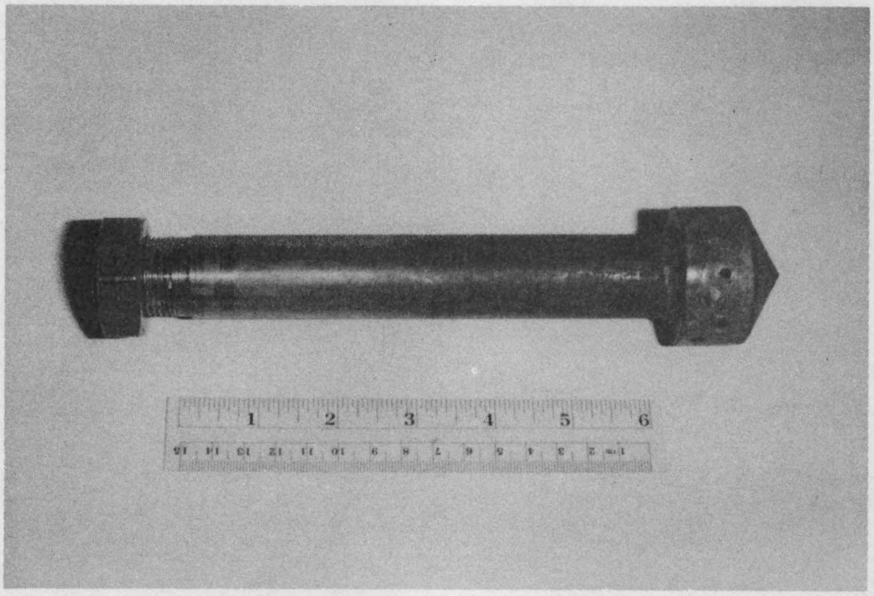

Figure 6.1. Bubble Cap Fluidization Device.

bubble caps were arranged in a square grid 18 inches on a side with 4.5 inches between cap centers. The center cap was omitted for the coal transport system. This matrix was centered in the 2 x 2 foot square bed area.

Qualitative results

Air only tests of the bubble cap fluidization system were conducted with tufts placed in the bed for flow visualization. The air circulated upward along the outer edges of the bed and downward in the center. This type of flow pattern would yield good mixing. The tufts also revealed the onset of turbulence along the grid plate. This was found to occur at a superficial velocity of about 5 feet per second. It is recommended that to achieve good mixing characteristics through turbulence, these caps should be operated at or above this velocity.

When limestone was placed into the bed and fluidized, bubbles were seen to coalesce at the first row of heat transfer tubes approximately 9 inches from the grid plate. This is shown in Figure 6.2. A small row of bubbles formed about 5 inches above the grid plate, resembling slug flow. The major portion of the fluidized bed of limestone was characterized by layers of bubbles forming and flowing through the limestone to the surface, shown in Figure 6.3. Along the bed walls which run parallel with the heat transfer tubes, large bubbles formed and rose. Because of the uniform bubble formation along a horizontal line the regime of fluidization was termed plug/bubbly.

Figure 6.2. Bubbles Coalesing at First Row of Heat Transfer Tubes for Bubble Cap Fluidization System.

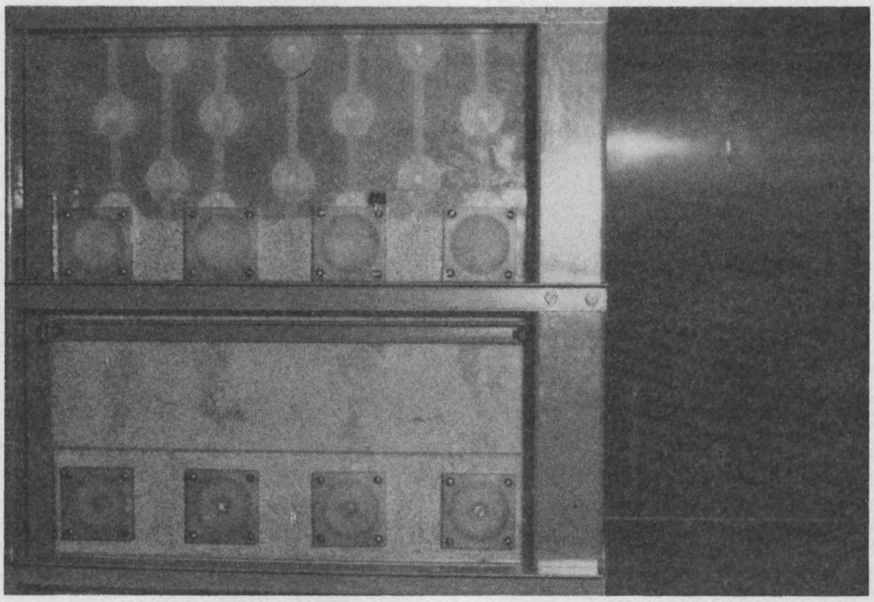

Figure 6.3. Row of Bubbles Flowing Through Limestone for Bubble Cap Fluidization System.

There were no sections where jets or large air flows were concentrated. The entire bed was fluidized uniformly. The upper surface of the bed was fairly violent when the bed was deep (around 2 feet slumped) and was rather calm for shallow beds (around 7 inches slumped).

Quantitative results - pressure drop

The pressure loss across the bubble cap fluidization system was measured for various superficial velocities. The results are shown in Figure 6.4. The data can be described very accurately by the relationship given in equation 6.1. This equation was obtained through a power law curve fit [16, p. 98]. P is given in inches of water when V_s is in feet per second (conditions are 14.3 psia and 80^{o}F).

$$\Delta P = 8.57\ V_s^{1.739} \qquad [r^2 = 0.973]. \qquad (6.1)$$

The r^2 which appears with equation 6.1 is the coefficient of determination which is a measure of how well the fit describes the variation of the dependent variable with respect to the independent variable. A value of r^2 equal to 1.000 indicates that 100% of the variation of P with respect to V_S is accounted for by the curve fit.

The bubble cap pressure loss is much greater than any of the other fluidization systems for which this data were available. These are also shown in Figure 6.4.

If an incompressible pipe flow analysis is performed on a bubble cap, this pressure loss can be accurately calculated. These calculations can be used to alter the design of this system to fit any desired conditions. This technique is described in Appendix E.

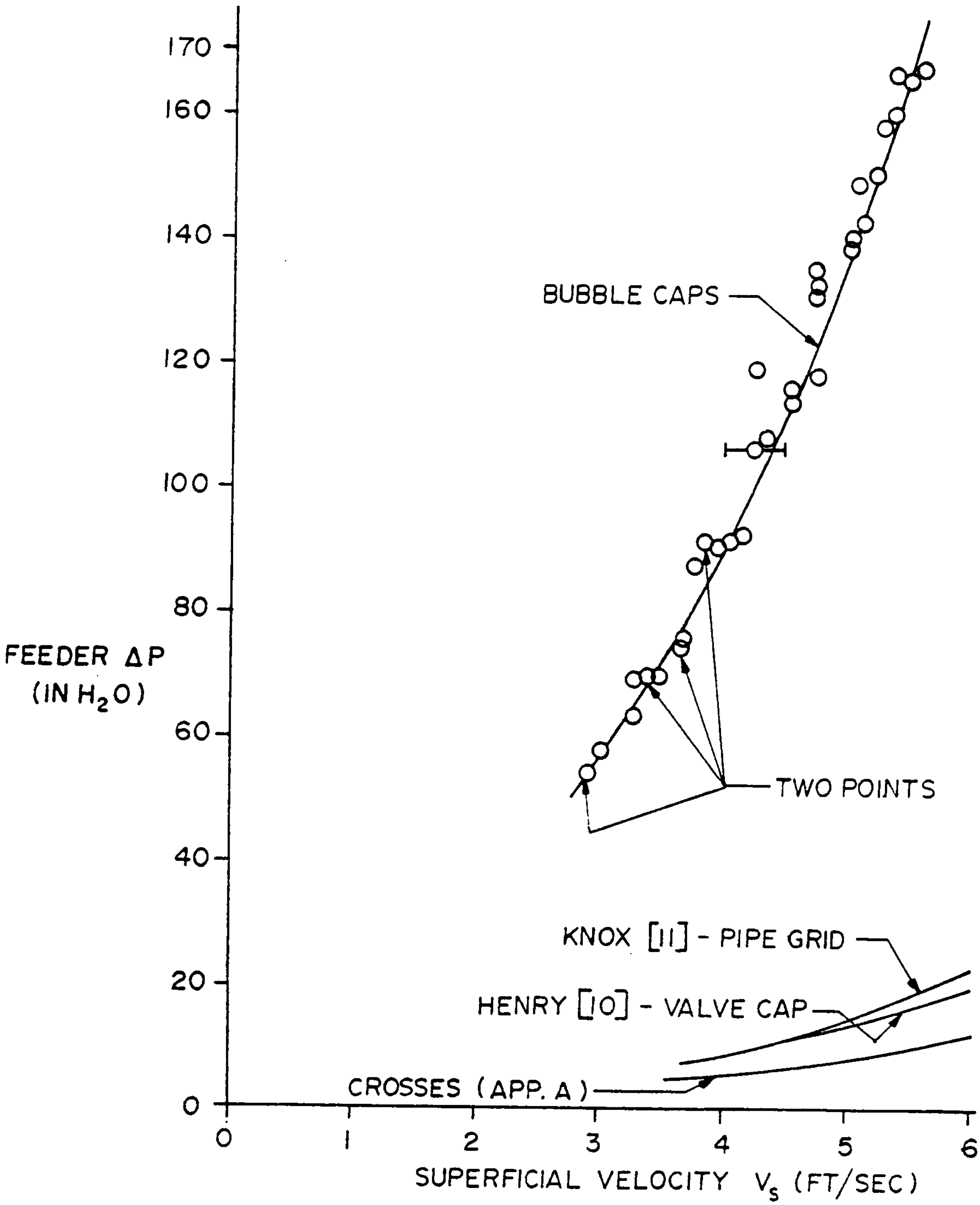

Figure 6.4. Pressure Loss Versus Superficial Velocity for Bubble Caps.

Amplitude and frequency of bed pressure

The average amplitude of the lower bed pressure fluctuation as a function of superficial velocity and bed depth is shown in Table 6.1. The amplitude is seen to increase with bed depth and superficial velocity. Both of these trends are common and were expected. The increase with superficial velocity occurs because the greater flow creates greater pressure pulses. Secondly, the greater bed depths require greater pressure pulses for the air to pass through the bed. The maximum amplitudes are also shown in Table 6.1. These are the result of a bubble passing by the pressure tap. Table 6.2 compares the average lower bed pressure amplitudes of the bubble cap fluidization system to those of the crosses (see Appendix A), the pipe grid [11] and the floating caps [10]. There are several notes concerning this table. One, since the pipe grid, the floating caps and the crosses experienced a much smaller pressure drop than the bubble caps, the blower could pump more air thus giving them a much greater superficial velocity range, up to about 8.5 ft/sec. The data for the floating caps, the pipe grid and the crosses were much more sparse in the superficial velocity range covered by the bubble caps, 3.5 to 5.3 ft/sec, consequently, some interpolation was required. Two, the total flow area for each feeder is given in Table 6.2. In cases where the flow area was variable, the configuration with the area closest to that of the bubble caps is presented. Third, two bed depths were chosen as a comparison basis, 6.0 and 15.5 inches. For the crosses and the pipe grid feeders, bed depths as close as possible to these two were chosen. The average amplitude of the floating cap feeder was not a function of bed depth.

TABLE 6.1

AMPLITUDES OF THE LOWER BED PRESSURE FOR THE BUBBLE CAP FLUIDIZATION SYSTEM

Bed Depth (in.)	6.0	12.5	15.5	15.75	25.0
Superficial Velocity Range(ft/sec)	Average Amplitudes				(± in. H_2O)
3.7-3.9	---	0.7	2.0	1.5	0.7
4.1-4.5	1.0	2.0	3.0	3.0	3.5
4.6-4.7	2.0	3.0	4.0	---	4.5
4.9-5.3	2.5	3.5	4.5	5.0	6.0
5.4	2.7	---	---	---	---
	Maximum Amplitude (in. H_2O)				
	+4.5	+7.5	+10.5	-10.2	+10.5

TABLE 6.2

COMPARISON OF THE LOWER BED PRESSURE AMPLITUDES IN INCHES OF WATER FOR THE BUBBLE CAPS, PIPE GRID, CROSSES AND FLOATING CAPS

Feeder	Bubble Cap		Pipe Grid [11]				(Appendix A) Crosses						Floating Cap [10]
Configuration (Flow Area ft^2)	No Variation (0.034)		HP1D[1] (0.100)		HP11D[1] (0.212)		A Mix[2] (1.361)		All +[2] (1.361)		All x[2] (1.361)		Cap Height (0.136)
Superficial Velocity Range (ft/sec) \ Bed Depth (in.)	6.0	15.5	5.8	14.9	4.7	15.4	7.0	16.25	7.0	16.75	7.0	16.25	Not a function of bed depth
3.5-3.9	---	2.0	0.1	0.5	0.2	0.6	---	---	---	0.7	---	---	1.0
4.1-4.5	1.0	3.0	0.2	1.0	0.2	1.2	---	1.0	---	1.1	---	---	4.0
4.6-4.7	2.0	4.0	0.2	1.1	0.2	1.3	0.2	1.1	0.3	1.3	1.0	1.1	4.0
4.9-5.3	2.5	4.5	0.3	1.5	0.3	1.7	0.4	1.3	0.9	2.0	1.0	1.2	4.0

[1]For full explanation see Knox [11], p. 131. HP1D stands for Hole Pattern 1 - Down.

[2]For explanation, see Appendix A.

Note: For the Pipe Grid, Floating Caps, and Crosses, interpolation was required. This was done using the velocity in the center of the range.

Study of Table 6.2 reveals that the bubble cap system has the greatest average amplitudes of all of the systems for both depths. This is most likely a result of the characteristic bubbly fluidization of the bubble caps.

The frequency of the lower bed pressure oscillation is presented in Table 6.3 as a function of bed depth and superficial velocity. The frequency tends to remain fairly constant with respect to superficial velocity, but decreases from 2.8 cycles per second to about 1.8 cycles per second for slumped bed depths increasing from 6.0 inches to 24.0 inches. This is because larger bubbles tend to form in deeper beds. Larger bubbles form less frequently because they require more air.

One noteworthy exception is the 3.3 cycles per second for the 25 inch deep bed at superficial velocity range of 3.7 to 3.9 feet per second. This is not a singularity; the same high frequencies were observed in the lower superficial velocity range (3.0 to 3.6 feet per second) of the other depths. These data were not presented because the pressure instrumentation did not have sufficient resolution to allow a good count to be obtained. It was possible, however, to determine that the frequency was somewhat higher, in some cases around 5.0 cycles per second. This occurs due to the fact that the frequency at low superficial velocities is the result of small bubbles. At higher superficial velocities, the frequency becomes the result of larger bubbles formed by the coalescence of the small bubbles.

The frequency of the lower bed pressure oscillations for the bubble cap system is compared to the frequencies of the other systems in Table 6.4. Henry [10] did not present data on the frequency of the

TABLE 6.3

FREQUENCIES OF THE LOWER BED PRESSURE FOR
THE BUBBLE CAP FLUIDIZATION SYSTEM

Superficial Velocity Range (ft/sec) \ Bed Depth (in.)	6.0	12.5	15.5	15.75	25.0
	Frequency (cycles/sec)				
3.7-3.9	---	2.0	1.9	2.1	3.3
4.1-4.5	2.5	2.4	2.0	2.1	1.7
4.6-4.7	2.7	2.3	2.1	---	1.8
4.7-5.3	2.8	2.5	2.0	2.1	1.7
5.4	2.8	---	---	---	---

TABLE 6.4

COMPARISON OF THE LOWER BED PRESSURE FREQUENCIES, IN CYCLES/SEC FOR THE BUBBLE CAPS, PIPE, GRID, AND CROSSES

Feeder	Bubble Cap		Pipe Grid [11]				Crosses (Appendix A)					
Configuration	No Variation (0.034)		HP1D[1] (0.100)		HP11D[1] (0.212)		Mix [2] (1.361)		All + [2] (1.361)		All x [2] (1.361)	
Bed Depth (in.) / Superficial Velocity Range (ft/sec)	6.0	15.5	5.8	14.9	4.7	15.4	7.0	16.25	7.0	16.75	7.0	16.25
3.5-3.9	---	2.0	4.0	---	---	3.8	---	2.5	---	2.6	---	---
4.1-4.5	2.5	2.4	3.9	3.3	4.8	3.0	---	2.6	---	2.0	---	---
4.6-4.7	2.7	2.3	3.9	3.3	4.8	3.0	5.0	2.6	4.2	2.1	6.0	2.5
4.9-5.3	2.8	2.5	3.8	3.2	4.9	3.1	5.0	2.5	5.1	2.3	5.8	2.7

[1]For full explanation see Knox [11], p. 131.

[2]For explanation, see Appendix A.

oscillations for his floating cap fluidizing feeder. The bubble caps' frequencies are about the same as the crosses for the deepest bed. The bubble caps' frequency did not change significantly when the bed was made shallow, however, the crosses did. The bubble caps' frequency was lower than the pipe grid's for both bed depths. All of the fluidization systems display the trend of decreasing frequency with increasing bed depth.

Bed expansion

Bed expansion (see Appendix C for definition of bed expansion) as calculated on a percentage basis versus superficial velocity is presented in Figure 6.5. The linear regression equation 6.2 for these data is given below. Expansion is given in percent when superficial velocity is in feet per second. This equation should not be applied for superficial velocities below 3.2 feet per second.

$$E = 17.07\, V_s - 54.60 \qquad [r^2 = 0.890.] \qquad (6.2)$$

Bubble cap bed expansion is compared to the other systems in Figure 6.6. The bubble caps yield greater bed expansion for a given superficial velocity than any other system. This is because the bubble caps distributed the fluidization air more uniformly. The bubble caps created no major air pathways and had few dead spots. This was conducive to bed expansion.

Conclusions

The bubble caps are an excellent fluidization system. They fluidized the bed uniformly experiencing only small dead zones in the bed corners. It should be emphasized that if the pressure loss characteristics of this system do not meet needed requirements, they can be

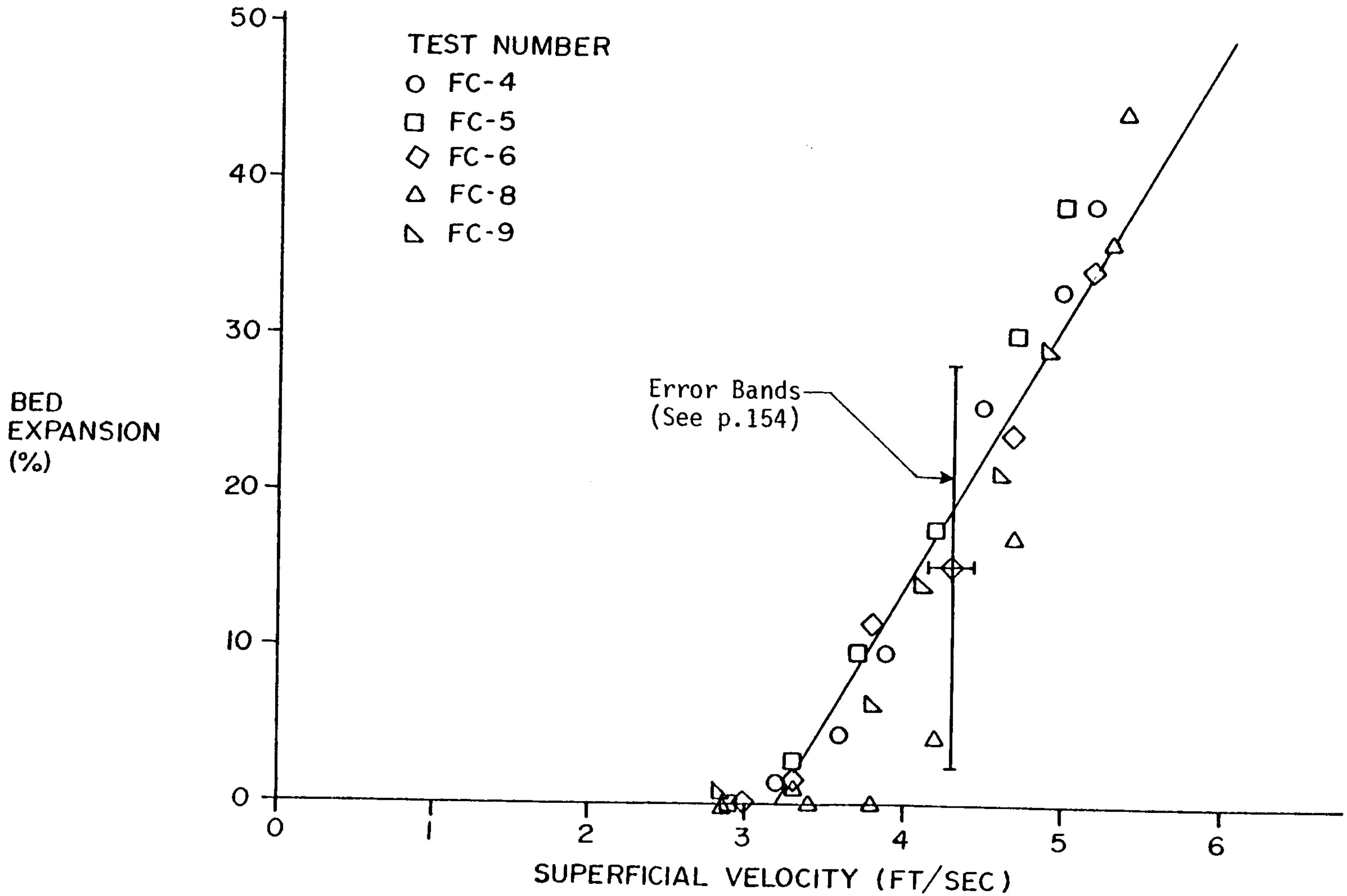

Figure 6.5. Percent Bed Expansion Versus Superficial Velocity for Bubble Caps.

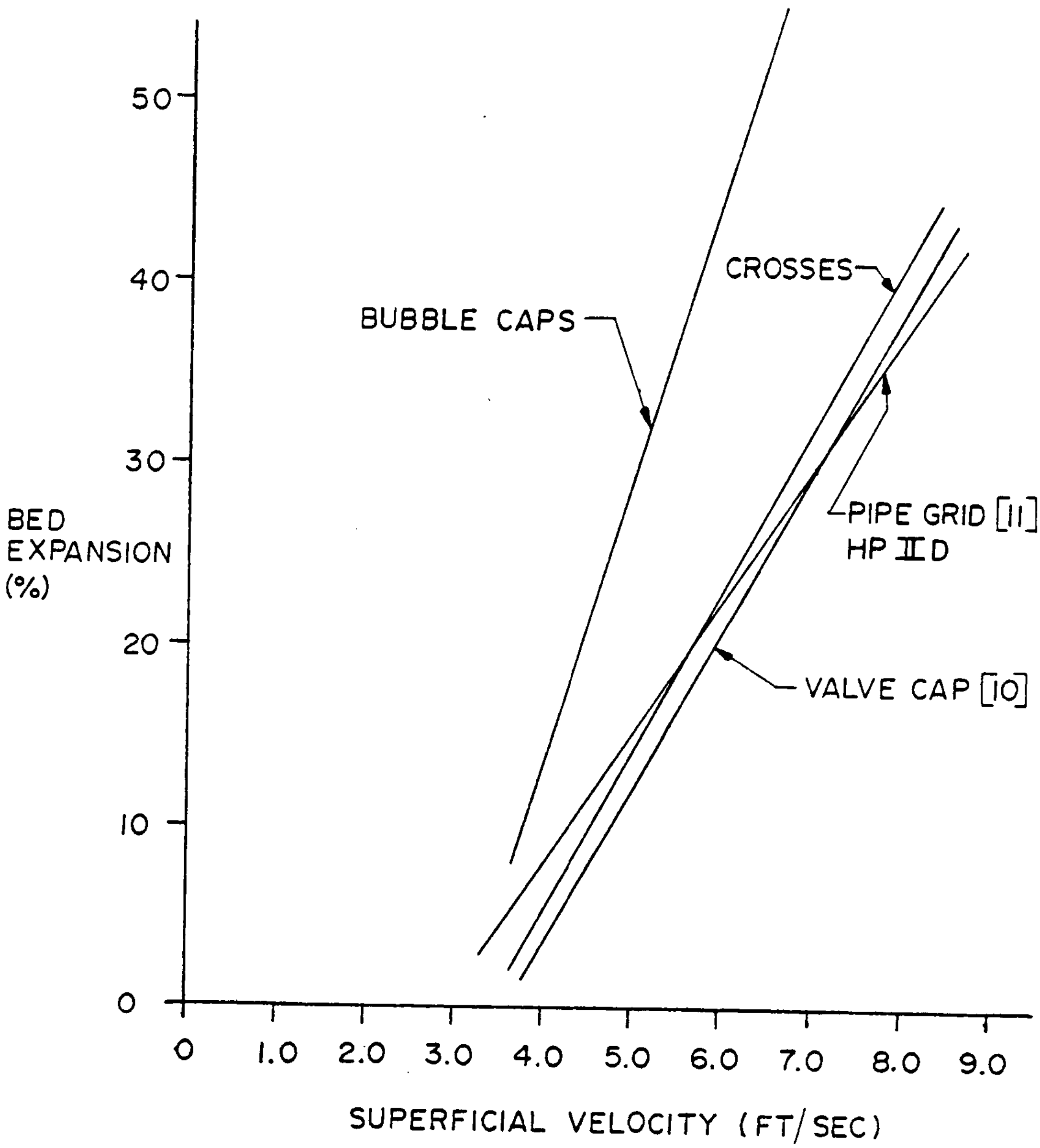

Figure 6.6. Percent Bed Expansion Versus Superficial Velocity for Various Fluidization Systems.

changed by the analytic procedure outlined in Appendix E. This capability makes this system highly adaptable.

The bubble caps represent the system to be employed in the 20MW pilot plant being constructed by the TVA. They are, therefore, a state-of-the-art system.

Valve Cap Below-Bed Coal Feed System

Introduction

A valve cap feed system is shown in Figure 6.7. It has two very desirable characteristics. One, when operating, it will distribute coal in all radial directions. Two, when not operating, it will seat on the feed pipe and prevent the bed from draining back into the coal feed line. The cap operates as a check valve. The original dimensions were suggested by the TVA.

The first design featured a cage made of square stock oriented with its diagonal placed horizontally to aid in moving limestone from between the cap and cage. This was done in hope that the cap would open completely during operation. Weld beads were placed between the cap and feed pipe following the recommendations of Henry [10]. This recommendation was for caps operated together in parallel and stated that caps would be more likely to open if they always had some small amount of air flow passing through them to clear away bed particles. The valve cap in this test was not operated in parallel with any other cap, but for utility use, it would be operated in this mode. The valve cap system was made removable from the bed and coal feed line to facilitate alteration.

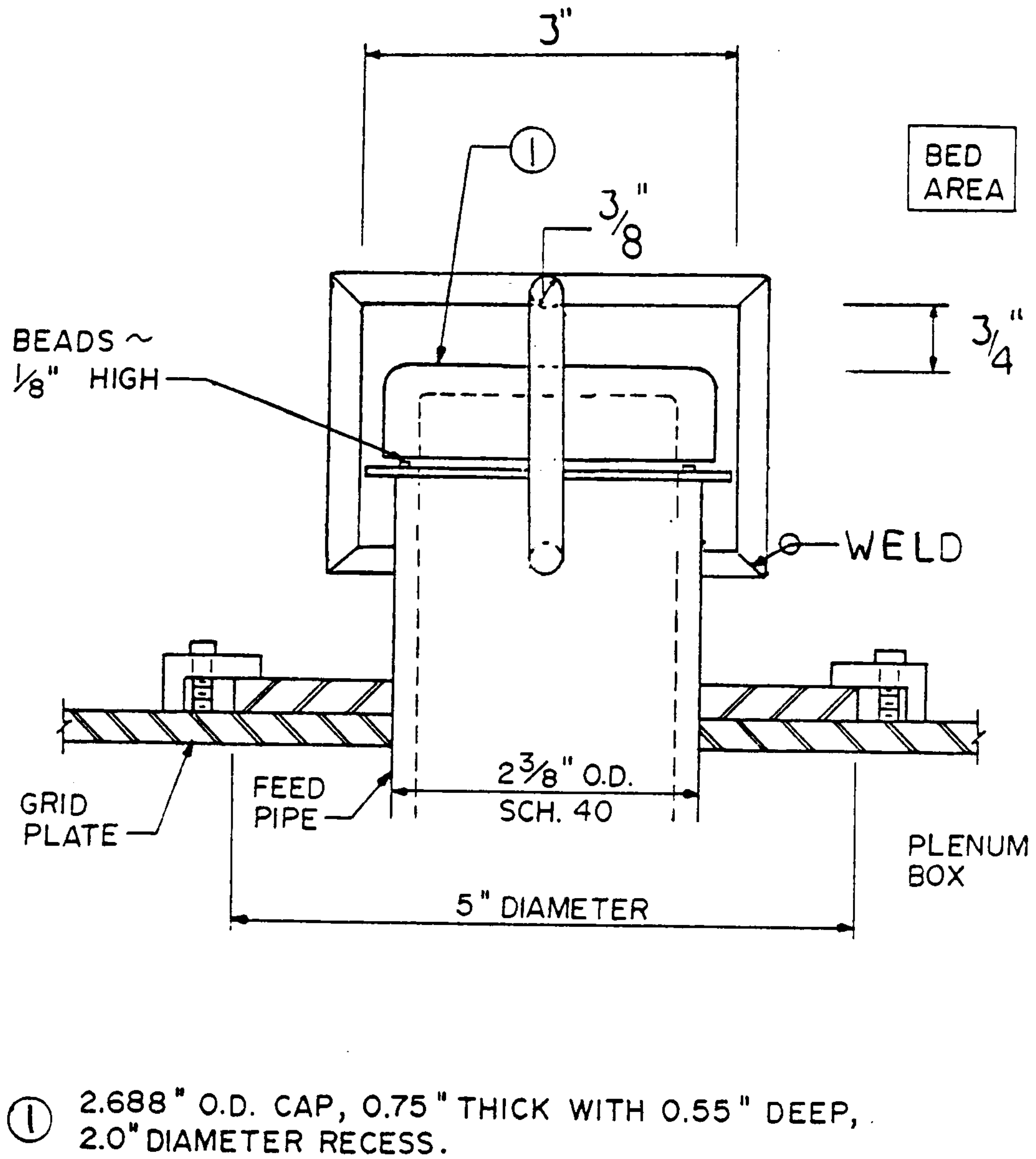

Figure 6.7. Valve Cap Feeder—Experimental Design.

Elementary force balance

An elementary force balance was performed upon the valve cap to determine the relationship between full-open flow rate and cap mass. The control volume employed is shown in Figure 6.8.

The cap has five major forces acting upon it.

1. The bed pressure force acting on the top surface.
2. The air momentum transport acting on the bottom surface.
3. The weight of the cap.
4. The force of the containment cage on the cap.
5. The air pressure force acting on the bottom of the cap.

The air flows vertically into the bottom of the cap and radially outward. The integral momentum equation is given in equation 6.3 [13, p. 145].

$$\Sigma F_z = \underset{\substack{\text{control}\\\text{surface}}}{\iint} V \frac{\rho}{g_c} \bar{V} \cdot d\bar{A} + \frac{\partial}{\partial t} \underset{\substack{\text{control}\\\text{volume}}}{\iiint} V \frac{\rho}{g_c} \, d(\text{Vol}) \qquad (6.3)$$

The terms in the equation are defined as follows. ΣF_z is the sum of the forces in the positive z direction shown in Figure 6.8. The density of the air at the conditions of the bed is denoted by ρ. The dimensional constant is denoted by g_c. V denotes the speed of the air, $\bar{V}$ the velocity. The differential area vector, denoted by $d\bar{A}$, points outward along the control surface. A differential volume element is written as d Vol. Time is indicated by t, thus $\frac{\partial}{\partial t}$ is a partial derivative with respect to time.

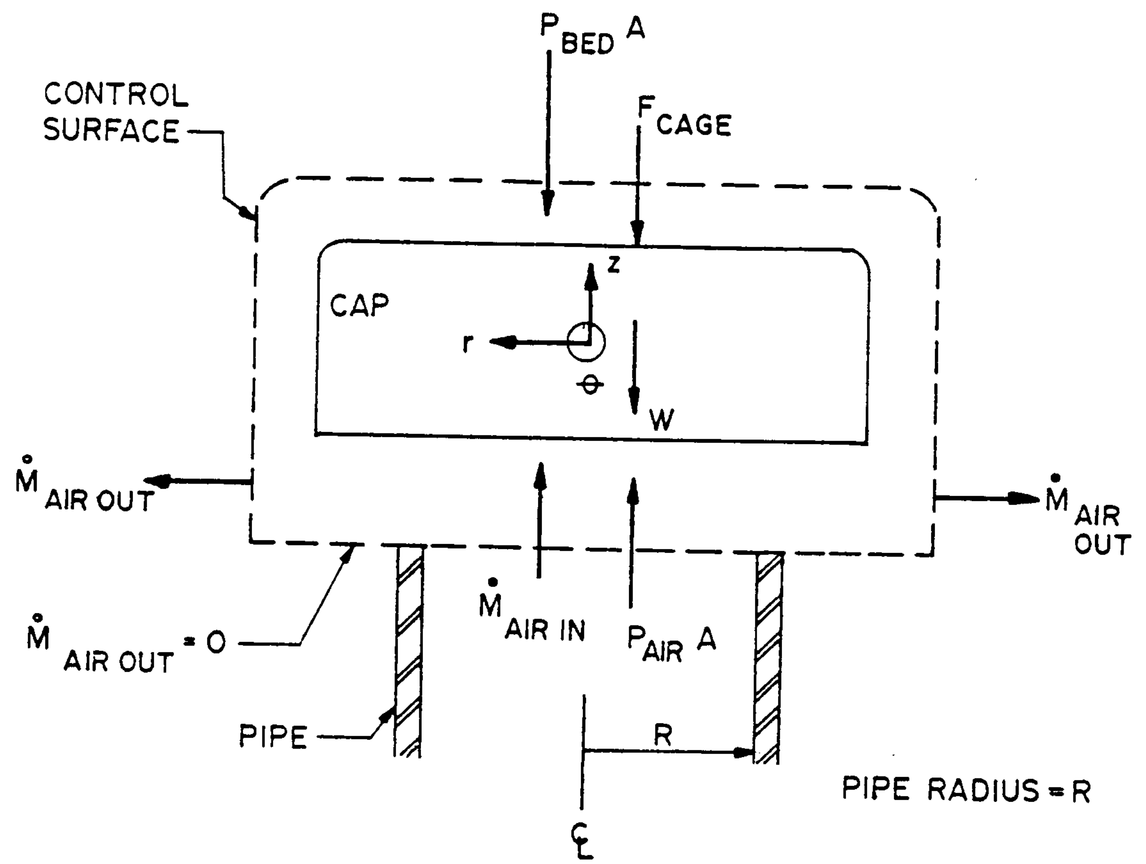

Figure 6.8. Control Volume for Elementary Force Balance.

Several assumptions were made to simplify the analysis. First, steady-state was assumed so that the time derivative would be zero. Second, the exit air was assumed to travel only in a horizontal plane, thus it did not contribute a momentum term in the vertical (z) direction. Third, the pressure of the air below the cap, (P_{Air}), was assumed to be approximately equal to the bed pressure above the cap (P_{Bed}), therefore, the two corresponding pressure forces would cancel. Fourth, the cage force was set equal to zero to determine the minimum air momemtum required to hold the cap open. With these assumptions, the sum of the forces in the vertical (z) direction becomes simply negative the cap weight (negative because it is directed downward). The differential area, dA is $r dr d\theta$ where θ is perpendicular to r and z in a horizontal plane. The dot product $\bar{V} \cdot d\bar{A}$ is negative for mass flux into the control volume. Equation 6.3 will now become equation 6.4.

$$- w = \int_0^{2\pi} \int_0^{R} \frac{\rho_{Air}}{g_c} V^2 \, r dr d\theta + 0. \tag{6.4}$$

Or, assuming ρ_{Air} and V are constant across the pipe exit, one obtains equation 6.5.

$$w = \frac{\rho_{Air}}{g_c} V^2 \int_0^{2\pi} \int_0^{R} r dr d\theta. \tag{6.5}$$

The double integral is simply the pipe area and will be denoted A_{Pipe}.

$$w = \frac{\rho_{Air}}{g_c} V^2 A_{Pipe}. \tag{6.6}$$

Since the design specifications given in Section 3 contain air flow rate, equation 6.6 will be rearranged by recalling that flow rate, Q, equals the product of velocity and area.

$$w = \frac{\rho_{Air}}{g_c} \frac{Q^2}{A_{Pipe}} . \tag{6.7}$$

Equation 6.7 gives an estimate of the maximum weight cap that can be supported by a given air flow. This weight will be denoted $W_{Air\ Only}$ to denote that it is the air flow only which supports this weight cap. Later, solid and air flows will be considered together.

It was decided that equation 6.7 could be modified to account for an additional force due to the higher pressure expected below the cap. A higher pressure is expected because of the pressure loss associated with expanding the flow from the pipe to bed conditions. A correction factor, called the momentum correction factor and denoted as K, was inserted in equation 6.7. This is shown in equation 6.8.

$$w_{Air\ Only} = K \frac{\rho_{Air}}{g_c} \frac{Q^2}{A_{Pipe}} . \tag{6.8}$$

Equation 6.8 can be further modified by using equation 6.9 and 6.10 where V_{Air} is the air velocity in the pipe and $\dot{m}_{Air}$ is the mass flow rate of the air.

$$Q = V_{Air} A_{Pipe} \tag{6.9}$$

$$\rho V_{Air} A_{Pipe} = \dot{m}_{Air} \tag{6.10}$$

Using these equations, equation 6.8 becomes equation 6.11.

$$w_{Air\ Only} = K \frac{\dot{m}_{Air} V_{Air}}{g_c} . \tag{6.11}$$

If solids flow is to be included, two additional terms must be defined. These are the slip ratio, S, and the coal mass to air mass flux ratio, J. The defining equations for these parameters are 6.12 and 6.13.

$$S = V_{Solids}/V_{Air} \qquad (6.12)$$

$$J = \dot{m}_{Solids}/\dot{m}_{Air} \qquad (6.13)$$

By analogy to the air only development, the weight supportable by solids alone, $w_{Solids\ Only}$, is given by equation 6.14.

$$w_{Solids\ Only} = \frac{\dot{m}_{Solids}\ V_{Solids}}{g_c} . \qquad (6.14)$$

Utilizing equations 6.12 and 6.13, equation 6.14 becomes:

$$w_{Solids\ Only} = \frac{\dot{m}_{Air}\ V_{Air}}{g_c}\ (JS). \qquad (6.15)$$

Note the absence of the momentum correction factor, K, in the solids equation. It was not necessary to account for a pressure distribution for the coal as it was for the air. Combining equations 6.11 and 6.15 gives the weight of any cap supportable by air and solids flow.

$$w_{Total} = w_{Air\ Only} + w_{Solids\ Only} = \frac{\dot{m}_{Air}\ V_{Air}}{g_c}\ (K+JS). \qquad (6.16)$$

Equations 6.11 and 6.16 will be used to evaluate K and S from experimental data.

Initial designs and tests with the valve cap system

The first caps which were manufactured are described in Table 6.5. The TVA-1 cap was used to perform initial tests to determine the basic behavior of the valve cap feed system. Several observations were made.

The cap opened and closed in a cycle. First it would begin to rise on one-side. The cap would tilt which would cause it to slide back against two of the four cage bars. Next, the tilt would increase until the rising side reached the cage top whereupon the other side of the cap would begin to rise. When this side rose to about half of the total free travel, the cap would quickly become fully open. Upon closing, the side not touching the cage supports would begin falling. This side would fall until it reached about half the free travel, whereupon, the cap would shift to the other side of the cage and fall until it reached the pipe. Because of the tilting, a collar was placed around the pipe, flush with the top surface, to prevent the cap from tilting below the pipe's lip and lodging between the cage and pipe.

The air flow from the feed system was directed radially outward from the cap. This was expected and will aid with mixing of coal into the bed.

The 0.75 inch thick cap was heavy and required a significant flow of air, approximately 165 cubic feet per minute, to operate fully open at 0.50 inch gap. As a result, it was not used in further tests.

Momentum correction factor tests

The two thin caps were used in tests to determine the value of the momentum correction factor K appearing in equation 6.8, as a function of cap free travel. The tests were performed with an open-top cage to

TABLE 6.5

INFORMATION FOR 3.5 INCH O.D. FLAT CAPS

Cap Name	Thickness (Inches)	Material	Mass (Grams)
TVA-1	0.750	Steel	911.90
UT-1	0.375	Steel	451.70
UT-2	0.375	Aluminum	168.95

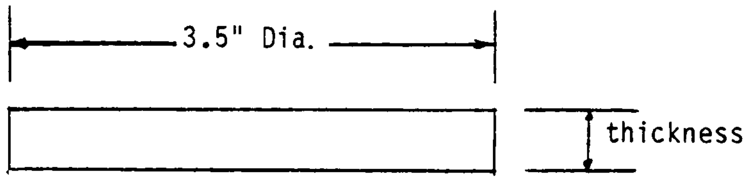

ensure there was no cage force exerted on the cap. The relationship between momemtum correction factor K and gap is shown in Figure 6.9. The line of Figure 6.9 is described by equation 6.9.

$$K = -0.84\ (\text{Gap}) + 1.93 \qquad [r^2 = 0.989] \qquad (6.17)$$

This equation only applies for gaps ranging from 0.50 inches to 1.0 inch. This equation can be used in conjunction with equation 6.8 to determine the maximum weight cap any air flow can support for a specified free travel. The momentum correction factor is greater than 1.0 because of the pressure force exerted by the air on the bottom surface of the cap.

2.688 inch diameter valve caps

The 3.5 inch outside diameter caps were too heavy to operate fully open at the required air flow rate. Consequently, it was decided to reduce the outside diameter of the cap in order to reduce the cap mass. The diameter used was 2.688 inches. The calculations required to arrive at this diameter are presented in Appendix D. Three flat caps were made with this outside diameter. The caps' thicknesses and masses are listed in Table 6.6. The 0.20 inch thick flat cap was designed to open fully with an air flow of 97.3 cubic feet per minute (80°F, 14.3 psia). The 0.45 inch thick flat cap was designed to open fully with an air flow rate of 97.3 cubic feet per minute and solids flow rate of 2.0 pounds of coal per pound of air or 7.5 pounds of coal per minute. The derivations used to determine these thicknesses are presented in Appendix D. The 0.75 inch thick cap was made to compare geometrically with the large 3.5 inch outside diameter cap.

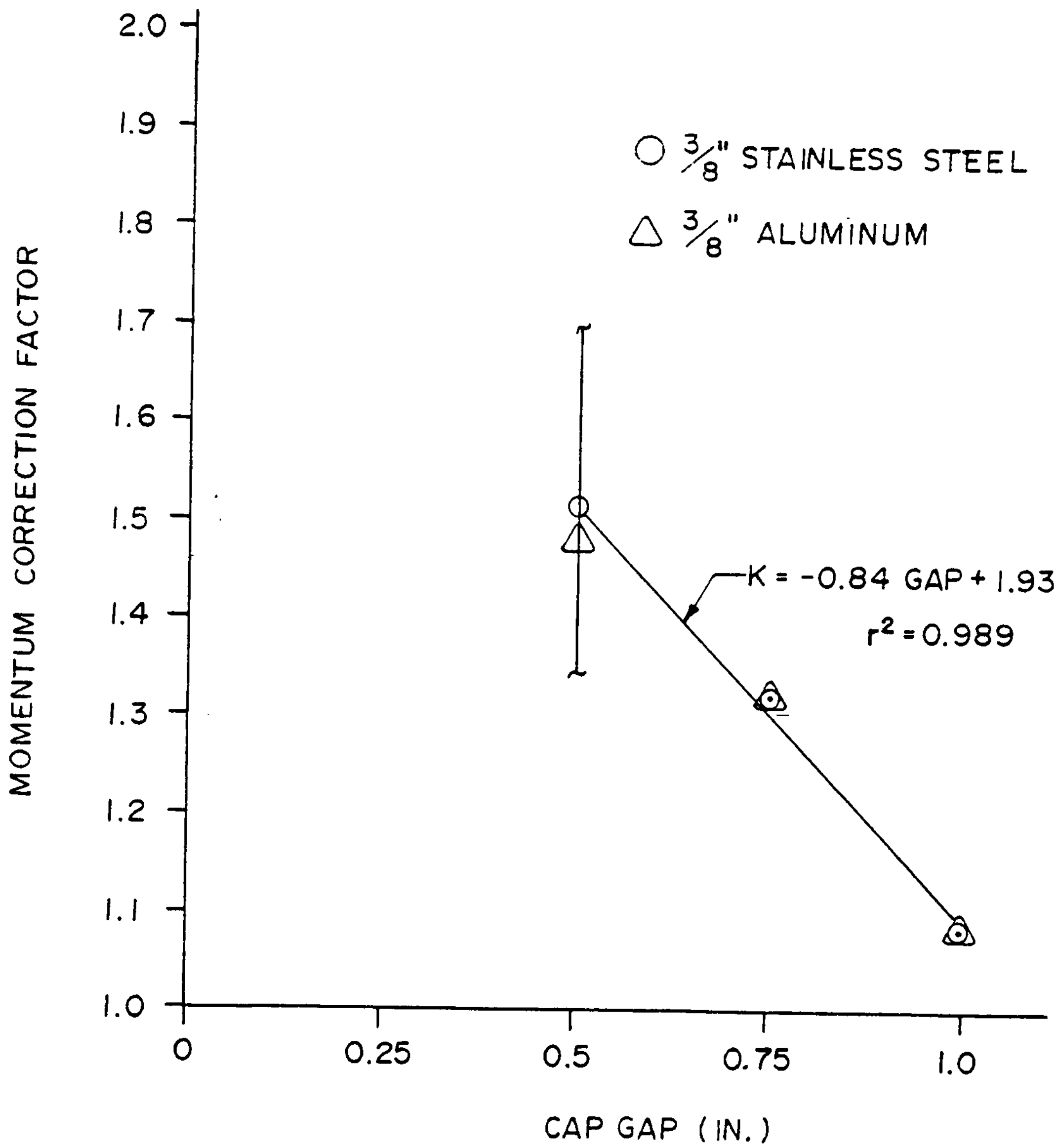

Figure 6.9. Momentum Correction Factor Versus Cap Gap for 3.5 Inch Diameter Valve Caps, Air Only.

TABLE 6.6

INFORMATION FOR 2.688 INCH O.D. FLAT CAPS

Cap Name	Thickness t (in.)	Recess Depth d (in.)	Mass (Grams)
F1	0.75	0 (Flat)	531.40
F2	0.45	0 (Flat)	323.90
F3	0.20	0 (Flat)	146.15
R1	0.625	0.25	349.40
R2	0.45	0.25	222.90
R3	0.625	0.425	274.00
R4	0.75	0.55	320.65
C1	Max. = 0.45 Min. = 0.10	0 (Convex)	215.90

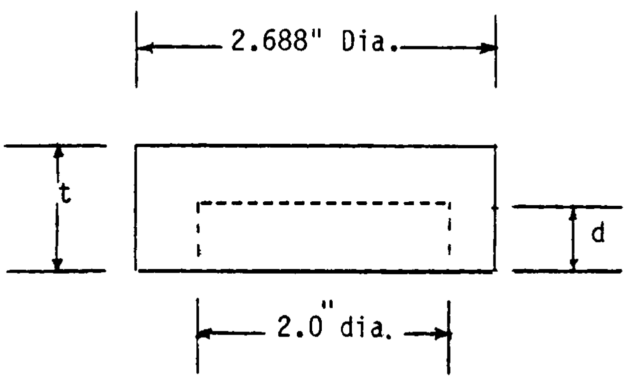

Several recessed caps were also manufactured. It was felt that the recess would capture coal particles and prevent wear on the underside of the cap. This concept is illustrated in Figure 6.10. The recesses were cut to various depths to investigate the effect this would have upon the cap wear characteristic. All of the recesses were made 2.0 inches in diameter which matched the feed pipe inside diameter. The important cap dimensions and masses are listed in Table 6.6.

One convex cap was manufactured to determine if it was possible to make a cap that would be more aerodynamically stable than the flat caps. It was believed that this cap might float at various levels instead of tilting as did the flat caps.

2.688 inch diameter caps — air only tests

All of the caps were tested with a 3.0 inch inside diameter cage and 0.5 inch free travel. Air only was passed through the feed system and the pressure differential was measured between a tap located approximately 1 foot below the valve cap and the lower bed pressure tap. This pressure drop is plotted as a function of air flow rate for all of the caps in Figures 6.11 through 6.18. Several points are noticed from these figures.

First, all of the caps operate with the same general characteristics. Initially, they are just rising from the seated position. This is the part of the figure where the pressure increases rapidly with respect to flow rate. Next, the caps begin to tilt, one side rising from the feed pipe until it hits against the cage. This is evidenced by the plateau in the pressure loss versus flow rate curve. The magnitude

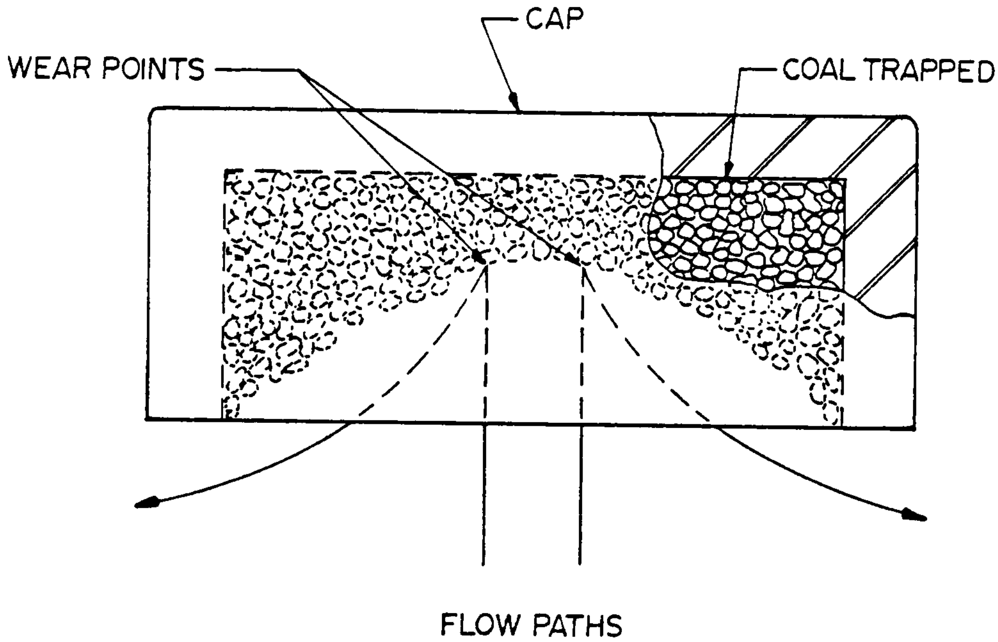

Figure 6.10. Trapped Coal in a Recessed Cap.

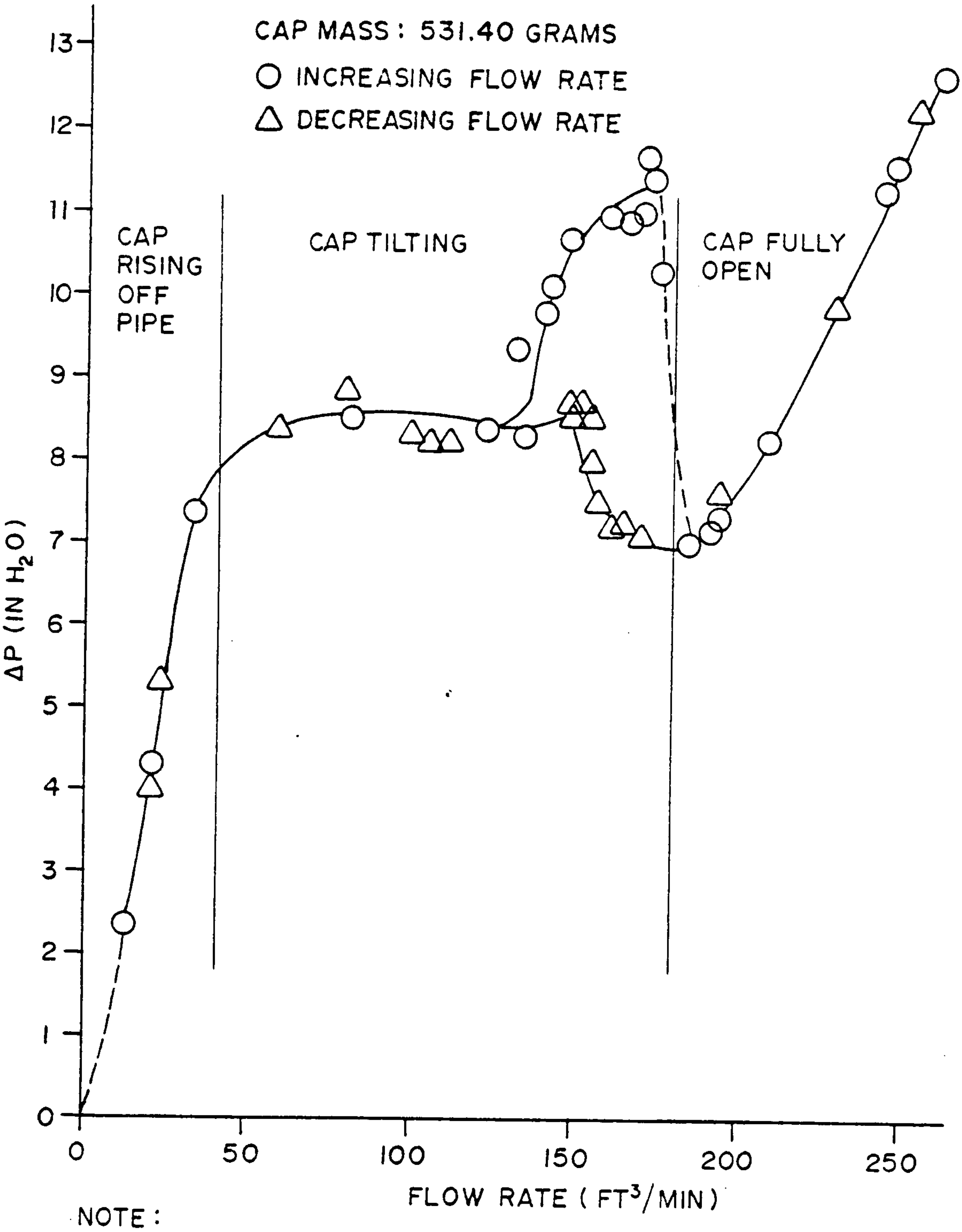

NOTE:
THE ERROR BANDS ARE SMALLER THAN THE SYMBOLS.

Figure 6.11. ΔP Versus Flow Rate for Flat Cap F1, 0.50 Inch Gap, 3 Inch Diameter Cage, Air Only.

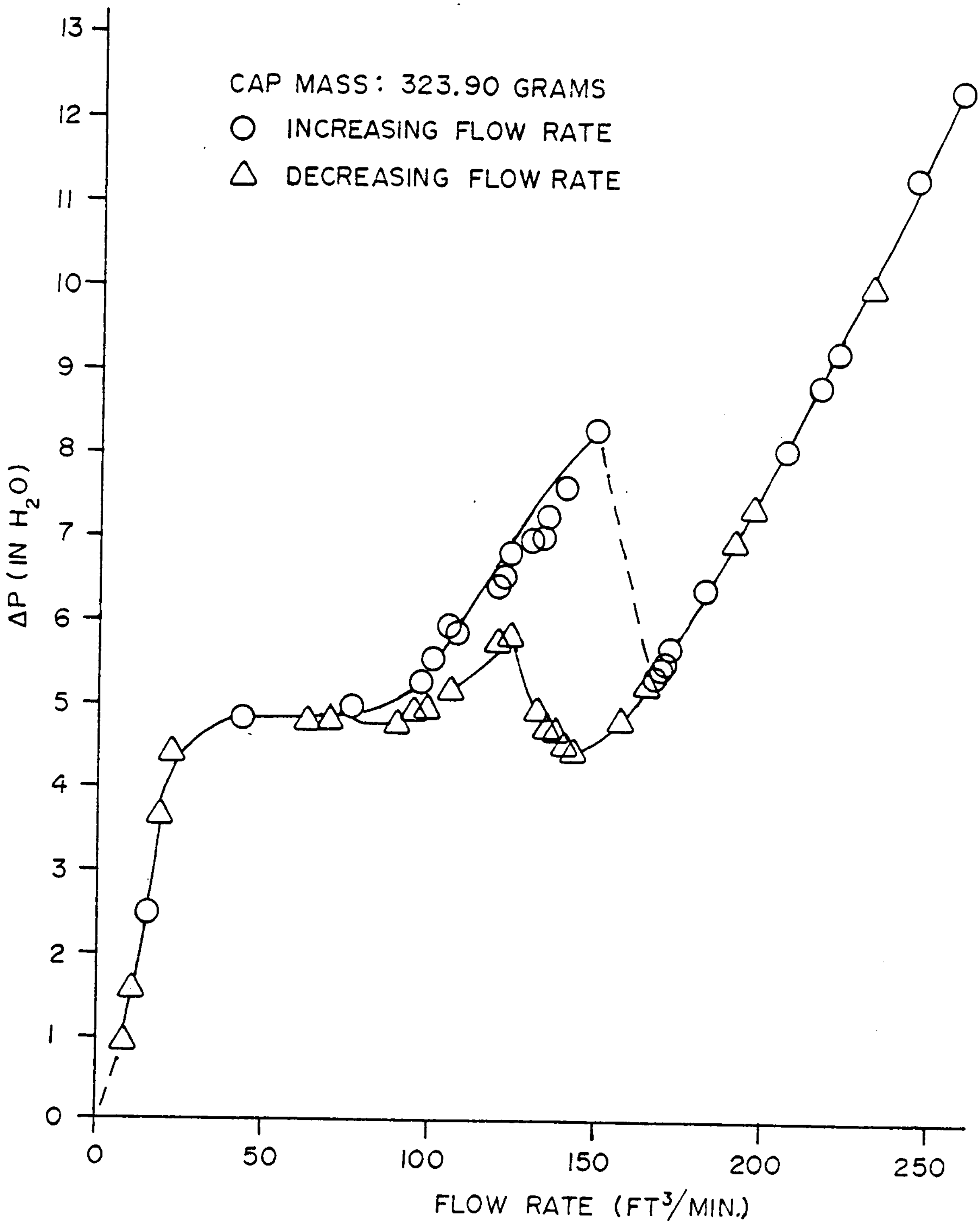

Figure 6.12. ΔP Versus Flow Rate for Flat Cap F2, 0.50 Inch Gap, 3 Inch Diameter Cage, Air Only.

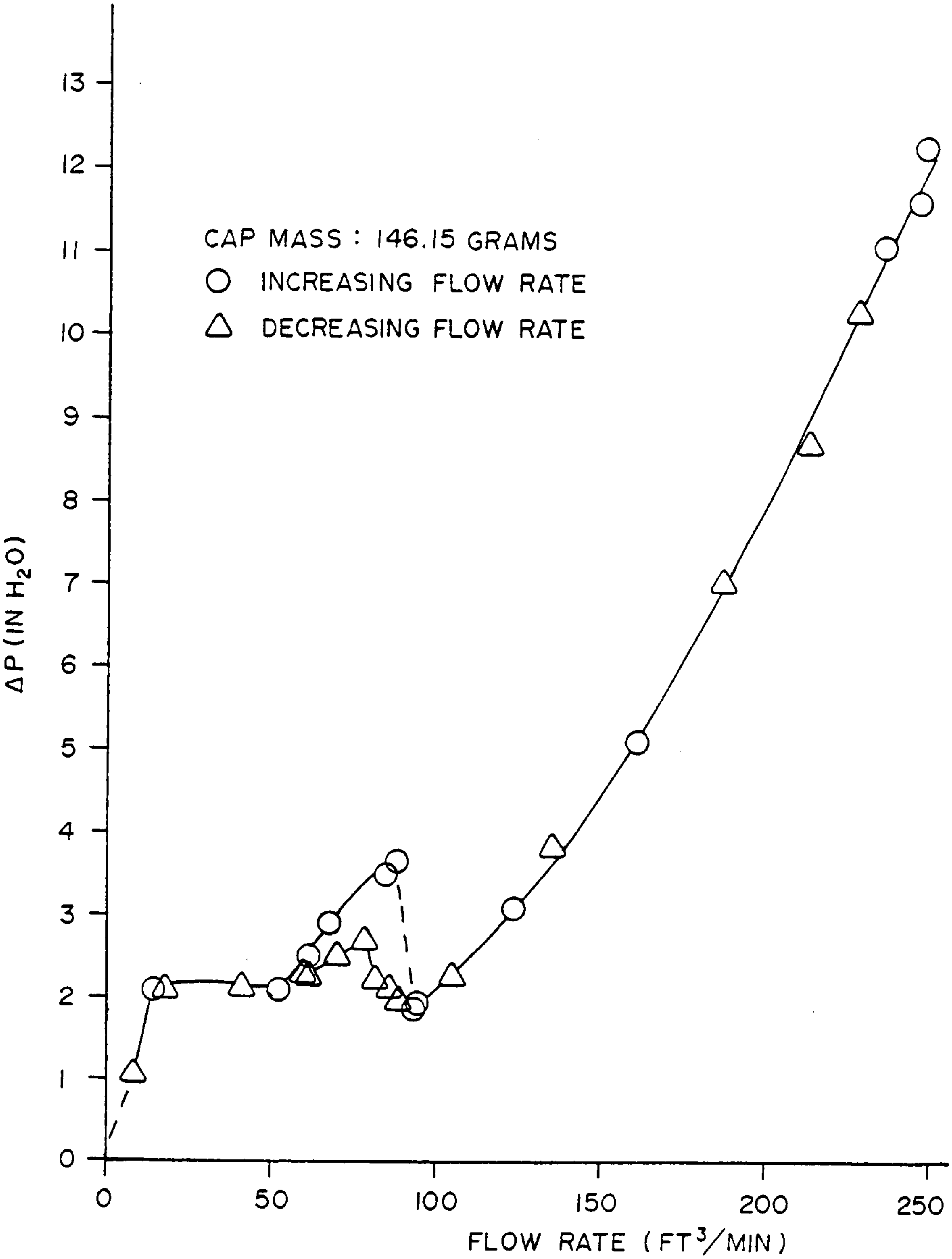

Figure 6.13. ΔP Versus Flow Rate for Flat Cap F3, 0.50 Inch Gap, 3 Inch Diameter Cage, Air Only.

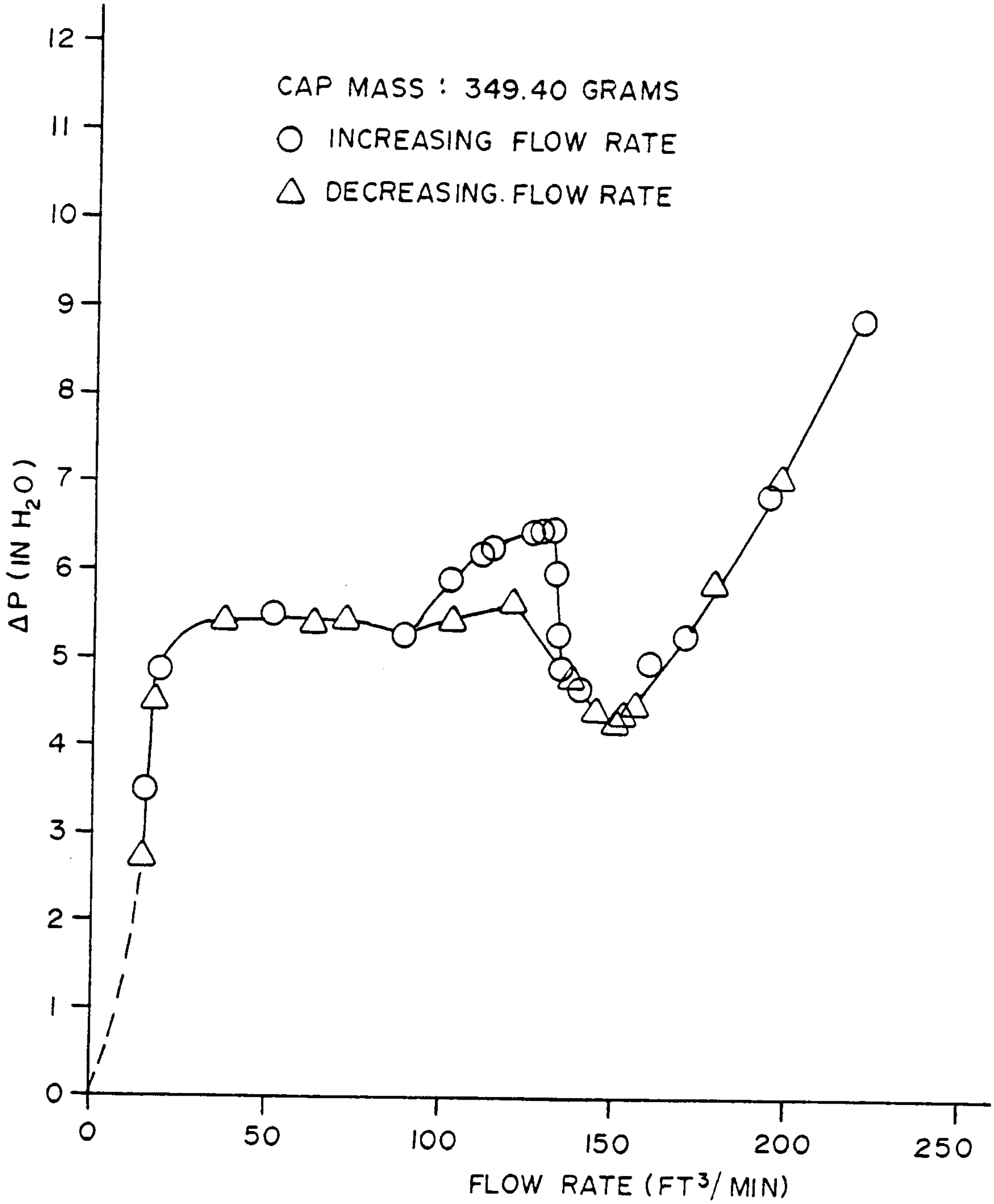

Figure 6.14. ΔP Versus Flow Rate for Recess Cap R1, 0.50 Inch Gap, 3 Inch Diameter Cage, Air Only.

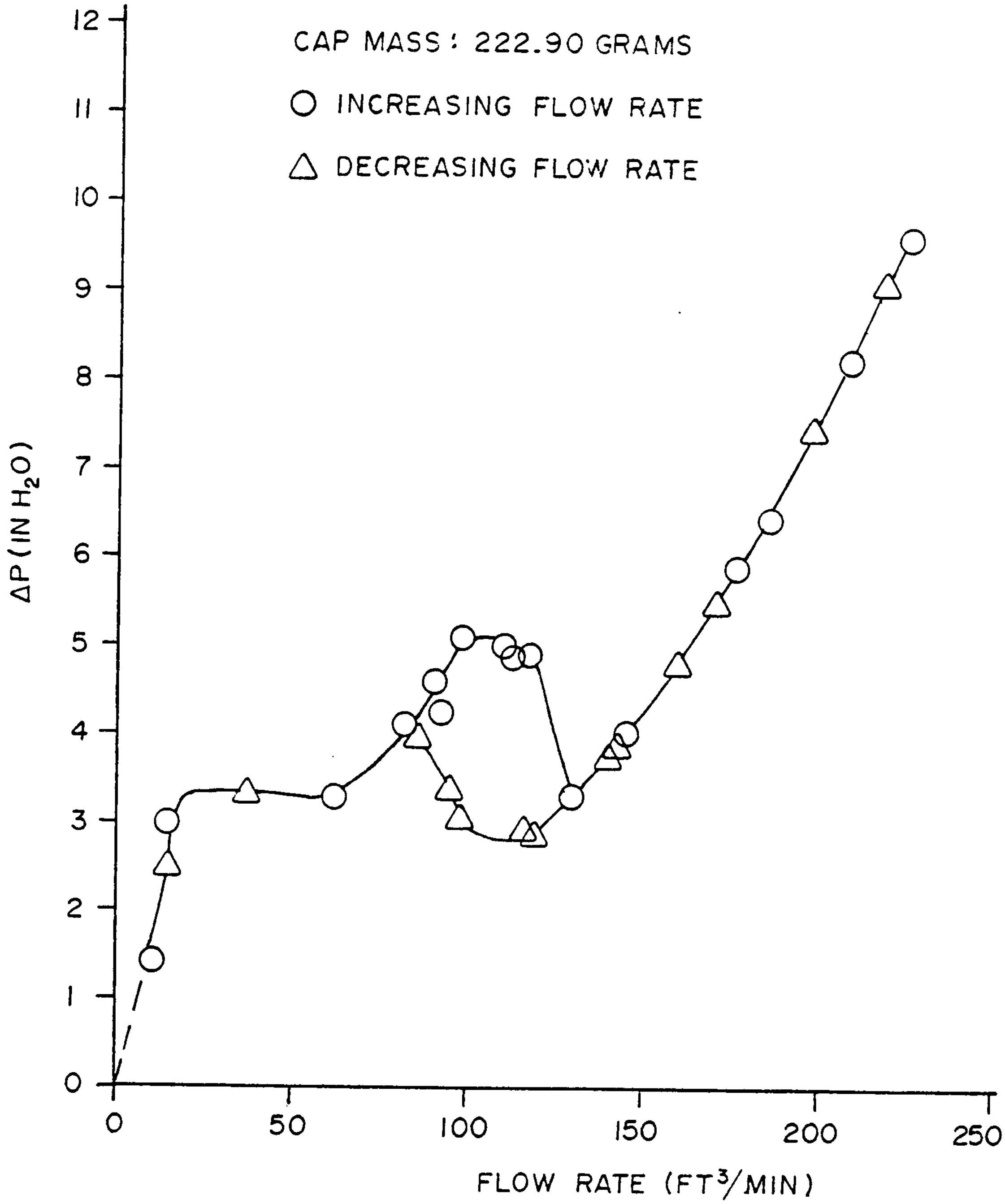

Figure 6.15. ΔP Versus Flow Rate for Recess Cap R2, 0.50 Inch Gap, 3 Inch Diameter Cage, Air Only.

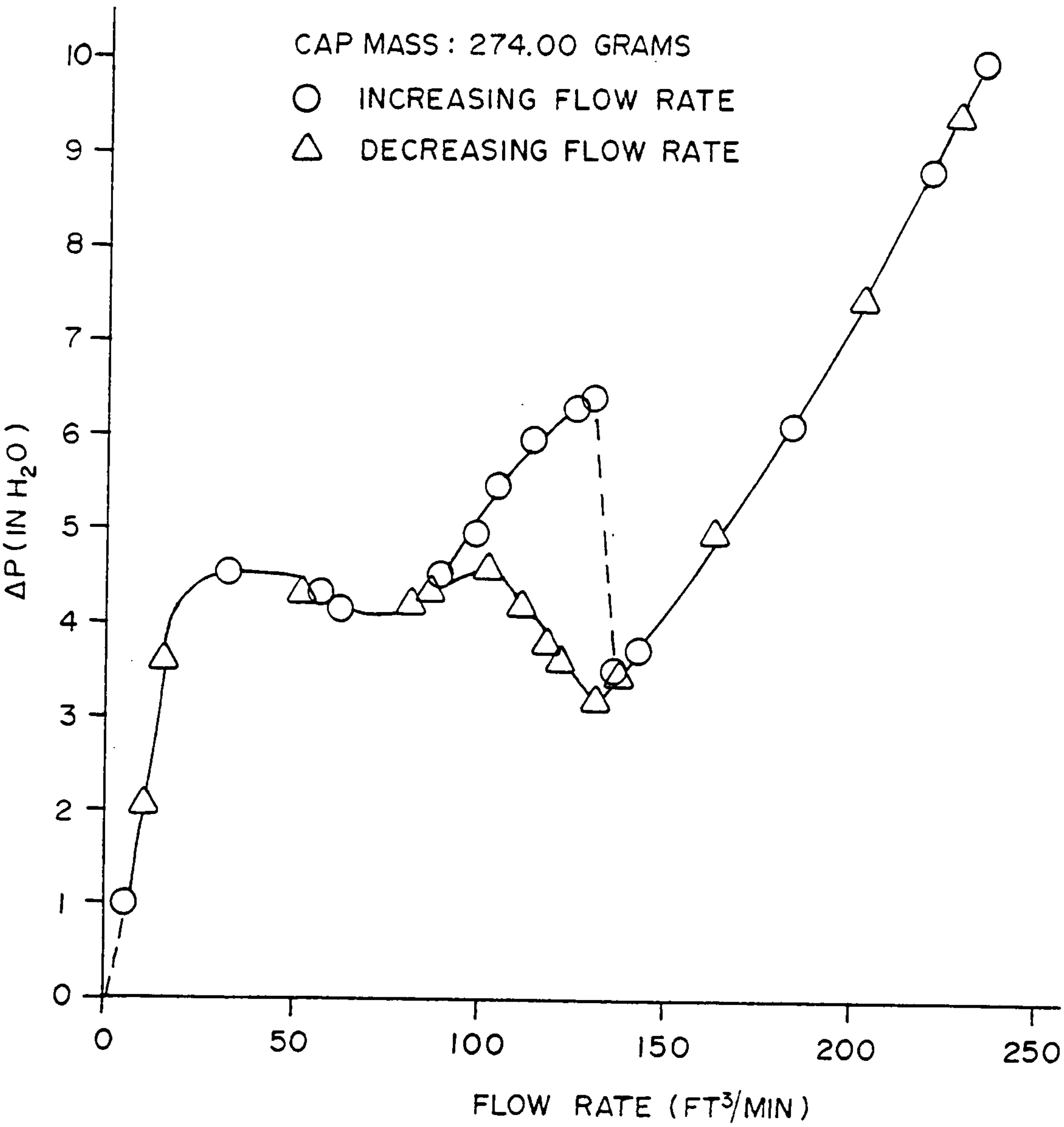

Figure 6.16. ΔP Versus Flow Rate for Recess Cap R3, 0.50 Inch Gap, 3 Inch Diameter Cage, Air Only.

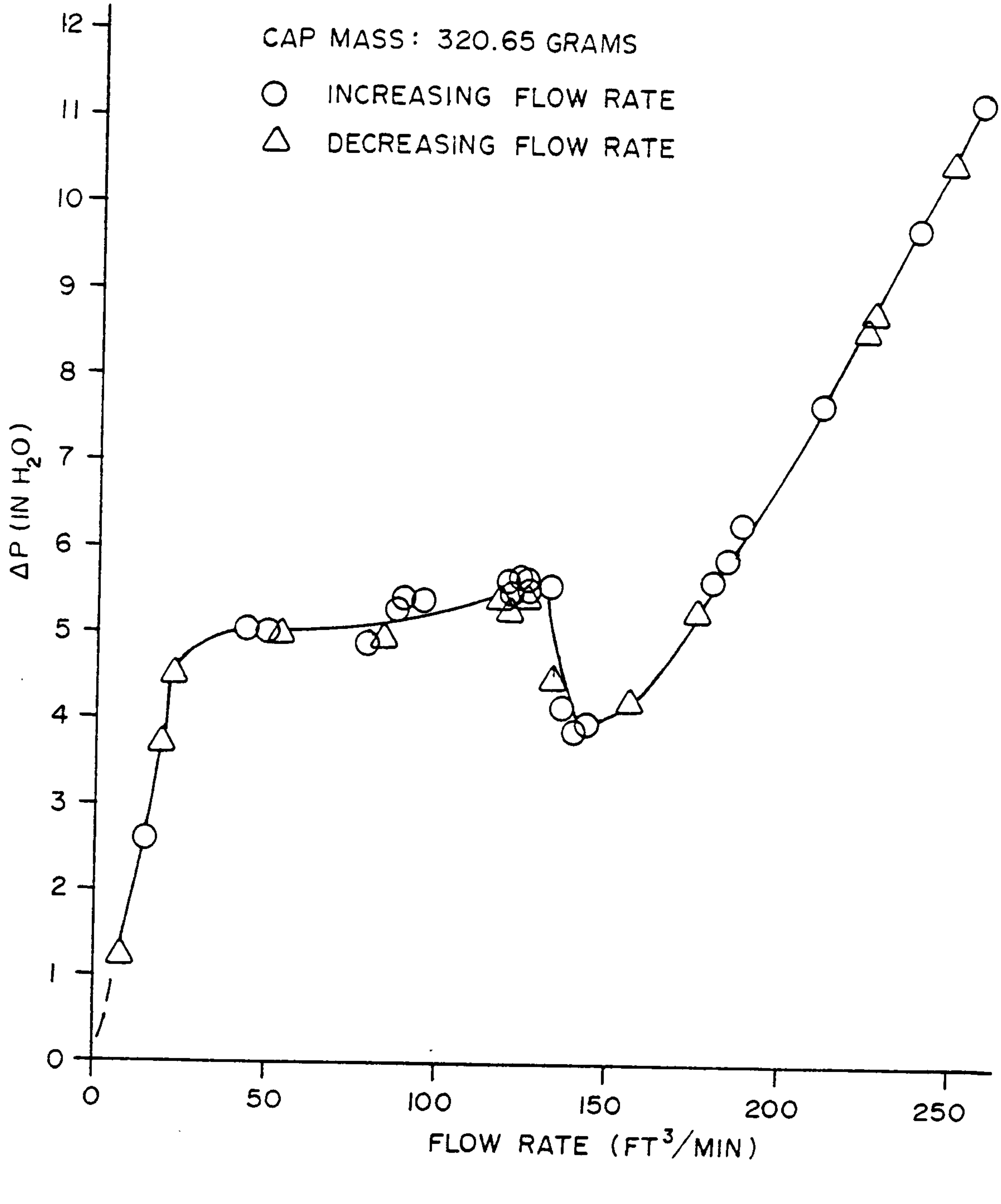

Figure 6.17. ΔP Versus Flow Rate for Recess Cap R4, 0.50 Inch Gap, 3 Inch Diameter Cage, Air Only.

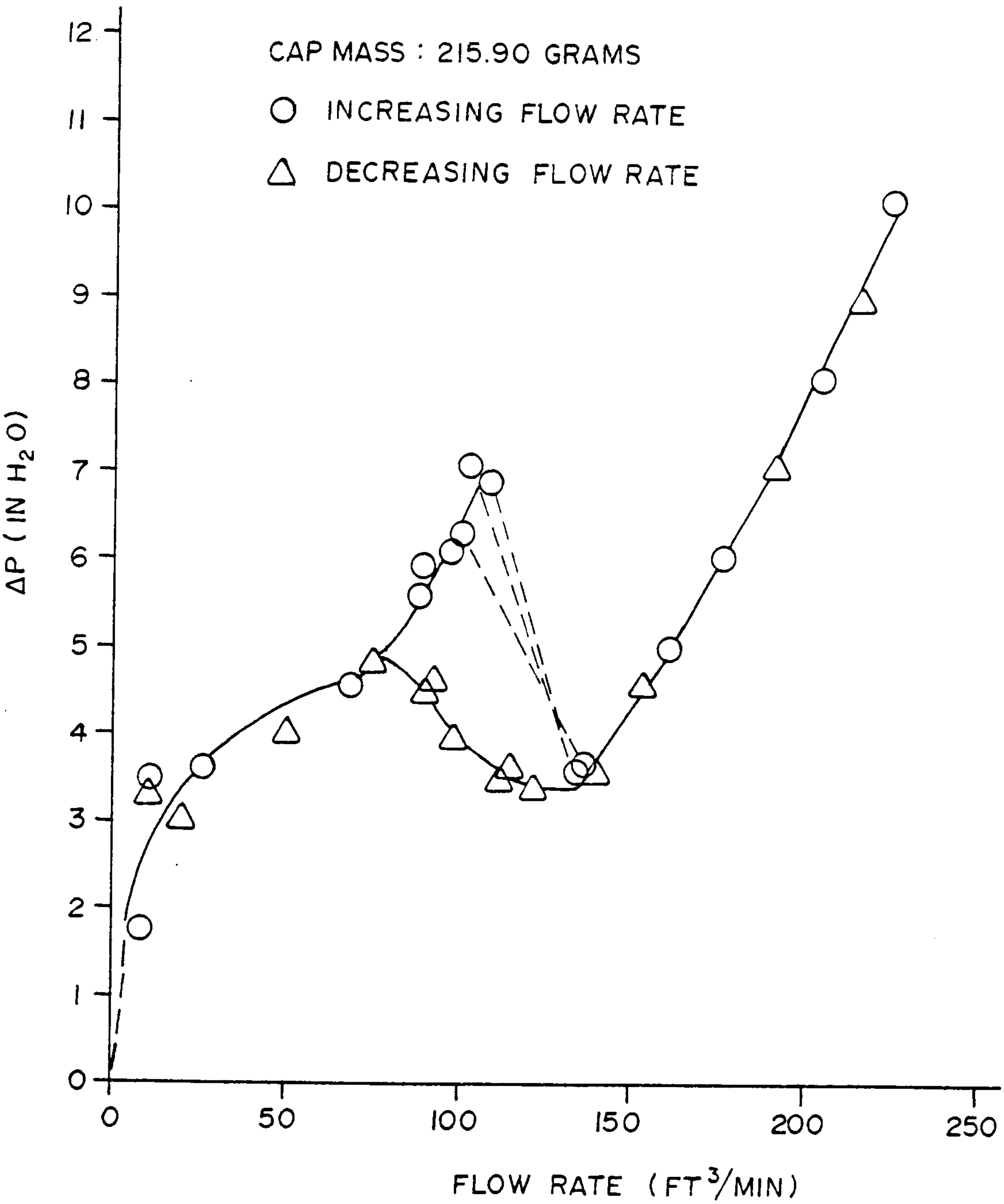

Figure 6.18. ΔP Versus Flow Rate for Convex Cap C1, 0.50 Inch Gap, 3 Inch Diameter Cage, Air Only.

of the pressure loss associated with this plateau is proportional to cap mass. Heavier caps plateau at higher values of ΔP. This is a result of the extra pressure force that is required to tilt a heavier cap. When flow rate is increased further, the pressure loss again begins to rise. The only exception to this is the recessed cap R4. This behavior will be explained later. This rising pressure loss is due to the down side of the cap rising off the feed pipe. The pressure loss versus flow rate curve eventually reaches a point where pressure loss drops drastically with a small increase in flow rate. This is indicative of the cap becoming fully opened. Once fully opened, the pressure loss varies with respect to flow rate as a power law function for all of the caps. The general form of the variation is shown in equation 6.18.

$$\Delta P = CQ^{x}. \tag{6.18}$$

The values of C and x for all of the caps are tabulated in Table 6.7. Geometrically similar caps (i.e., flat caps compared to flat caps) follow the exact same curve when fully open. This is because the mass of the cap does not affect flow rate once the cap is completely open. Although not readily evident from Table 6.7, the recessed caps had a lower pressure loss for a given fully open flow rate than did the flat caps. In fact, caps with deeper recesses, had lower pressure losses.

When the air flow rate was decreased, (data points indicated by triangular symbols) the pressure loss characteristic followed the fully open curve until the falling off point was reached. This is evidenced on the figures by the lowest point of the fully open curve. The flow rate corresponding to this point is the lowest possible flow rate that

TABLE 6.7

PRESSURE DROP VERSUS FLOW RATE EQUATIONS FOR
2.688 INCH DIAMETER CAPS AT 0.5 INCH GAP

General Equation: $\Delta P = CQ^x$
Units : $\Delta P \equiv$ in H_2O, $Q \equiv ft^3/min$
Conditions: T = 80° F, P = 14.3 psia

Cap Names	Recess (in.)	C X10^4	x	r^2
F1,F2,F3	0.0	3.106	1.91	0.998
R1,R2	0.25	2.855	1.92	0.995
R3	0.425	1.943	1.99	1.000
R4	0.55	2.251	1.95	0.998

These values obtained from power law curve fit program [16, p.98].

can support the cap in a fully open position. These flow rates are tabulated in Table 6.8. For geometrically similar caps, the flow rates are proportional to the square root of mass. Heavier caps require more air flow to remain fully open.

Momentum correction factor (K) is also calculated for each cap using the experimentally determined flow rate and mass in equation 6.8. These values for K are seen to be somewhat lower than the value for 3.5 inch diameter caps with 0.5 inch gap calculated from equation 6.9. This is because the larger diameter caps experienced a greater pressure force due to the pressure below the cap being exerted over a larger area.

As the flow rate is continually reduced, the pressure loss increases sharply from the minimum value to the plateau, where the cap is now tilting with one edge touching the cage and the opposite edge resting upon the feed pipe. The closing cycle now follows the same path as the opening pressure loss cycle.

All of the cycles (except cap R4) displayed the same hysteresis characteristic. That is, more flow was required to fully open the cap than was needed to support it after it became fully opened. This hysteresis can be explained with the aid of Figure 6.19.

In the top portion of Figure 6.19, the schematic cap is rising. The important forces influencing hysteresis are the friction force due to the cage, the cap weight and the air force. As the cap rises, the friction force opposes the force applied by the flowing air. For the falling cap, illustrated by the bottom part of the Figure 6.19, the friction force acts to aid the air force. This difference is believed to cause the hysteresis. The air force required to lift the cap must

TABLE 6.8

MINIMUM FLOW RATES REQUIRED TO SUPPORT FULLY OPEN 2.688 INCH DIAMETER VALVE CAPS AT 0.50 INCH GAP

Cap Name	1 Mass (Grams)	2 Fully Open Flow Rate From Experiment (S.C.F.M.)	Momentum Correction Factor K*
F1	531.40	180.0	1.24
F2	323.90	142.0	1.22
F3	146.15	93.0	1.28
R1	349.40	150.0	1.18
R2	222.90	115.0	1.28
R3	274.00	130.0	1.23
R4	320.65	143.0	1.19
C1	215.90	135.0	0.90

*Calculated from 1 and 2 with equation 6.8.

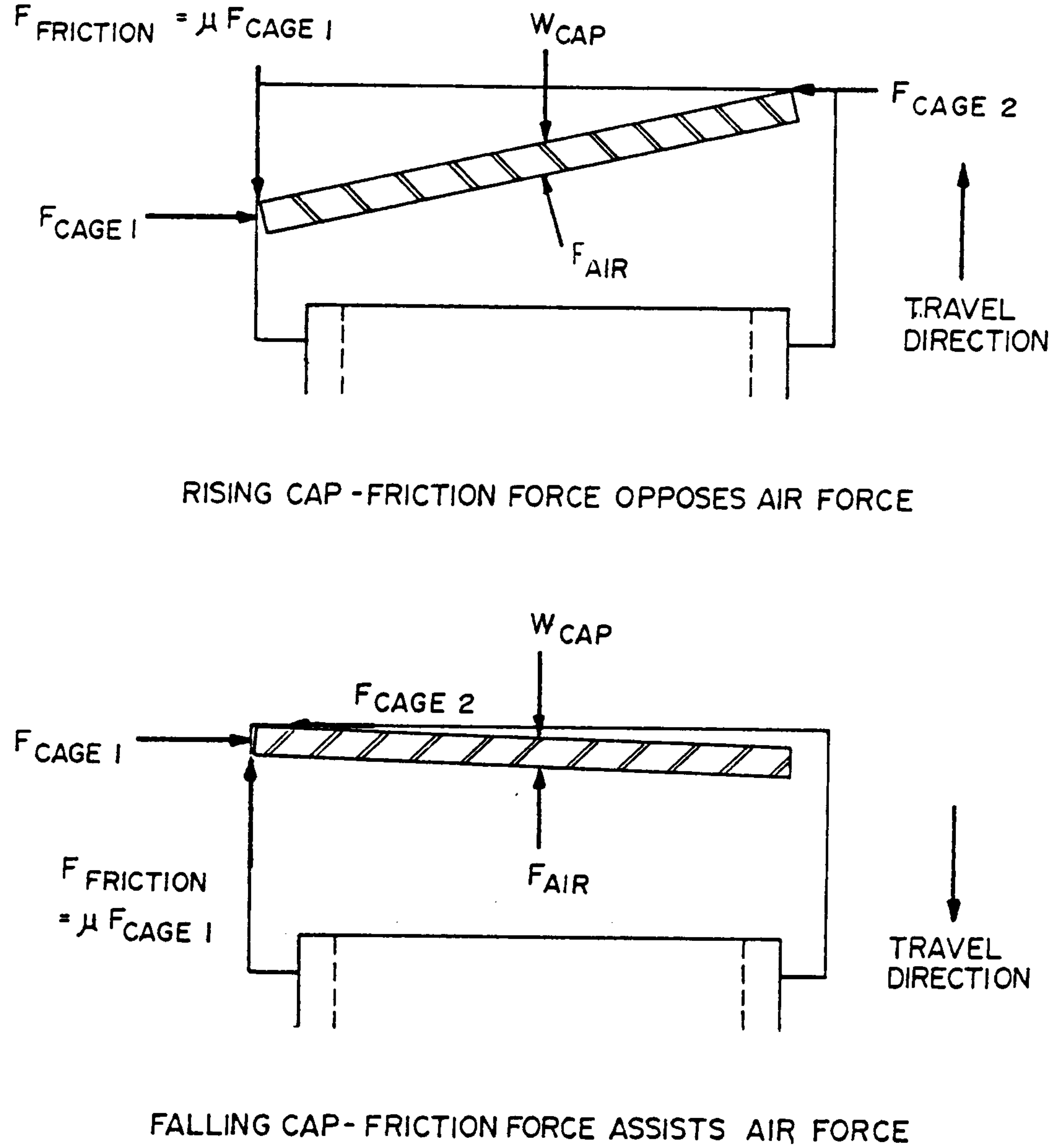

Figure 6.19. Forces on a Valve Cap Involved with Hysteresis.

overcome friction, whereas, the air force required to support a fully open cap is assisted by the cage friction.

Figure 6.17, page 61, for the deep recessed cap, R4, shows no hysteresis. This can be explained by referring to Figure 6.20. The air striking a flat cap can smoothly flow by as shown in the top part of the figure, however, air striking the deep recessed cap must flow around the recess wall. This imparts an additional force to the cap and aids in lifting. The removal of hysteresis by the deep recess is noteworthy, but should not, in itself, be considered an important aspect of cap design.

Three of the caps were tested at 0.75 inch gap: flat cap F2 and recessed caps R1 and R2. The results of these air tests are presented in Figures 6.21 through 6.23 and Tables 6.9 and 6.10. Several ideas can be discussed using these results.

The plateau, where the cap is tilting, is not affected by this change in gap. It is primarily a function of cap mass. This is evident from comparing Figure 6.12, page 56, and Figure 6.21.

Figure 6.22 shows that recess cap R1 does not experience any hysteresis at 0.75 inch gap. This is in contrast to its behavior at 0.50 inch gap illustrated in Figure 6.16 on page 60. The reason this cap shows no hysteresis at the 0.75 inch gap and does at 0.50 inch gap is because the recess is more able to deflect the flow at this gap as compared to the smaller gap.

Table 6.9 lists the coefficients and the exponents for the fully open curve fits. Again, geometrically similar caps show the same fully open pressure loss characteristic. The fully open pressure loss versus

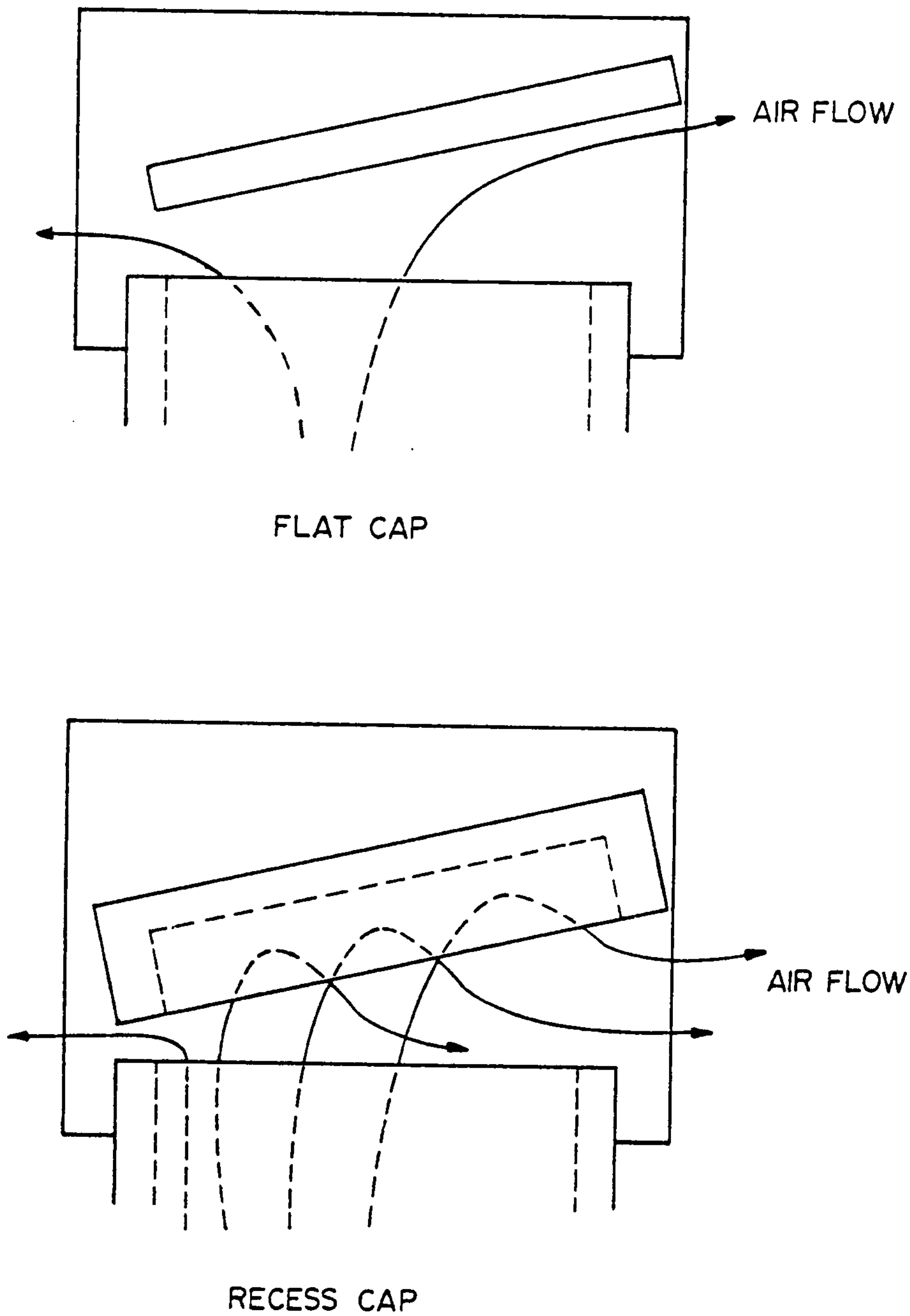

Figure 6.20. Comparison of Air Flow for Flat Cap and Recessed Cap.

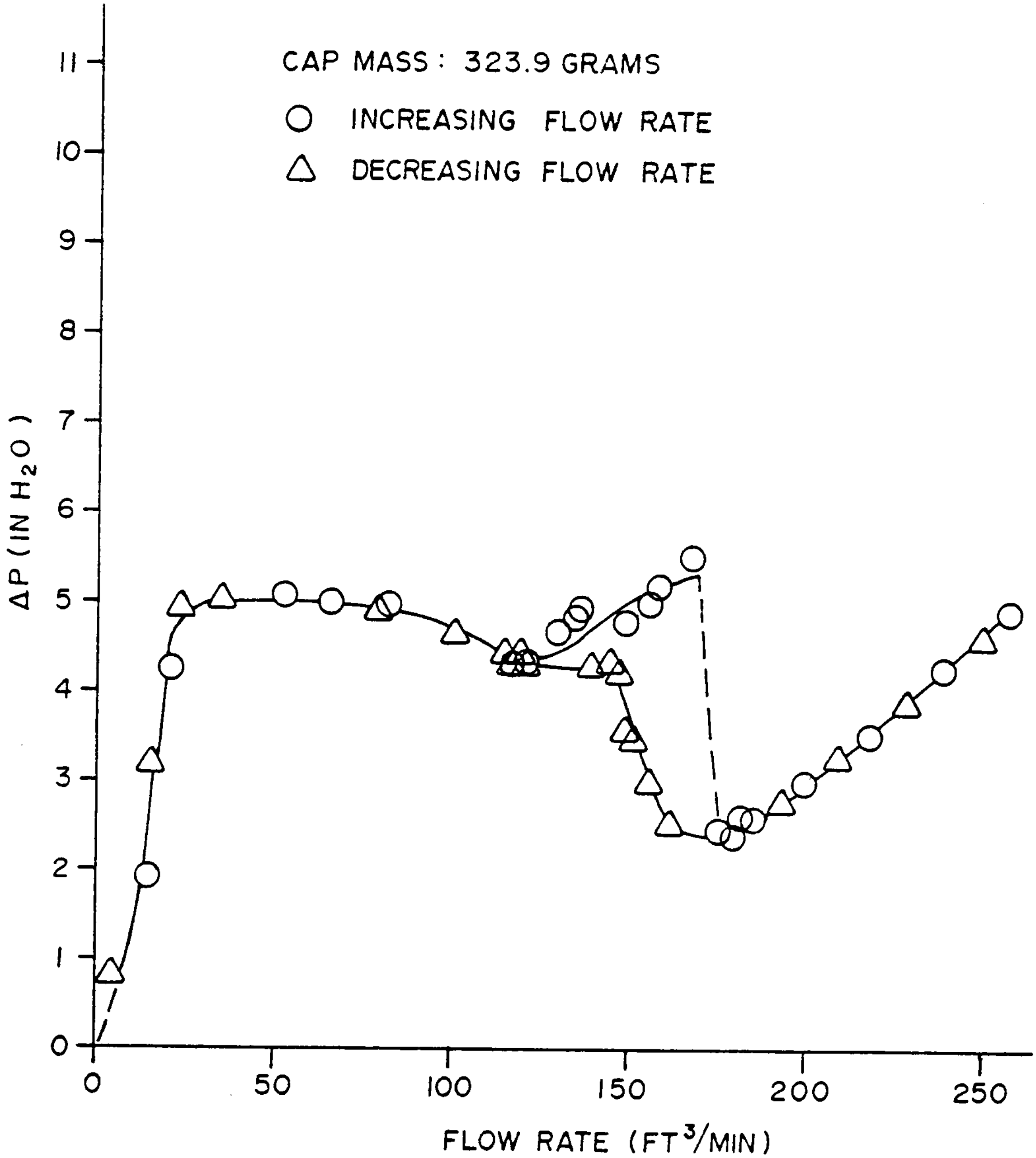

Figure 6.21. ΔP Versus Flow Rate for Flat Cap F2, 0.75 Inch Gap, 3 inch Diameter Cage, Air Only.

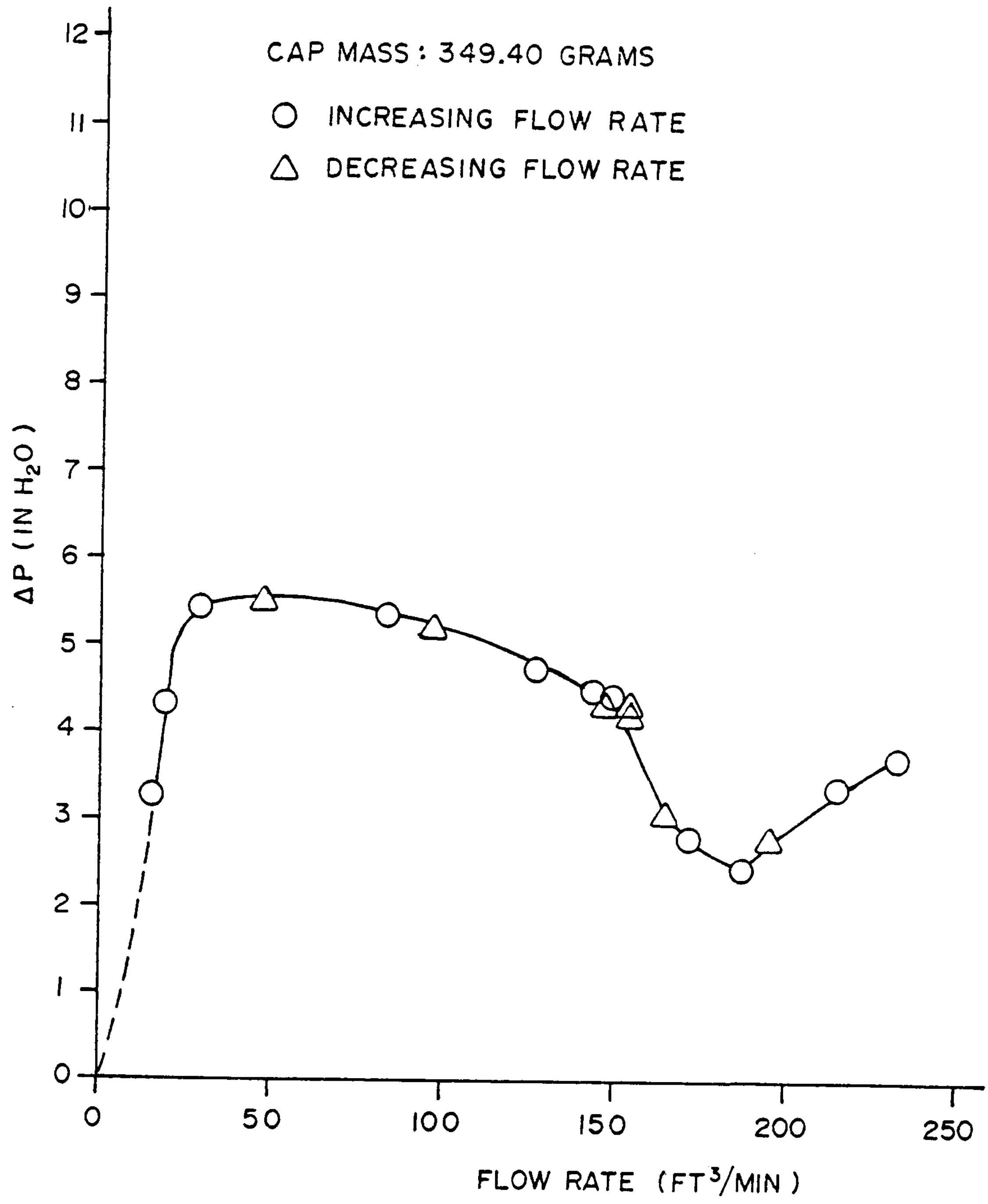

Figure 6.22. ΔP Versus Flow Rate for Recess Cap R1, 0.75 Inch Gap, 3 Inch Diameter Cage, Air Only.

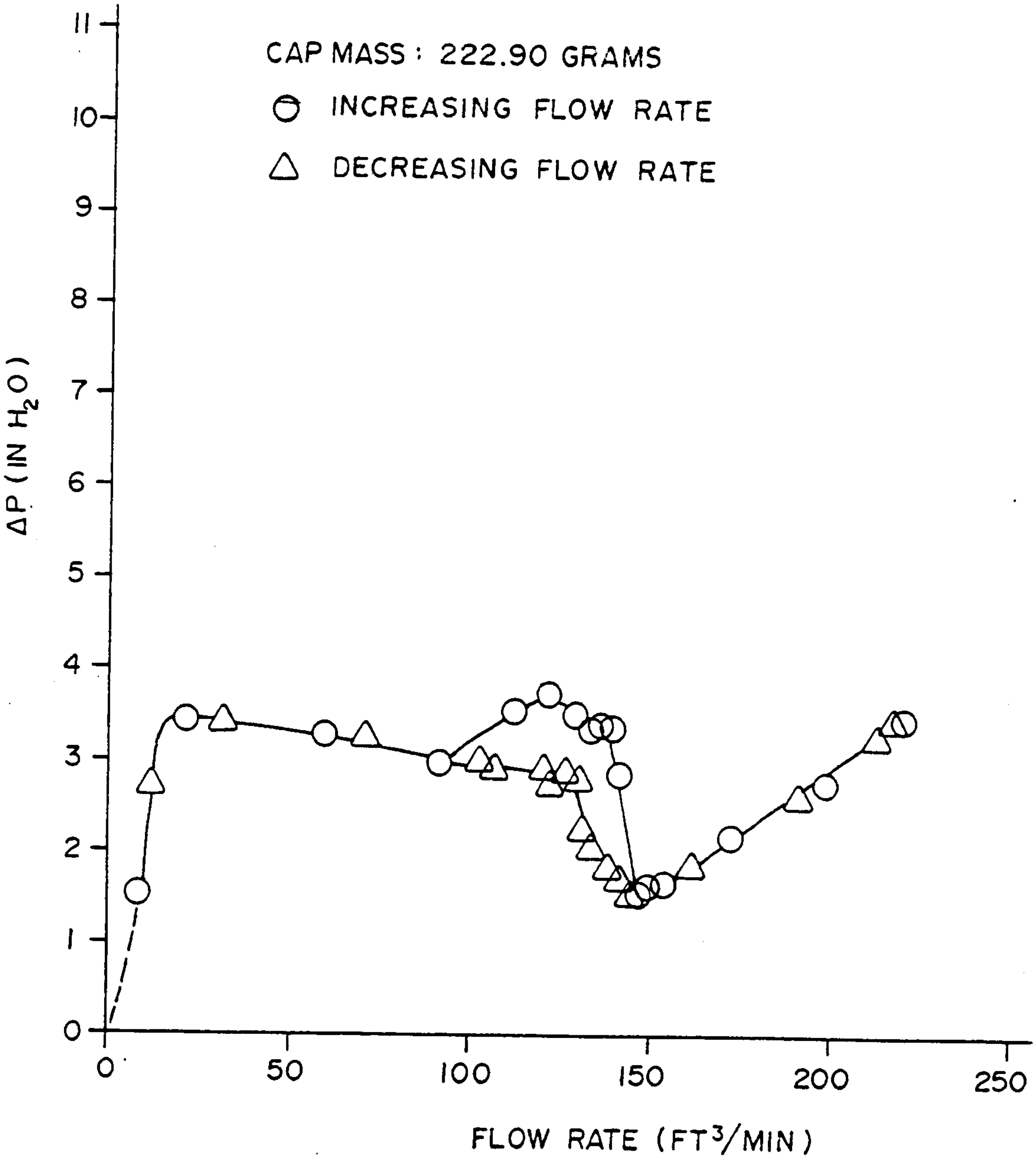

Figure 6.23. ΔP Versus Flow Rate for Recess Cap R2, 0.75 Inch Gap, 3 Inch Diameter Cage, Air Only.

TABLE 6.9

PRESSURE DROP VERSUS FLOW RATE EQUATIONS FOR 2.688 INCH DIAMETER VALVE CAPS AT 0.75 INCH GAP

General Equation: $\Delta P = CQ^x$
Units : $\Delta P \equiv$ in H_2O, $Q \equiv ft^3/min$
Conditions: $T = 80°F$, $P = 14.3$ psia

Cap Names	Recess (in.)	C $X10^4$	x	r^2
F2	0, Flat	1.388	1.89	0.992
R1,R2	0.25	0.724	2.00	0.996

These values obtained from power law curve fit program [16, p.98].

TABLE 6.10

MINIMUM FLOW RATES REQUIRED TO SUPPORT FULLY OPEN
2.688 INCH DIAMETER VALVE CAPS AT 0.75 INCH GAP

Cap Name	1 Mass (Grams)	2 Fully Open Flow Rate From Experiment (S.C.F.M.)	Momentum Correction Factor K*
F2	323.90	175.0	0.80
R1	349.40	187.5	0.75
R2	222.90	147.0	0.78

*Calculated from 1 and 2 with equation 6.8.

flow rate curve for either the flat cap or the recessed caps at a 0.75 inch gap is lower than the fully open pressure loss versus flow rate curve for the comparable cap at 0.50 inch gap. The larger free travel helps to lessen the resistance to flow.

Table 6.10 presents the minimum flow rate required to support each cap in a fully open position. Momentum correction factors for these caps as determined from equation 6.8 are also listed. Comparing values for minimum flow rate listed in Table 6.10 to those listed in Table 6.8, page 66, for similar caps, reveals that more air is required to support a fully open cap at 0.75 inch gap than is required at 0.50 inch gap. This is because the air can more easily pass around the caps when they are at a 0.75 inch gap thus reducing the pressure beneath the caps. The greater flow rate also causes smaller momentum correction factors to be calculated for the 0.75 inch gaps. This trend is evidenced by the convex cap. The caps' aerodynamic shape allowed the air to flow around it with less resistance, consequently, giving a lower value of momentum correction factor K (see Table 6.8, page 66).

Air only tests — discussion

The air only tests were performed in a careful manner to insure that steady-state was achieved. The air flow was allowed to reach equilibrium at every point. The caps were raised and lowered slowly and numerous data points were recorded. Several up and down cycles were done and the results were highly repeatable.

The caps' free travel was set with steel bars having thicknesses equal to the desired gaps. The gaps were checked in eight locations with precision calipers and 0.031 inches was the maximum allowable error. This error was always positive; in other words, the gap was no more than 0.031 inches larger than desired. There was no possible way in which the gap could be smaller than the desired height.

The results of these tests can be utilized to compare the relative performance of various caps. Opening, closing and operating characteristics can be discerned from these tests. Effects of cap design, mass and cage design can be determined. These tests are quick, easy and relatively simple to interpret.

The two shortcomings of these tests are that the caps are opened slowly and that no limestone was present in the bed. The data were not intended to model these conditions; this was left for the following test series.

Air only dynamic tests — introduction

Air only dynamic tests were performed on some of the caps to determine their behavior when operated in a dynamic mode (i.e., opened and shut quickly). Data were taken with a strip chart recorder and several cycles were performed.

Air only dynamic tests — results

When the caps were opened quickly (on the order of 2 seconds), they did not generally follow the steady-state air only curves because of the time lag of the experimental system, however, when the flow reached equilibrium, the equilibrium point would always lie on the steady-state air only test curves.

When the caps were closed quickly, the flow would fall to zero and the pressure would drop shortly thereafter.

If the caps were opened and closed faster than the air only tests, but not as fast as above (on the order of 10 seconds), the pressure loss versus flow rate curves would show the same shape as the steady-state air only tests, but the curve would be displaced. The pressure loss was somewhat lower because of the system time lag. Hysteresis was still present and the final equilibrium pressure loss-flow rate operating point would always lie on the steady-state air only test line.

Air only dynamic tests—discussion

The air only dynamic tests simply illustrate the fact that the caps will operate somewhere along their steady-state air only test curves regardless of their previous flow history.

This type of test shows that hysteresis should not be of any concern to the actual cap operation. If the caps are opened rapidly, then the hysteresis would not hinder the cap opening.

Coal and air tests—introduction

Tests were performed with various caps at 0.5 inch gap employing coal and air flow only. Different coal mass flow rates varying from 17.5 pounds per minute to 35.0 pounds per minute were used. These values were picked because they correspond to approximately 2.5 and 5.0 pounds of coal per pound of air respectively for the flow conditions of Chapter 3. It was felt that this was a representative range of ratios for a fluidized bed combustion unit based on one feed point per nine square feet of bed area. Pressure loss versus flow rate data were obtained along with basic observations.

Coal and air tests—results

Observations of the caps illustrated several points.

1. A tilted cap dumps most of the coal to its open side. This is highly undesirable and should be avoided under all circumstances. Uneven coal distribution such as this leads to poor sulfur capture, high carbon monoxide emissions and poor combustion.
2. The flat caps, when fully open, are always offset from the pipe centerline. This is because of the way the caps tilt upon opening. The deflecting air produces a force on the tilting cap driving it offcenter and against the cage supports. This offset causes some maldistribution of coal, slightly more being fed to the side away from this offset (i.e., if the cap is against the cage bars on the right side, more coal is fed to the left side). The different amount of coal was not enough to create concern especially when one considers that the cap will probably change offset positions while operating in a limestone bed because of the forces exerted on the cap by the fluctuating bed. The convex cap did not exhibit the "maldistribution of coal" characteristic. Regardless of the offset direction, coal was always distributed equally. This is a point in favor of the convex cap.
3. The recess which was cut into the flat caps did not affect coal distribution. The recess caps behaved exactly as the flat caps during coal feeding distributing slightly more coal to the side opposite the offset.

The pressure loss versus flow rate curve for the 0.45 inch thick flat cap, F2, at 0.50 inch gap is shown in Figure 6.24 for a coal mass flow rate of 17.5 pounds per minute. This is compared to the air only curve.

The additional momentum supplied by the coal reduces the air flow required to keep the cap fully open from 142 cubic feet per minute to 118 cubic feet per minute. At this flow, the weight of the cap is given by equation 6.19.

$$w_{Total} = w_{Air\ Only} + w_{Solids\ Only} = \frac{\dot{m}_{Air}\ V_{Air}}{g_c}\ (K+JS). \qquad (6.19)$$

The symbols in this equation are defined in the discussion covering its development.

For $80^{o}F$ and 14.3 psia, the product of mass flow rate and velocity divided by g_c is 0.405 lbf. The cap weight is 0.714 lbf thus (K+JS) is equal to 1.765. From Table 6.8, page 66, K is equal to 1.22. The coal mass flow rate to air mass flow rate ratio, J, at these conditions was 2.018. These values allow the coal slip velocity, S, to be determined as 0.27. This value of S is lower than values typically found in literature which are around 0.80 [17]. This suggests further investigation is needed in this area.

The presence of the coal shifts the fully open curve about 20 cfm. At a given flow rate, the coal plus air pressure loss is larger than the air only pressure loss for a fully open cap. This is because the coal restricts the air passageway, in effect decreasing the gap. The increase is about 20 percent at these conditions.

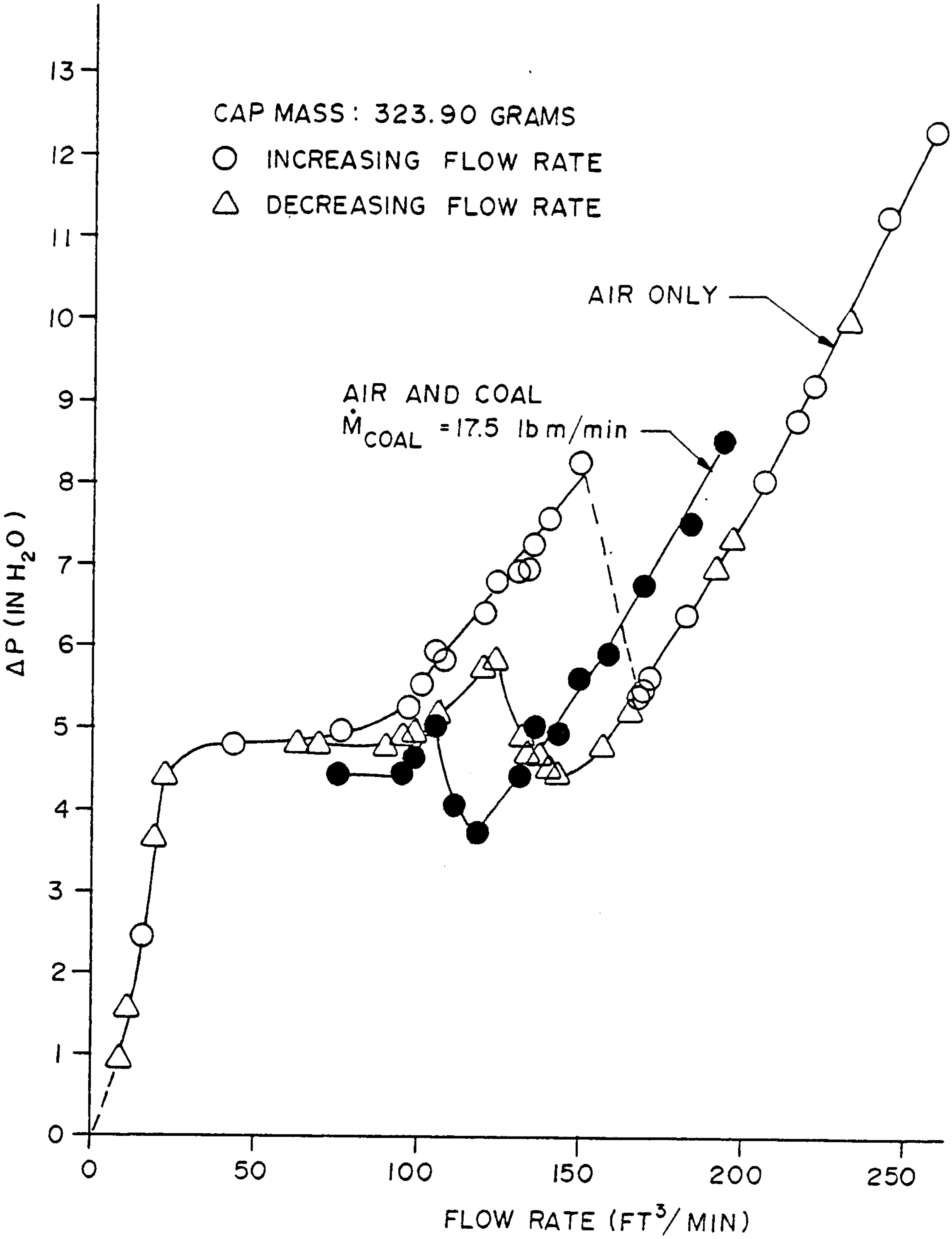

Figure 6.24. ΔP Versus Flow Rate for Flat Cap F2, 0.50 Inch Gap, 3 Inch Diameter Cage, Air Only and Air Plus Coal.

Only one mass flow rate of coal was presented of the five flow rates tested between 17.5 and 35.0 pounds per minute, because over the test range the mass flow rate did not appreciably affect the pressure loss curve.

Coal and air tests—discussion

The added momentum of the coal flow is significant enough to consider in a cap design. The conservative designer, however, should design a cap to open with air flow only and have the coal flow be an added margin of safety.

The increased pressure loss due to the presence of the coal should not significantly affect the system performance.

Limestone tests—introduction

The valve caps were tested in the fluidized bed test facility with various depths of limestone ranging from 6 inches to 26 inches when slumped. The caps were opened and shut, slowly and rapidly, in a cyclic fashion. Pressure loss versus flow rate data were obtained using a strip chart recorder.

Limestone tests—results

Different valve caps were cycled well over 100 times and no hangups occurred with this geometrical configuration; 3.0 inch inside diameter cage and 2.688 inch outside diameter cap. The three inch inside diameter cage was chosen on the following design basis. The clearance between the cage inside diameter should be at least 1.25 times the largest possible bed particle to avoid hangup. Three inches equals 2.688 inches plus the product of 1.25 and the size of the largest bed particle (0.25 inch).

The valve caps worked very well in preventing drainback. No bed material ever entered the feed line when the transport air was stopped.

When the cap was opened in the limestone, the equilibrium pressure-loss flow rate point did not lie on the air only graph. The pressure loss was much greater at a given flow rate. When comparisons were made with flat plate data (see Appendix B), the cap was found to have a 0.25 inch gap instead of the 0.50 inch gap that was set. This was caused by limestone being trapped between the cap and cage, thus reducing the operating gap. The cage design used was conducive to entrapping bed material because the top was made of 0.50 inch wide cross bars. (This cage top was bolted, instead of welded, to the vertical supports.) See Figure 6.25. To facilitate opening, the cage was redesigned as shown in Figure 6.26 to reduce the contact area between the cap and cage. This is not the only working design, but was simple to build and install. This design was tested in limestone and worked well. The operating point fell almost on the air only test line indicating that only very small limestone particles were trapped between the cap and cage. The point to remember when designing a cage is to minimize the contact area between the cage and cap. Sharp edges, instead of blunt, are very effective for moving limestone from between the cap and cage.

Another notable result of the limestone tests was that the rising hysteresis in the pressure loss versus flow rate curve was effectively eliminated.

The hysteresis was eliminated because the valve cap did not have to wait for the pressure to build up. The control valve was opened

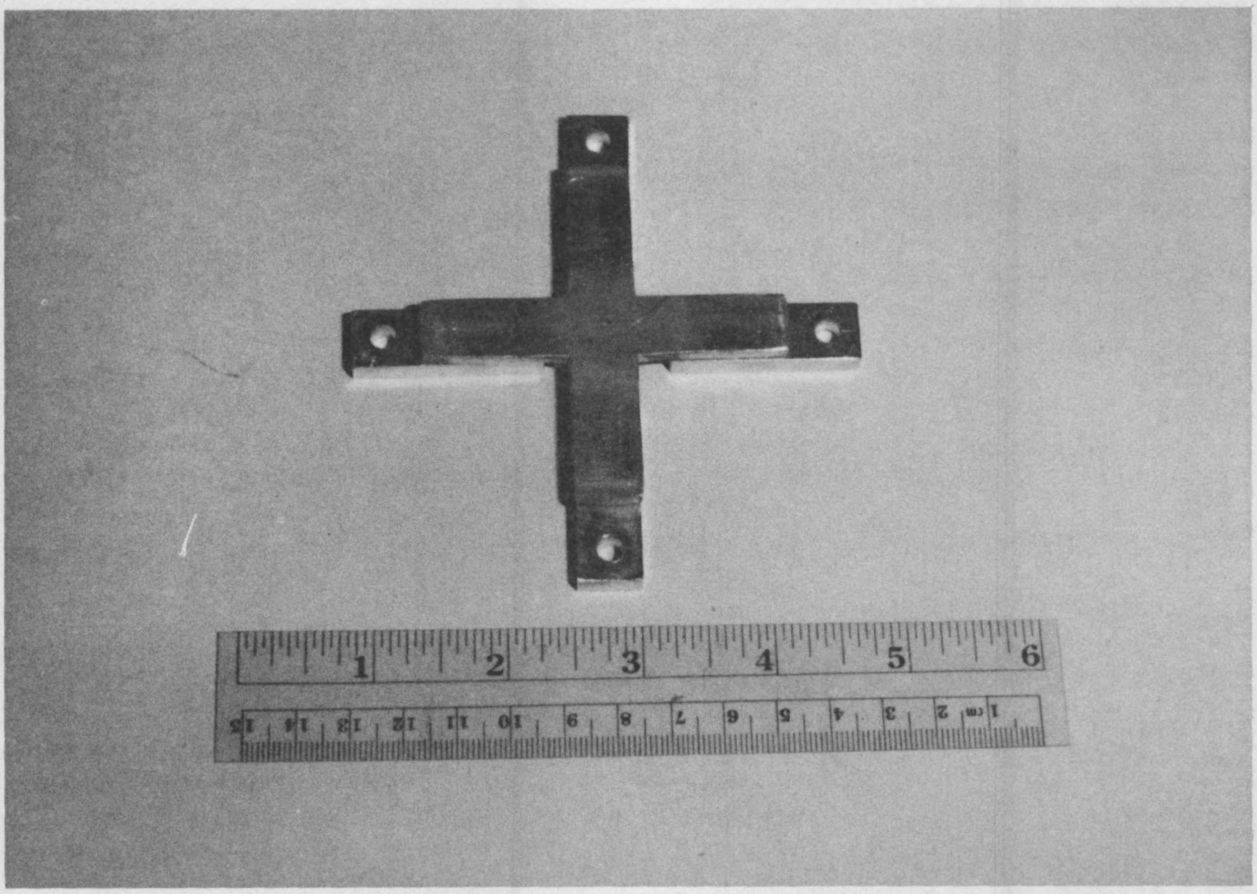

Figure 6.25. Original Cage Top.

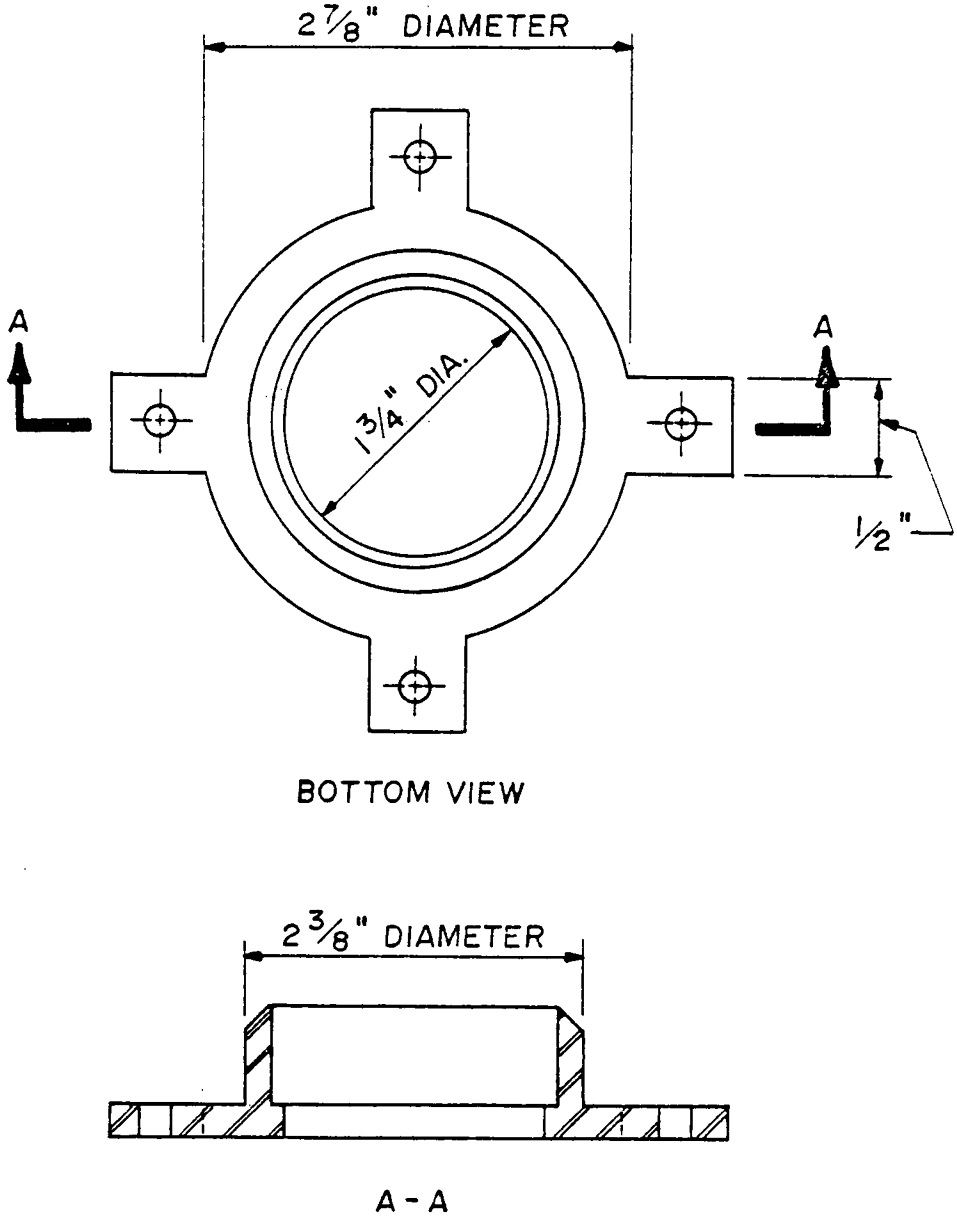

Figure 6.26. Redesigned Cage Top.

quickly enough so that the pressure below the cap was almost instantaneously above that required for opening. The cap was "blown" open.

Limestone tests—discussion

The valve cap operates in limestone at equilibrium along the air only curve. The valve cap is very effective for preventing bed drainback. It was also very reliable, not hanging up in well over 100 cycles.

Hysteresis is removed with rapid operation., The only other operational difference between air only and limestone operation is an occasional pressure pulse that travels down the feed line due to a bed pressure fluctuation.

Coal feed tests—introduction

The coal feed tests are actual models of the coal feeding process in a fluidized bed. Coal was introduced into the fluidized bed through the coal feed system and bed samples were taken with the sample probes. The samples were analyzed for the coal mass present as a result of the feed system.

The analysis produced a map of the bed illustrating where coal rich or lean areas existed. (The tests are described in more detail in Chapter 5 and the analysis in Appendix C).

The coal mass flow rate was always set at 25 pounds per minute. This was picked because it corresponds to the requirements set in Chapter 3.

Two cap gaps were studied as well as two different caps. The gaps were 0.50 inches and 0.75 inches and the two caps were the 0.45 inch thick flat cap (F2) and the 0.75 inch thick, 0.55 inch recessed cap (R4).

Two different sample times were tried to investigate mixing in the fluidized bed and to determine what sampling time was truly representative. The samples were taken for 10 seconds at 20 seconds and 50 seconds into the feed. The samples of coal averaged about 75 grams and typically ranged from 60 to 90 grams. Sometimes a bubble would be passing by as the probe was closed and the sample mass might be as low as 30 grams. The sampling volume of the probes was 3.32 cubic inches.

Coal feed tests—results

The first tests presented are those used to determine the amount of coal present in the bed due to the less than 100 percent efficient recycle. This coal was referred to as background coal and the concentration was determined to be constant for each test and over the entire bed.

The data for one of the two background tests are shown in Figure 6.27. The data for all of the coal feed tests are presented in this same format and its explanation follows. The map shows the exact location of the sample port in the bed. The number to the right of the slash is the corrected coal mass to limestone mass percent ratio calculated as described in Appendix C ($\bar{R}^*$ is the average of the value and σ is the standard deviation of this set). The term "corrected" is used to denote that the coal mass has had the background coal mass removed. This means the coal mass reflects only the coal present as a consequence of feeding. The number to the left of the slash is the corrected coal mass to limestone mass ratio at this location compared to the bed average coal mass to limestone mass ratio on a percentage basis. This is also discussed in Appendix C and will be called the comparison percent ratio to denote that it is a comparison to the bed average ratio as a

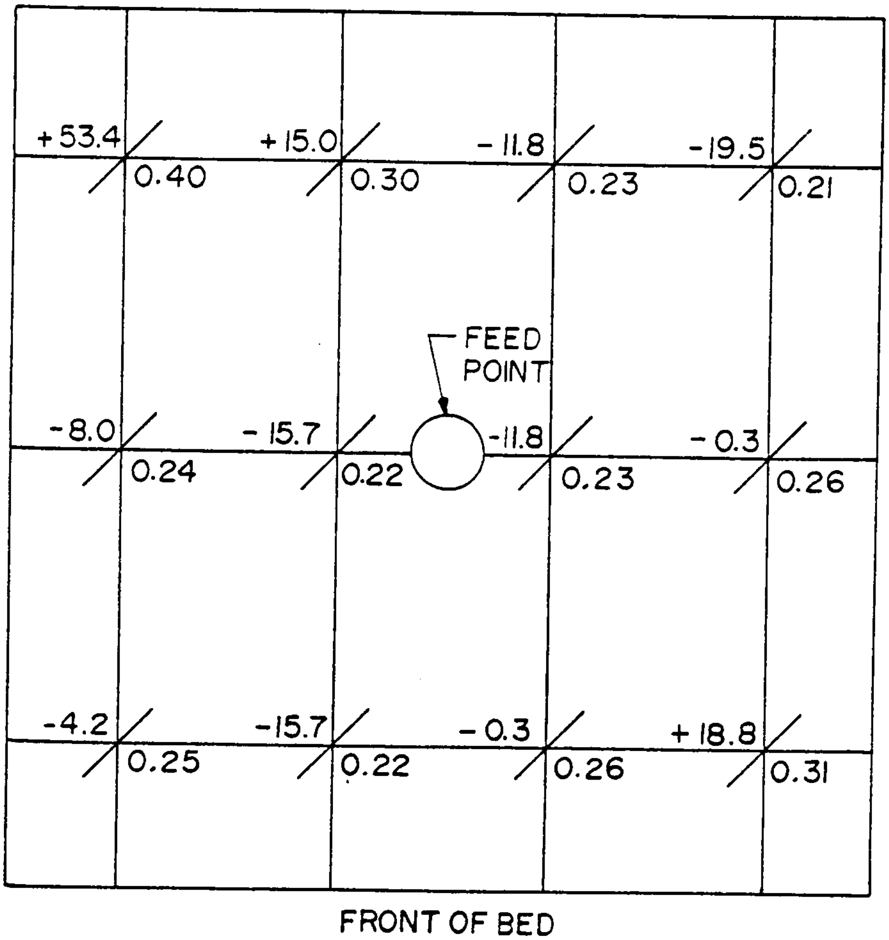

$\overline{R}^* = 0.26\ \%$
$\sigma = 0.05\ \%$

CAP: R4 GAP: 0.50 in. CAGE I.D.: 3.0 in.
AVERAGE TRANSPORT AIR FLOW RATE: 0 cfm.
COAL FEED RATE: 0 lbm/min. SAMPLE TIME: 20 sec
PROBE HEIGHT: 1 ft. LIMESTONE DEPTH: 25.0 in.
BED SUPERFICIAL VELOCITY: 4.5 fps.

Figure 6.27. Coal Feed Data Reduction—Background.

percent. This number indicates whether the location is coal rich or lean compared to the bed average.

The background data shows a somewhat random arrangement of positive and negative percentages. There were a lot more negative percentages than positive, which was due to the one very high positive (+53.4) and the two near zero negatives (-0.3). The average background coal mass to limestone mass ratio was 0.26 percent. This was the value used for the background ratio for all of the tests. The standard deviation for this data set was 0.05 percent. This will be compared with other standard deviations from different data sets.

The data of Figure 6.28 are a random sample with the 0.45 inch thick flat cap (F2) at 0.50 inch gap taken 20 seconds into the coal feed with the probes at the one foot level. The one foot level indicates that the line of four probes was one foot above the grid plate. This is about 10 inches above the injection point. This cap was open and was not tilting which is indicated by the fact that there are no extremely high or extremely low comparison percent ratios. This is typical of a random map and was substantiated by several repeated tests. The average corrected coal mass to limestone mass ratio was 2.09 percent and the standard deviation for this data set was 0.47 percent. The coal feeding increased the average corrected coal mass to limestone mass ratio by a factor of eight and the standard deviation by a factor of nine.

There are four locations that do not fall within one standard deviation of the average. These are the locations with mass ratios of 1.4, 2.9, 1.6 and 2.8 percent. This indicates that the coal feed data are more scattered than the background data.

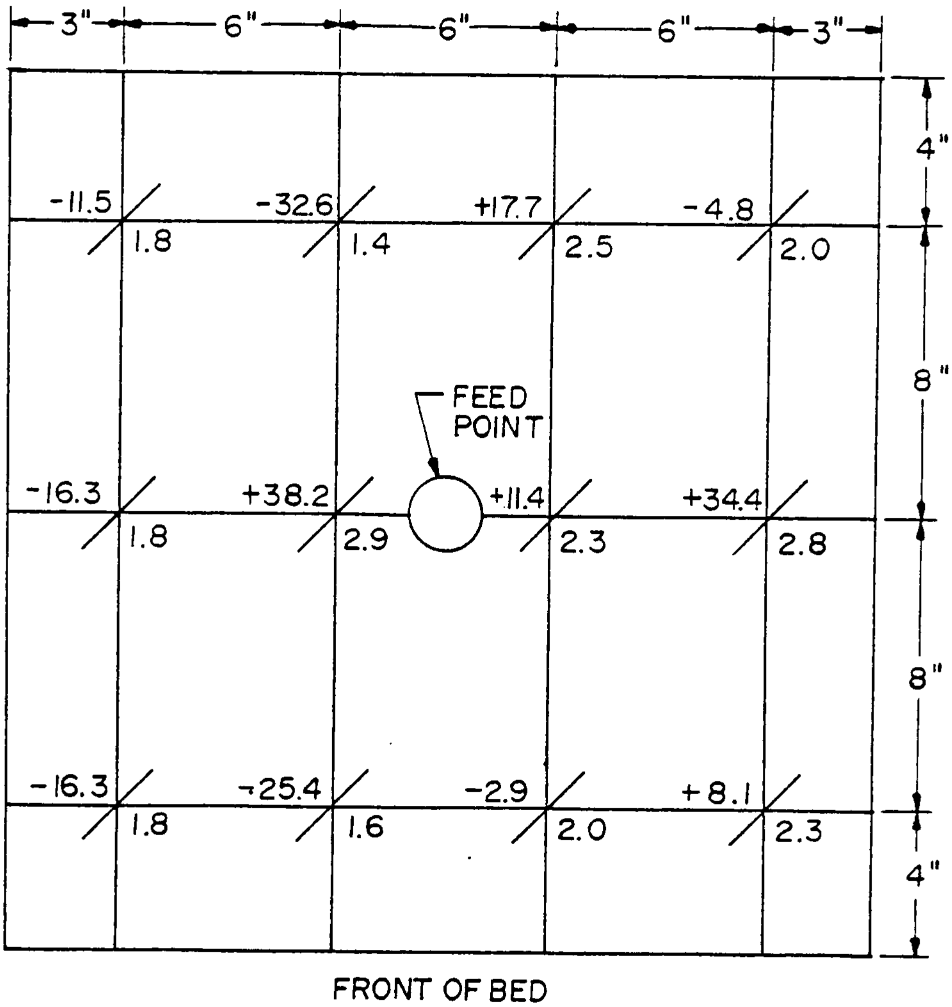

$\overline{R}^* = 2.09\ \%$
$\sigma = 0.47\ \%$

CAP: F2 GAP: 0.50 in. CAGE I.D.: 3.0 in.
AVERAGE TRANSPORT AIR FLOW RATE: 169 cfm.
COAL FEED RATE: 25 lbm/min. SAMPLE TIME: 20sec.
PROBE HEIGHT: 1 ft. LIMESTONE DEPTH: 25.9 in.
BED SUPERFICIAL VELOCITY: 5.0 fps.

Figure 6.28. Coal Feed Data Reduction—Cap F2, 0.50 Inch Gap, 20 Second Sample Point.

When the samples were taken at 50 seconds into the feed, the comparison percent ratios were always random, even for one particular test in which the coal feed line clogged. This indicated that 50 seconds was too long to wait and that the coal initially injected by the coal feed system had already been well mixed within the bed. This does, however, attest to the excellent mixing characteristics of a fluidized bed.

Figure 6.29 shows a typical random sample with the 0.45 inch thick flat cap, F2, at 0.50 inch gap taken 50 seconds into the feed with the probes at the one foot level. The average mass ratio ($\bar{R}$*) is greater for this test than for the 20 second sample test shown in Figure 6.28. This is a result of the greater amount of coal injected and the mixing within the bed. The 50 second sample time was not used again after it was judged as being too long.

Figure 6.30 is an excellent example of the problem that might be encountered when a cap does not fully open and operates at a tilt. This test used the 0.45 inch thick flat cap, F2, at 0.75 inch gap with the probes on the one foot level and the samples being taken at 20 seconds. The transport air flow rate was set at 112 cubic feet per minute which was, as shown in Figure 6.21 on page 70 or Table 6.10 on page 74, far too low to keep the cap fully open. At least 175 cubic feet per minute were required to keep this cap open. The cap was obviously tilted so that it biased coal in one direction, which is indicated by the +87.4 comparison percent ratio. The side opposite to the coal rich area was lean which was evidenced by the entire side having a negative comparison percent ratio. Clearly, this mode of operation in a bed would be very detrimental to bed performance. The coal rich area would become a reducing zone and the coal lean area would become an oxidizing zone.

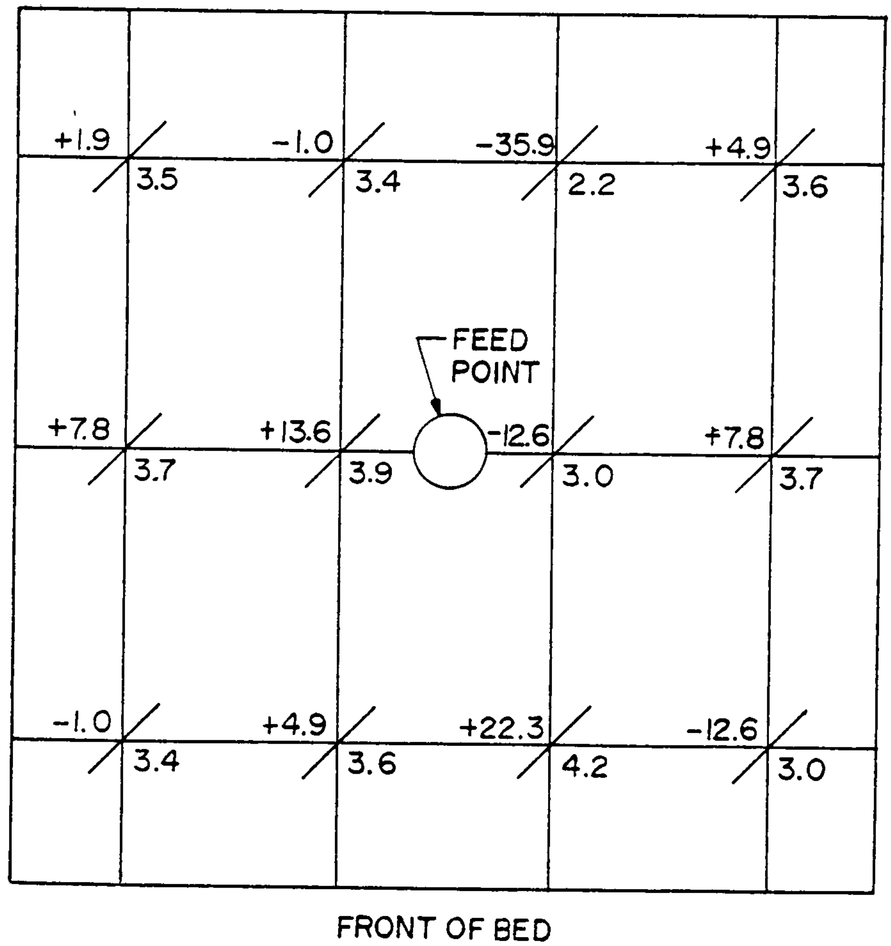

$\overline{R}^* = 3.43\ \%$
$\sigma = 0.51\ \%$

CAP: F2 GAP: 0.50 in. CAGE I.D.: 3.0 in.
AVERAGE TRANSPORT AIR FLOW RATE: 131 cfm.
COAL FEED RATE: 25 lbm/min. SAMPLE TIME: 50 sec.
PROBE HEIGHT: 1 ft. LIMESTONE DEPTH: 25.5 in.
BED SUPERFICIAL VELOCITY: 5.1 fps.

Figure 6.29. Coal Feed Data Reduction—Cap F2, 0.50 Inch Gap, 50 Second Sample Point.

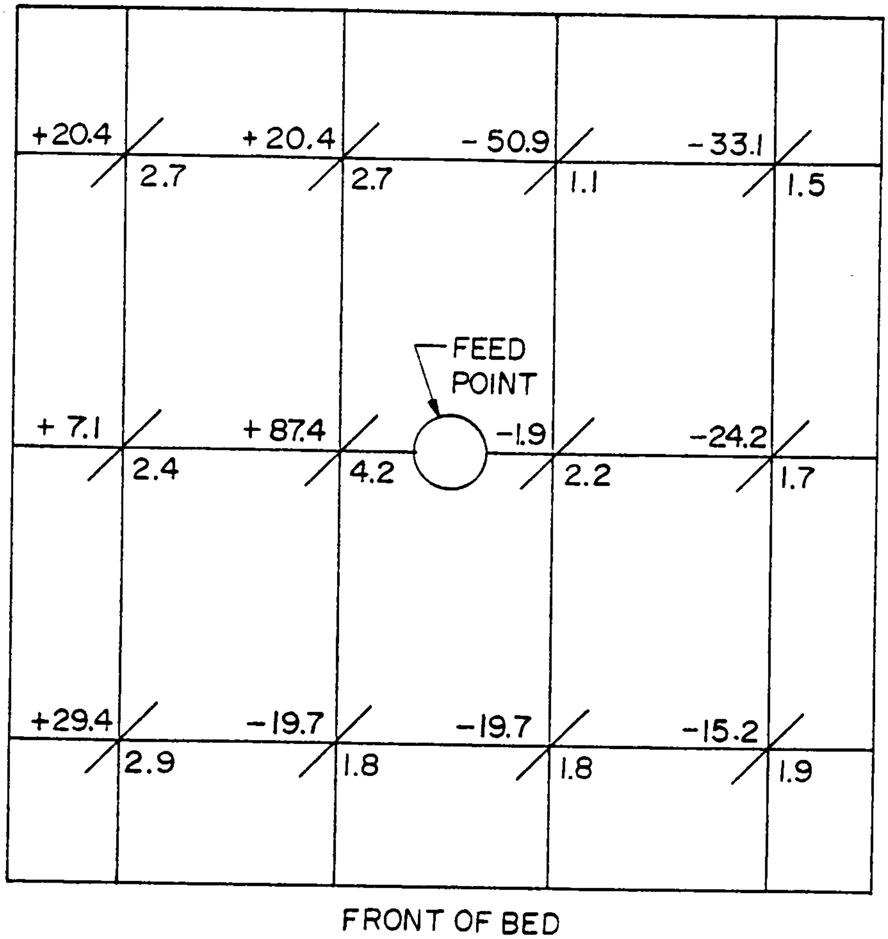

$\overline{R}^* = 2.24\ \%$
$\sigma = 0.82\ \%$

CAP: F2 GAP: 0.75 in. CAGE I.D.: 3.0 in.
AVERAGE TRANSPORT AIR FLOW RATE: 112 cfm.
COAL FEED RATE: 25 lbm/min. SAMPLE TIME: 20 sec.
PROBE HEIGTH: 1 ft. LIMESTONE DEPTH: 24.5 in.
BED SUPERFICIAL VELOCITY: 5.0 fps.

Figure 6.30. Coal Feed Data Reduction—Cap F2, 0.75 Inch Gap, 20 Second Sample Point.

A coal feed test was done on the 0.75 inch thick, 0.55 inch recess cap, R4, at 0.50 inch gap. The probes were on the one foot level and the samples were taken at 20 seconds. Figure 6.31 shows these data which are also random. The average coal distribution mass ratio was also about the same as the average mass ratio for the flat cap under identical test conditions. The average ratio for this test was 1.97 percent compared with 2.09 percent for the flat cap test. This test illustrates that recessing the cap does not affect the coal feeding performance.

A test was done with the probes at the two foot level using the 0.45 inch thick flat cap, F2. This test simply showed that the coal distribution was also random on this plane of the bed. The bed average mass ratio for the two foot level was approximately the same as the bed average mass ratio for the one foot level (2.08 percent for the two foot compared to a typical valve of 2.09 percent for the one foot). This again illustrated how well the fluidized bed mixes.

Repeatability checks were done with some of the tests. Figure 6.32 shows a run which compares with Figure 6.31. The average mass ratios agree with in 8.7 percent. Figures 6.33 and 6.34 show two tests which are repeats of Figure 6.28 on page 89. They show the same general trends and numerical values.

Coal feed tests—discussion

The coal feed tests revealed many facts about coal feeding with the valve cap feed system and the bubble cap fluidization system.

First, the coal feed tests showed that coal can be distributed randomly throughout the entire bed by the valve cap feed system. These

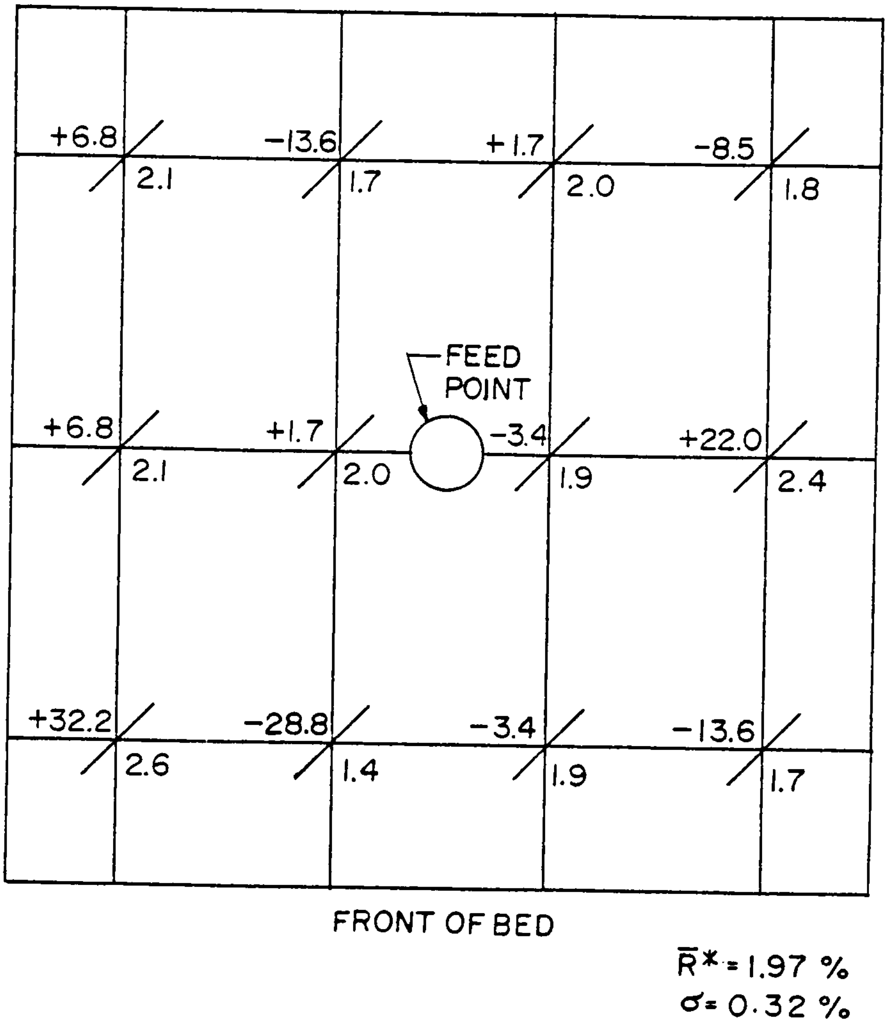

CAP: R4 GAP: 0.50 in. CAGE I.D.: 3.0 in.
AVERAGE TRANSPORT AIR FLOW RATE: 135 cfm.
COAL FEED RATE: 25 lbm/min. SAMPLE TIME: 20 sec.
PROBE HEIGHT: 1 ft. LIMESTONE DEPTH: 25.5 in.
BED SUPERFICIAL VELOCITY: 5.0 fps.

Figure 6.31. Coal Feed Data Reduction—Cap R4, 0.50 Inch Gap, 20 Second Sample Point.

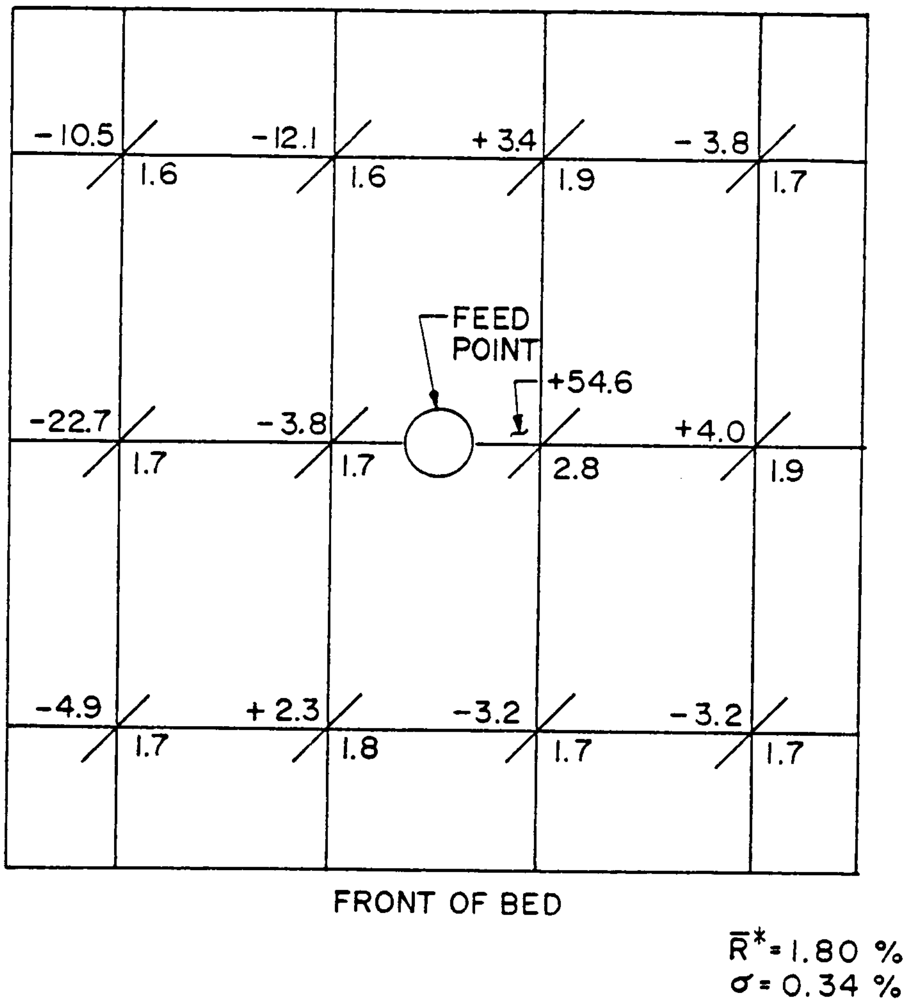

CAP: R4 GAP: 0.50 in. CAGE I.D.: 3.0 in.
AVERAGE TRANSPORT AIR FLOW RATE: 152 cfm.
COAL FEED RATE: 25 lbm/min. SAMPLE TIME: 20 sec
PROBE HEIGHT: 1 ft. LIMESTONE DEPTH: 25.2 in.
BED SUPERFICIAL VELOCITY: 5.0 fps.

Figure 6.32. Coal Feed Data Reduction—Cap R4, 0.50 Inch Gap, 20 Second Sample Point, Repeat 1 of Figure 6.31.

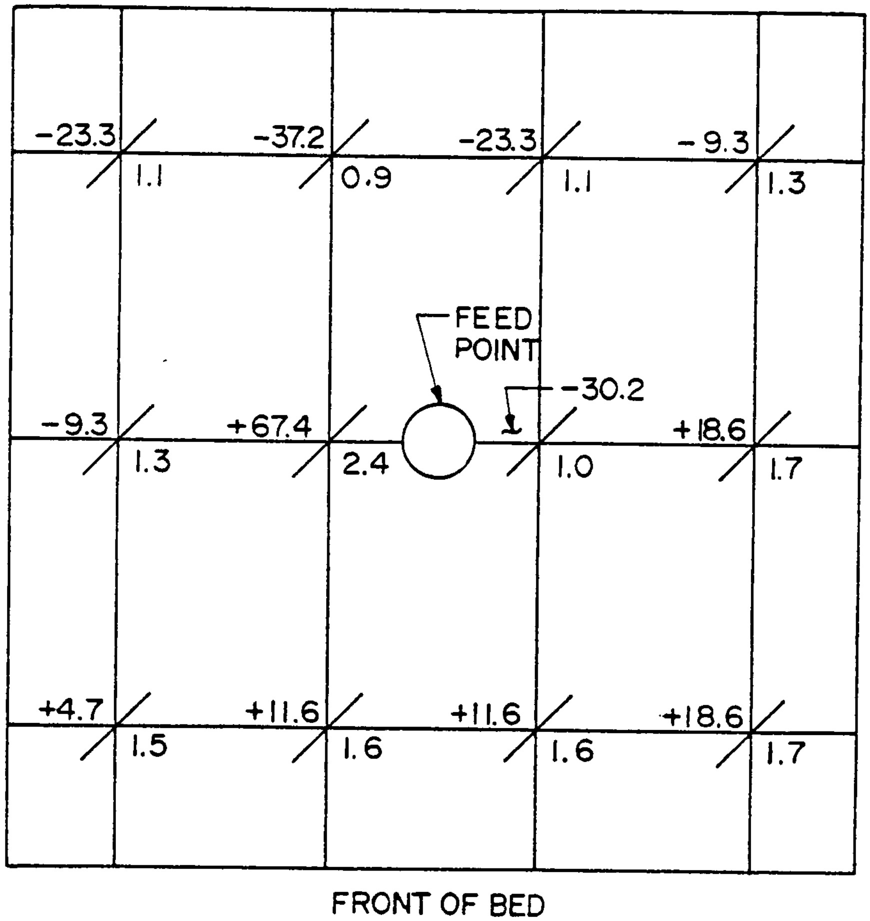

$\bar{R}^{*} = 1.43\%$
$= 0.41\%$

CAP: F2 GAP: 0.50 in. CAGE I.D.: 3.0 in.
AVERAGE TRANSPORT AIR FLOW RATE: 101 cfm.
COAL FEED RATE: 25 lbm/min. SAMPLE TIME: 20 sec
PROBE HEIGHT: 1 ft. LIMESTONE DEPTH: 25.2 in.
BED SUPERFICIAL VELOCITY: 5.0 fps.

Figure 6.33. Coal Feed Data Reduction—Cap F2, 0.50 Inch Gap, 20 Second Sample Point, Repeat 1 of Figure 6.28.

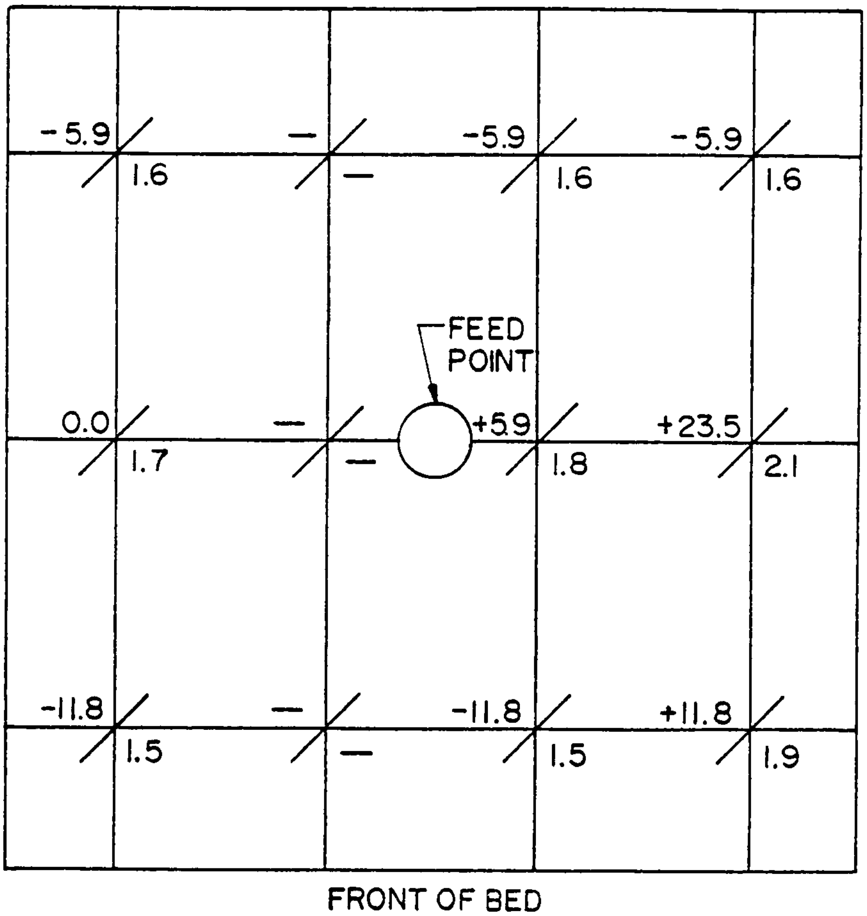

$\bar{R}^* = 1.70\ \%$
$\sigma = 0.20\ \%$

CAP: F2 GAP: 0.50 in. CAGE I.D.: 3.0 in.
AVERAGE TRANSPORT AIR FLOW RATE: 127 cfm.
COAL FEED RATE: 25 lbm/min. SAMPLE TIME: 20 sec
PROBE HEIGHT: 1 ft. LIMESTONE DEPTH: 24.8 in.
BED SUPERFICIAL VELOCITY: 4.9 fps.

NOTE:
THE COLUMN OF SLASHES INDICATE THAT THIS PROBE FAILED TO OPEN.

Figure 6.34. Coal Feed Data Reduction—Cap F2, 0.50 Inch Gap, 20 Second Sample Point, Repeat 2 of Figure 6.28.

tests illustrated the excellent mixing characteristics of a fluidized bed. As a consequence of these mixing characteristics, the coal feed tests revealed that 50 seconds was too long to wait for sampling with this type of tracing.

These tests revealed two important facts about valve caps in specific. First, they must be operated fully open. If the cap is tilted, coal lean, oxidizing zones, and coal rich, reducing zones, will occur. This will lead to poor combustion. Secondly, a recessed cap will not degrade the system coal feeding performance.

The coal feed tests are the best model to an actual fluidized bed without burning coal. Actual combustion tests are the next necessary step in thoroughly evaluating any feed system including the valve cap.

These coal feed tests were performed in a bed with a total cross sectional area of 4 square feet. This same feed system will typically be used to feed 9 square feet of bed cross section. The differences would be lower concentrations for each sample location because of the extra feed area being serviced by the feed point and a possible radial concentration gradient. It is believed that these differences would not be detrimental to the overall system operation.

Wear characteristic study—introduction

A fluidized bed coal feed device is subjected to very abrasive conditions when high velocity air laden with coal impinges upon its surfaces. The valve caps, being the component of this system which bear the brunt of the feed stream, should be designed to combat wear.

Three different cap shapes were studied to compare their wear characteristics. The three shapes tested were the flat cap, the convex cap and the recessed cap. The flat cap was the standard against which the other caps were compared. It was felt that the convex cap might wear mostly in the center thus allowing the edges to be made very thin. This would help decrease the cap mass.

The recess caps were designed with wear as a major consideration. It was felt that if the recess was deep enough, coal might collect in the cap. This would, in effect, be a cap made of steel and coal, with the main wear being directed on the coal. This was illustrated in Figure 6.10 on page 54.

The wear characteristic study was conducted for a coal mass flow rate of 25 pounds per minute and an air flow rate of 160 cubic feet per minute. The caps' bottom surfaces were painted with a thin layer of flat black paint. A 0.50 minute feed time was chosen after a few initial tries at 2.0 and 1.0 minutes proved to be too long; the paint layer was applied too thin and it would all wear off.

<u>Wear characteristic study——results</u>

The results of the wear characteristic tests are shown in Figure 6.35. The flat cap and the convex cap have no paint over most of their surfaces. This is characteristic of a high level of wear.

The black crescent where the paint remained is a direct result of the opening characteristic of the caps. Since they always rested upon two of the cage supports when rising, the caps were always off center when open. This created the crescent shape.

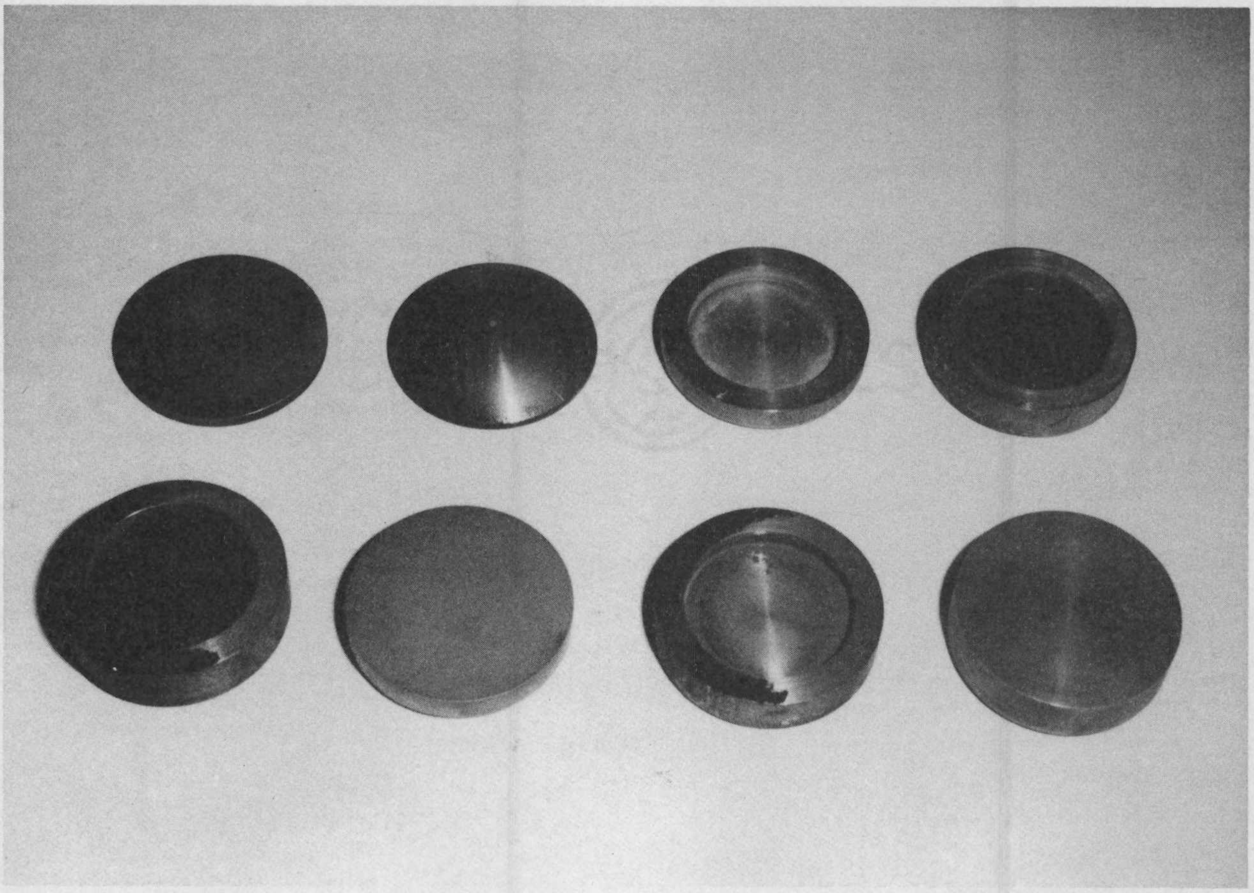

Figure 6.35. Wear Characteristic Tests with Various Caps.

Caps:	F3	C1	R2	R3
	R4	F2	R1	F1

The 0.25 inch deep recess has no paint over most of its surface, except near the recessed corners where the coal probably collects. In contrast, the 0.425 inch deep and the 0.55 inch deep recess caps have paint over most all of their inner surfaces. This is characteristic of reduced wear. This is very significant because it shows most of the wear will be on the collected coal. Thus a properly recessed cap could reduce the total cap mass and not sacrifice cap life.

Wear characteristic study—discussion

This study illustrates the probable benefit of a recessed cap, low mass and reduced wear. For this reason, the recessed cap, with recess depth of at least 0.425 inches is the best cap to use with the valve cap system.

The wear characteristic study is by no means a definitive test. Further wear tests with caps being subjected to coal flow for extended time periods are required to determine if the recess does truly prevent wear. It is believed, however, that the recessed cap will at least retard cap wear.

Closure

These tests of the small diameter valve cap give a good basis for selecting a proper cap for any application. The next chapter will discuss a particular cap design to satisfy the conditions of Chapter 3. It will also discuss the best possible cage designs and present recommendations for future testing of valve cap feed systems.

CHAPTER 7

CONCLUSIONS AND RECOMMENDATIONS

Fluidization System

The bubble cap fluidization system uniformly fluidizes a limestone bed and prevents bed drainback. This system has been in use in the EPRI 6x6 foot test facility and has operated successfully in actual combustion tests. The pressure loss versus superficial velocity relationship can be predicted and altered as outlined in Appendix E. For this reason, this system can be adapted to meet the various design conditions which might be encountered in industrial application.

The TVA has selected this system for the 20MW pilot plant. Tests at this facility should increase the available data for this system.

Valve Cap Coal Feed System

Introduction

The valve cap coal feed system operated fully open can evenly distribute coal to a fluidized bed. The valve cap system can reliably prevent bed drainback. A valve cap does not require any external actuating device. For these reasons, the valve cap is one of the most effective and reliable below-bed coal feed systems for a fluidized bed, however, it must be carefully designed to operate at the required flow rate for the specified bed temperature and pressure.

Cap

The primary objective of cap design is to create a proper balance between cap mass and transport air flow rate. The cap diameter must be made large enough to cover the feed pipe, but small enough so that the cap mass does not become too great.

A cap should be designed that is resistive to wear. The design which resists wear most is the recessed cap. To minimize cap weight by reducing leg height, the shallowest recess which retards wear should be selected. The diameter of the recess should be at least as large as the exit of the feed pipe to insure proper wear retardation.

A cap should be constructed with sufficiently thick top and wall sections to prevent deformation when the bed is slumped and the cap must support a static load. Effective values for these thicknesses will have to be determined with actual combustion bed tests.

Finally, the cap should be constructed of a hardened steel or stellite in order to withstand the harsh environment of a fluidized bed.

Cap design to meet chapter 3 specifications

A particular cap was designed to meet the specifications presented in Chapter 3. The cap was required to remain fully open with a transport air flow rate of 97.3 cubic feet per minute at 80°F at 14.3 psia. The cap was to operate in conjunction with a 2.0 inch diameter schedule 40 feed pipe and a coal mass flux to air mass flux ratio, (J), of 3.5.

The design was initiated by employing equation 6.16 repeated below.

$$w_{Total} = w_{Air\ Only} + w_{Solids\ Only} = \frac{\dot{m}_{Air} V_{Air}}{g_c} (K+JS). \qquad (6.16)$$

A cap gap of 0.75 inches was chosen adhering to a "coal industry" rule of thumb which states that the minimum opening should be equal to three times the maximum dimension of the largest particle. For this gap, the momentum correction factor, K, was assumed to be 0.75 from the data of Table 6.10 on page 74. The slip velocity S was calculated in Chapter 6 to be approximately 0.27. A value of 1.0 was used for the coal mass flux to air mass flux ratio to account for turndown during operation. Using equation 7.1, the maximum supportable mass was determined to be 138.9 grams (0.306 pounds).

A recessed cap of 2.688 inches outside diameter was picked as a design basis. To effectively retard wear, a 0.425 inch recess was the minimum depth allowed, consequently, this value was used to reduce the cap mass. The cap was designed to be 0.555 inches tall overall with 0.10 inch thick recess walls. This cap has a mass of 137.1 grams (0.302 pounds) if made from steel with a density of 7.73 grams per cubic centimeter (0.279 pounds per cubic inch).

Cage

The cage design and cap design must be compatible. The diametrical clearance between the cage and the cap should be at least 1.25 times the largest dimension of the largest bed particle. This will prevent cap hangup due to particle entrapment between the cap and the cage. The 2.688 inch diameter cap and 3.0 inch inside diameter cage meets this criterion for 0.25 inch maximum particle dimension ($3.0 = 2.688 + 1.25 \times 0.25$). The cage diameter cannot be made larger and the cap still effectively cover the 2.0 inch diameter schedule 40 feed pipe during no feed conditions. The cage and cap combination could be made smaller in diameter to reduce the cap weight, however, a smaller diameter cap might experience difficulty in obtaining a good radial distribution of coal.

The vertical support bars of the cage can be made from stock having any cross section, however, the circular bars used in this investigation proved effective. Support bars should be made small enough to avoid affecting coal feeding or valve cap operation. They should be made of stock with large enough cross section to insure that they do not fail during operation. As with the cap design, a hardened steel would be the best material choice for a long operating life.

The cage top should be designed to minimize the contact area between itself and the fully open cap. One acceptable design was presented in Figure 6.25, page 84.

Recommendations

Fluidization system

The bubble cap fluidization system is a well tested and proven system. Further testing should concentrate on hot bed studies to increase the available data base.

New fluidization systems should be designed and tested for application under different conditions.

Coal feed system

The most definitive test for a coal feed system is an actual combustion test in a hot bed. This would reveal exactly how well a particular system can feed coal, prevent bed drainback and withstand wear. Extended hot bed tests are necessary to truly judge a coal feed system.

In a combustion bed, start-up and shut-down cycles could be investigated to determine proper procedures. Rates of change for the transport air flow rate could be investigated to determine the effect upon system operation.

"Strength" tests could be conducted on candidate cap designs to determine the minimum tolerable thicknesses for critical sections.

Actual wear tests should also be conducted on valve cap designs. These tests should be performed for extended periods of time under actual combustion bed conditions including representative coal flow rates.

The cage design should be studied in a greater depth. The most prominent change should be from four-bar supports to three-bar.

New cage tops should be investigated to determine if more effective designs can be obtained for moving particles from in between the cage and the cap.

Finally, innovative coal feed systems should continue to be designed and investigated to further fluidized bed technology.

LIST OF REFERENCES

LIST OF REFERENCES

1. Babcock and Wilcox, Steam/Its Generation and Use, 161 East 42nd Street, New York, New York, 1978.

2. Walker, D. J., R. A. McIlroy, and H. B. Lange, "Fluidized Bed Combustion Technology for Industrial Boilers of the Future - A Progress Report," Report prepared by the Babcock and Wilcox Company, February 1979.

3. Ehrlich, Shelton, "History of the Development of the Fluidized-Bed Boiler," The Proceedings of the Fourth International Conference on Fluidized-Bed Combustion, Presented on December 9, 1975, Published by the MITRE Corp., May 1975, pp. 15-20.

4. Fluidized Combustion Company, "Preliminary Design and Cost Estimate for an Atmospheric Fluidized Bed Steam Generator," Report prepared for the TVA/DOE, April 28, 1978.

5. Babcock and Wilcox, "Conceptual Studies and Preliminary Design of a Fluid Bed Fired Boiler for Service in an Electric Utility," Report prepared for the TVA/DOE, April 28, 1978.

6. Combustion Engineering, Preliminary Design Study for a Fluidized Bed Demonstration Unit," Report prepared for the TVA/DOE, June 1, 1978.

7. Wilkerson, H. J. and R. J. Krane, "State-of-the-Art Coal and Limestone Feeding for Atmospheric Fluidized Bed Combustion," Report prepared for the TVA, September 24, 1979, ME-AFBC-79-2.

8. Zenz, F. A., "How Flow Phenomena Affect Design of Fluidized Beds," Chemical Engineering, Vol. 84, No. 27, December 19, 1977, pp. 81-91.

9. Zenz, F. A. and D. F. Othmer, Fluidization and Fluid-Particle Systems, Reinhold Publishing Corporation, New York, 1960.

10. Henry, Rodney L., "Combined Feeding of Coal and Air to a Model Fluidized Bed Using Valve Caps," Master's Thesis, The University of Tennessee, Department of Mechanical and Aerospace Engineering, March 1981, ME-AFBC-81-5.

11. Knox, Gary D., "Combined Fluidization and Coal Feeding in a Model Fluidized Bed -- Pipe Grid Feeder," Master's Thesis, The University of Tennessee, Department of Mechanical and Aerospace Engineering, March 1981, ME-AFBC-81-4.

12. Babcock and Wilcox, "Preliminary Design of a 570MW Atmospheric Fluidized Bed Boiler," Report prepared for the Stone and Webster Engineering Corporation, November 30, 1977.

13. Roberson, J. A. and C. T. Crowe, Engineering Fluid Mechanics, Houghton, Mifflin Company, Boston, Massachusetts, 1975.

14. Bradshaw, P., Experimental Fluid Mechanics, Pergammon Press, New York, New York, 1970.

15. Canada, G. S., M. S. McLaughlin, and F. Staub, "Flow-Regimes and Void Fraction in Gas Fluidization of Large Particles in Beds Without Tube Banks," Fluidization: Application to Coal Conversion Processes, Vol. 74, Issue 176, 1978, Published by the American Institute of Chemical Engineers, pp. 14-26.

16. Hewlett-Packard, Hewlett-Packard HP-25 Applications Programs, Hewlett-Packard Corporation, 1975.

17. Zenz, F. A., "Conveyability of Materials of Mixed Particle Size," I&EC Fundamentals, Vol. 3, February 1964, pp. 65-76.

18. Holman, J. P., Experimental Methods for Engineers, McGraw-Hill Publishing Company, New York, New York, 1978.

19. White, Frank M., Fluid Mechanics, McGraw-Hill Book Company, New York, New York, 1979.

APPENDICES

APPENDIX A

COMBINED COAL FEEDING AND FLUIDIZATION WITH FOUR ARM CROSSES

Introduction

Basics

Combined feeders are defined as feeders which combine all of the fluidization air and transport air into one system that fluidizes the bed and delivers coal. These systems must simultaneously satisfy uniform coal distribution and uniform bed fluidization. Combined feeders have advantages as well as disadvantages compared to feeders which separate the coal feed and fluidization functions.

Summary of advantages and disadvantages

The major advantage of a combined feeder is its superior ability to avoid clogging due to insufficient conveying velocity or agglomerating of the coal.

Combined feeders can open heavier valving devices because of the greater air flow passing through their system.

The major disadvantage of combined feeders is their dual role. These systems must properly fluidize the bed as well as effectively deliver coal.

Another disadvantage is erosion in the system. The high velocities associated with the large air flows can create many material design problems in the coal feed system.

Coal distribution may or may not be improved depending upon feeder design and placement within the bed. There is some concern with combined feeders about creating explosive mixtures of coal and air, therefore, mixing must be done immediately prior to injection into the bed. This could be another disadvantage for combined feeding.

Four Arm Cross

Introduction

The four arm crosses were designed as a combined feed system. The four arm cross is a pipe split in four directions. Each arm of the cross is 90 degrees from the two adjacent arms and makes an angle of 90 degrees with the base pipe (see Figure A.1).

Design

As a design basis, the four arm cross was to provide a pressure drop equal to one-third of the pressure drop across a four foot deep fluidized bed at a superficial velocity of 7.5 feet per second. This was determined in the following manner.

Assume that a four foot deep fluidized bed is expanded 50 percent. This would make the slumped depth 4.0 feet divided by 1.5 or 2.67 feet. The pressure loss across 2.67 feet of slumped bed is simply equal to the limestone weight. From Knox [11, p. 89], the bulk density of the limestone is 92 pounds per cubic foot, therefore, the pressure loss, P_L, is:

$$P_L = (92 \text{ lbf/ft}^3)\ (2.67 \text{ ft})\ (144 \text{ in}^2/\text{ft}^2)^{-1}$$

P_L = 1.71 pounds per square inch (psi).

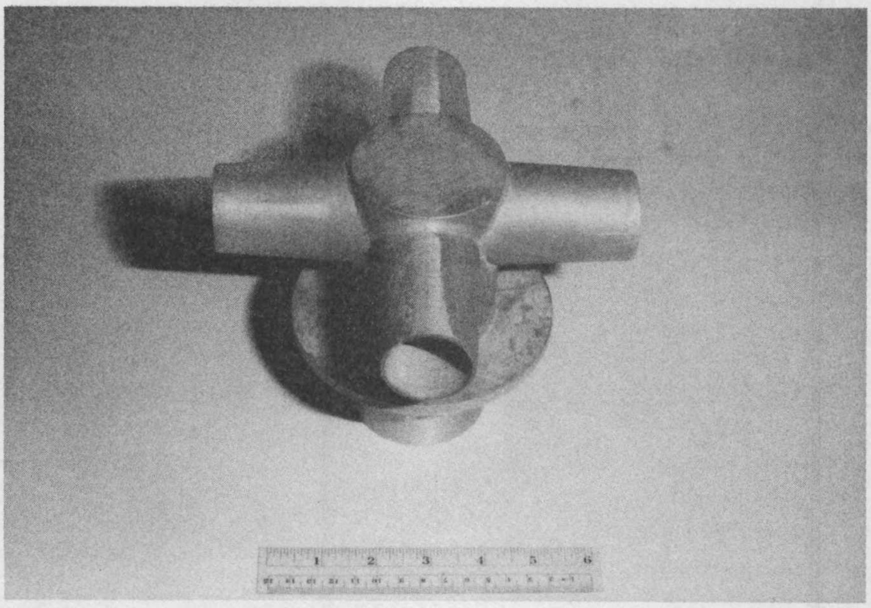

Figure A.1. Cross Feeder Out of Bed.

One-third of this value is the desired loss across the cross system, equal to 0.57 psi. Referring to the work of Henry [10, p. 155], this pressure loss was found to correspond to a floating cap with maximum cap height of one inch at superficial velocity of 7.8 feet per second. For a 2.5 inch diameter cap, the total flow area is 7.85 in^2. Because it was believed that the cross would experience a lower pressure loss than the floating cap, this area was reduced one-third making the total cross flow area 5.23 in^2. This flow area would require a hole 1.29 inches in diameter in each of the four cross arms. Each arm was made 1.6 inches in outside diameter to allow the hole size to be increased by 15 percent.

In order to determine what length arm was necessary, some further assumptions were made. First, the angle of repose of the limestone in an arm was assumed to be 30 degrees. The angle of repose is defined as the angle from the horizontal made by the limestone when resting in a free pile. Thirty degrees was picked with the aid of Zenz [9]. Using the maximum designed diameter of 1.48 inches, the limestone would reach $1.48/(\tan 30^o) = 2.56$ inches into the arm. To avoid drainback, the cross arm was made approximately this length.

The centerline of the arms were placed 2.375 inches above the grid plate surface to allow approxmiately 1.5 inches of nonfluidized limestone to rest on the plate. In an actual hot bed, this nonfluidized zone would help to insulate the grid plate and help keep it from becoming too hot. This would reduce the possibility of the plate warping or breaking from the weight of the limestone when the bed is slumped.

The inside diameter of the base of the cross was made 2.5 inches in diameter to match with the existing bed systems. The final cross design is presented in Figure A.2.

Horizontal jet penetration was calculated to determine if the crosses would fluidize all parts of the bed. Zenz [17, p. 2] presents a figure with nondimensional penetration depth P/D_0 (nondimensionalized with respect to exit diameter) versus the product of gas exit velocity in feet per second and square root of gas density in pounds per cubic foot. The exit velocity was determined by dividing the design point flow rate of 1,800 cubic feet per minute by the total exit area of 16 times the flow area of one cross arm. The design point diameter of 1.29 inches was used. The exist velocity, V_0, was calculated to be 207 feet per second. The gas density used was 0.0735 pounds per cubic foot. Thus, the product of velocity and gas density was 56. From Figure 4 in Zenz [17, p. 2], the dimensionless penetration depth, P/D_0, is approximately 4. For an exit diameter of 1.29 inches, the penetration depth, P_0, is 5.2 inches. This number must be considered with respect to a particular arrangement of the crosses within the bed.

The crosses were arranged in 2 foot by 2 foot bed in a square pattern one foot per side, centered in the bed. Refer to Figure A.3. The orientation shown is probably the most critical when considering bed penetration because the distance, D, between confronting arms is greatest. This distance was determined as follows: $D = (12)^2+(12)^2 - 2d$. The cross arm length measured from the centerline of the base, d, is 3.75 inches so D = 9.47 inches. This is less than the total penetration depth from both cross arms, twice the depth from one arm (10.4 inches). Therefore, the jets from each arm will interfere, promoting good mixing.

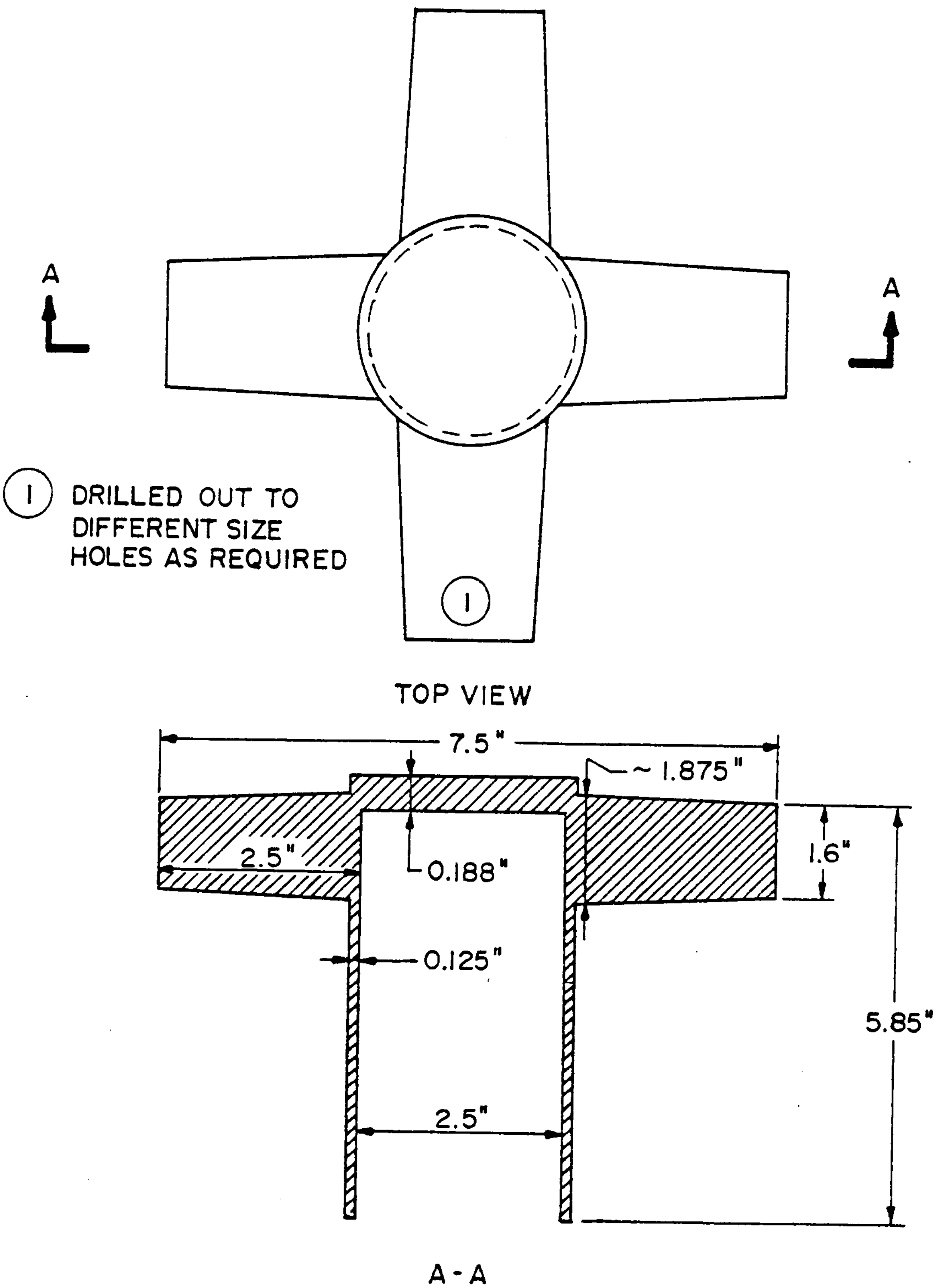

Figure A.2. Cross Feeder Design.

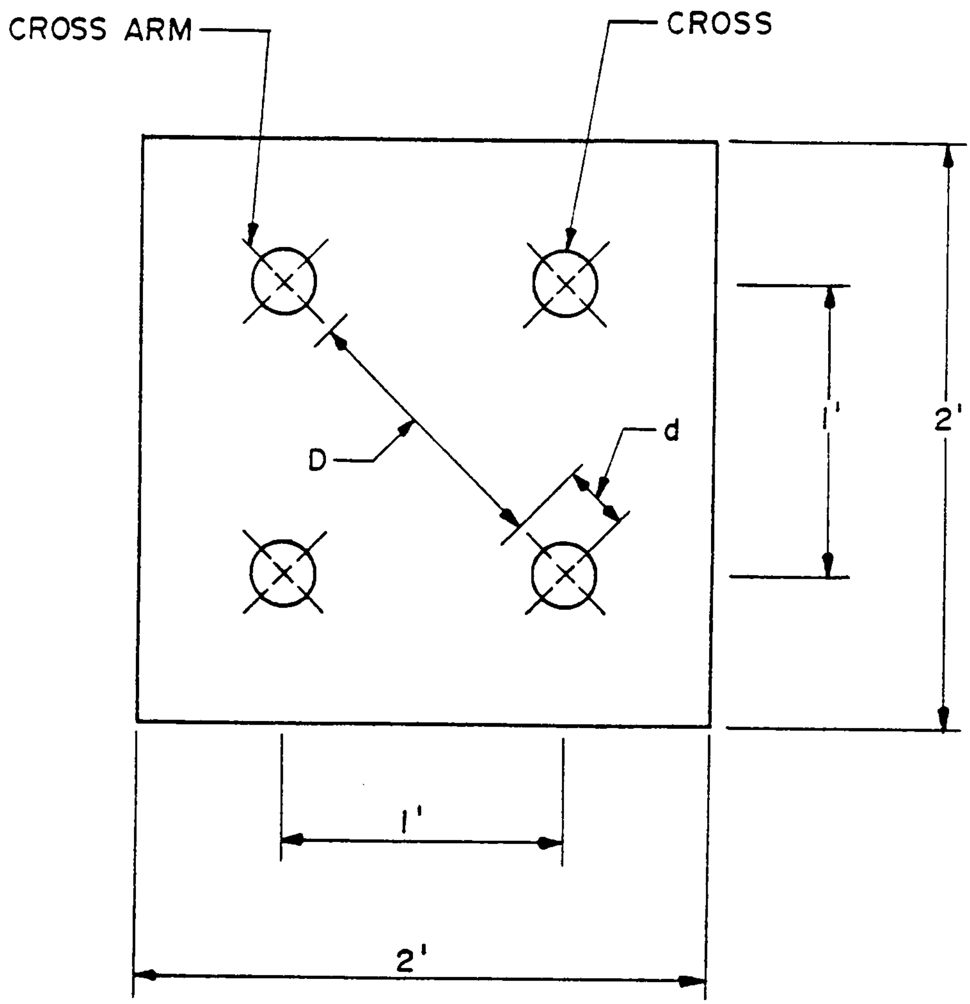

Figure A.3. Bed Dimensions and Cross Arrangement.

Qualitative results

Fluidization with the four-arm cross is shown in Figure A.4. Several points are evident from the figure. The main characteristic of the cross fluidization is the large jets. Most of the air from the crosses is concentrated in the streams eminating from the cross arms. This is not good from a mixing viewpoint, nor is conducive to uniform fluidization. As a result of these jets, large bubbles formed within the bed. The regime of fluidization was bubbly.

The top plane of the bed was violent as a result of the large bubbles breaking the surface. The bed height would vary approximately plus and minus five inches.

Large nonfluidized zones were present in many regions of the bed. Between jets and in the corners was where most of the dead limestone rested. These dead regions approximated 25 percent of the bed material at the grid plate. These dead regions would cause poor mixing, uneven bed temperatures and poor combustion.

Qualitatively, a comparison of this system's characteristic fluidization to that of Henry's feeder shows the crosses to be inferior. Henry's system operated in the turbulent flow regime which is superior from a mixing standpoint, than the bubbly flow regime. The characteristic fluidization of the crosses and Knox's in-bed pipe feed system was very similar. Videotapes of these feeders in operation are available through The University of Tennessee Mechanical and Aerospace Engineering Department located in Dougherty Hall.

Bed drainback

The crosses prevented bed drainback when the bed was slumped, however, it should be emphasized that these conditions do not exactly

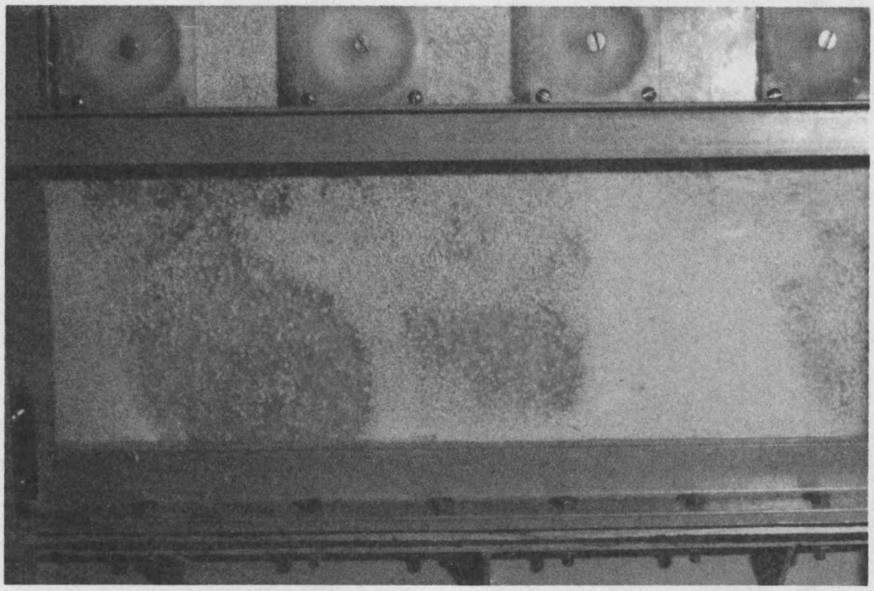

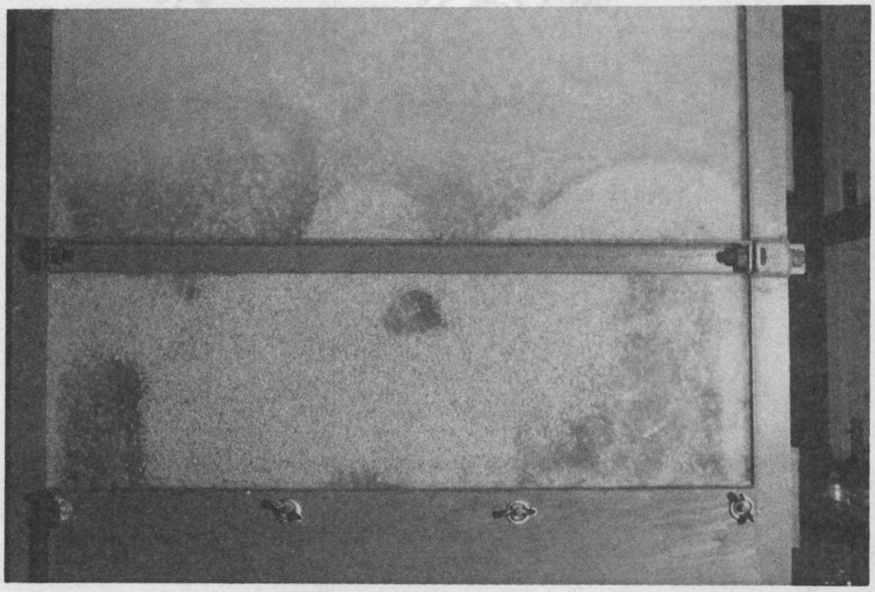

Figure A.4. Fluidization with the Crosses.

match those of an actual operating fluidized bed. In actuality, slumped bed sections would be in contact with fluidized sections and interaction between the two would cause some agitation in the slumped bed. Since this bed does not move at all when slumped, bed drainback tests in this facility cannot conclusively show that the crosses would truly prevent bed drainback.

Quantitative results

The crosses were tested only with the limestone and air tests, because the fluidization was so poor that the crosses were deemed unappropriate as a fluidized bed combined coal and air feeder. Nevertheless, the results of the air and limestone tests are presented.

Pressure drop

Figure A.5 shows feeder pressure drop from the plenum box to the exit plane of the crosses, versus bed superficial velocity for different cross orientations. The orientations are named and depicted schematically on Figure A.5. It is interesting to note the effect orientation has upon the pressure loss. The configuration with the least pressure drop at all superficial velocities was with all of the crosses in an x position. This occurred because the fluidization air formed into a large bubble in the center, where the crosses were all aimed, creating an easy path for the air to travel through the bed. The configuration with the next least pressure drop was with all of the crosses in the plus orientation. This arrangement allowed four smaller bubbles (or pathways) to form between each cross. Finally, the configuration with the greatest pressure loss (mixed configuration), had two

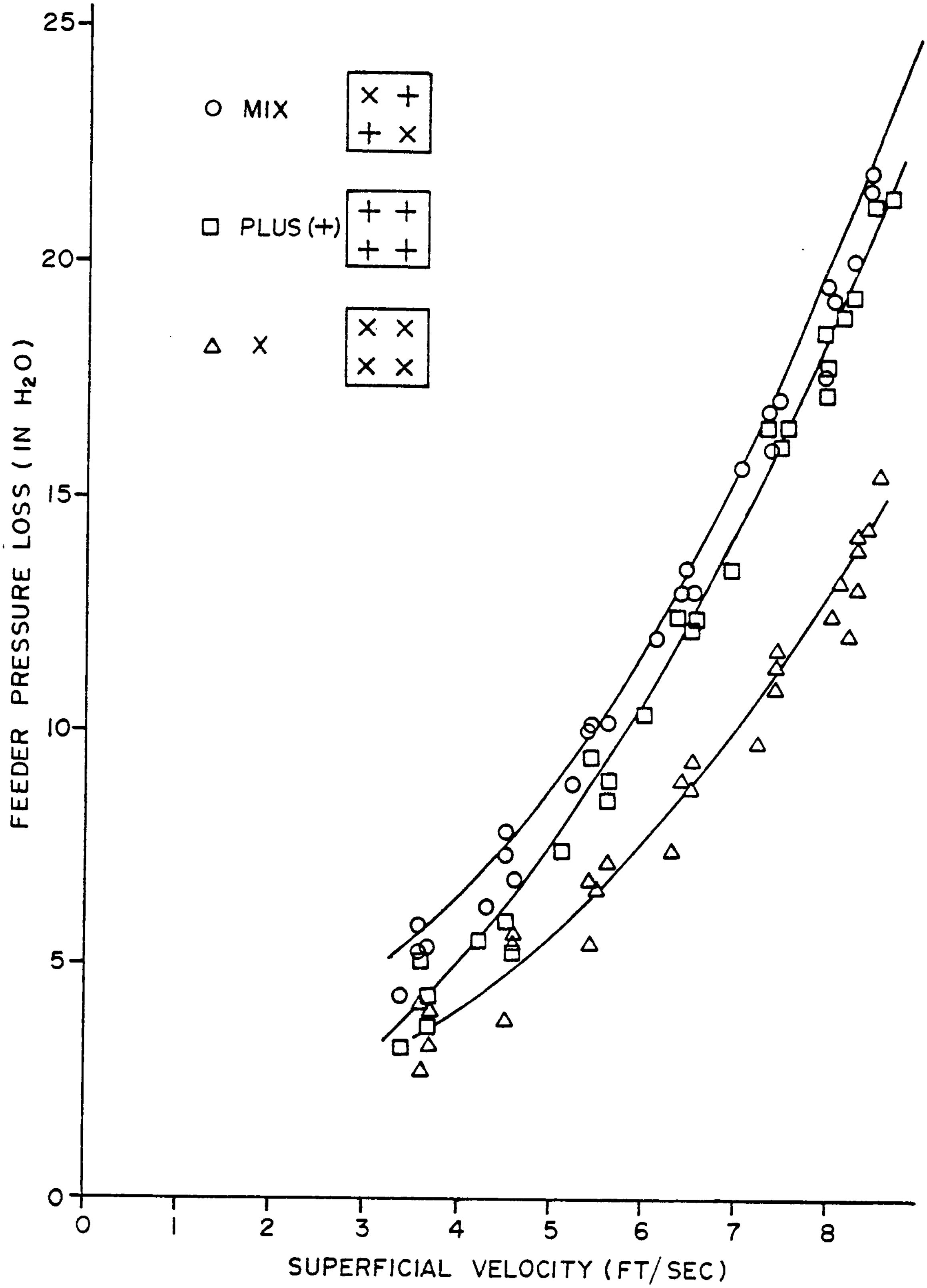

Figure A.5. Pressure Loss Versus Superficial Velocity for Cross Feeder, Various Configurations.

x position crosses and two plus position crosses placed diagonally opposite one another. Only one small main pathway was formed between the two x position crosses.

This explanation of the air flow passages within the bed was substantiated by observations of the limestone surface after the bed was drained. Because of the placement of the drain line approximately two inches of limestone remained in the bed after draining. The feeders always left a characteristic pattern in the surface of the remaining limestone. The all x configuration left a 10 inch diameter hole in the center that extended all the way to the grid plate. Smaller holes were present along the sides. A large center crater was evidence of the central air flow. The all plus configuration left four craters that did not extend to the grid plate between each cross, as well as small holes along the bed perimeter. The plus and x (mixed) configuration left one center crater that reached the grid plate and two smaller holes near the x placed crosses. The limestone patterns are shown in Figure A.6.

Power law curve fits were determined for each configuration by the use of a linear regression program [16, p. 98]. The data are seen to agree very well with the specific curves. The relationships and corresponding orientations are given in Table A.1.

Figure A.7 illustrates the decrease in pressure drop obtained by increasing the cross arm diameter from 1.30 inches to 1.42 inches (9 percent). This method of decreasing pressure loss might be necessary to make this system usable. Larger arm units could decrease the tendency for jets to occur or at least decrease their length of bed penetration. This diameter's pressure loss versus superficial velocity equation is also listed in Table A.1.

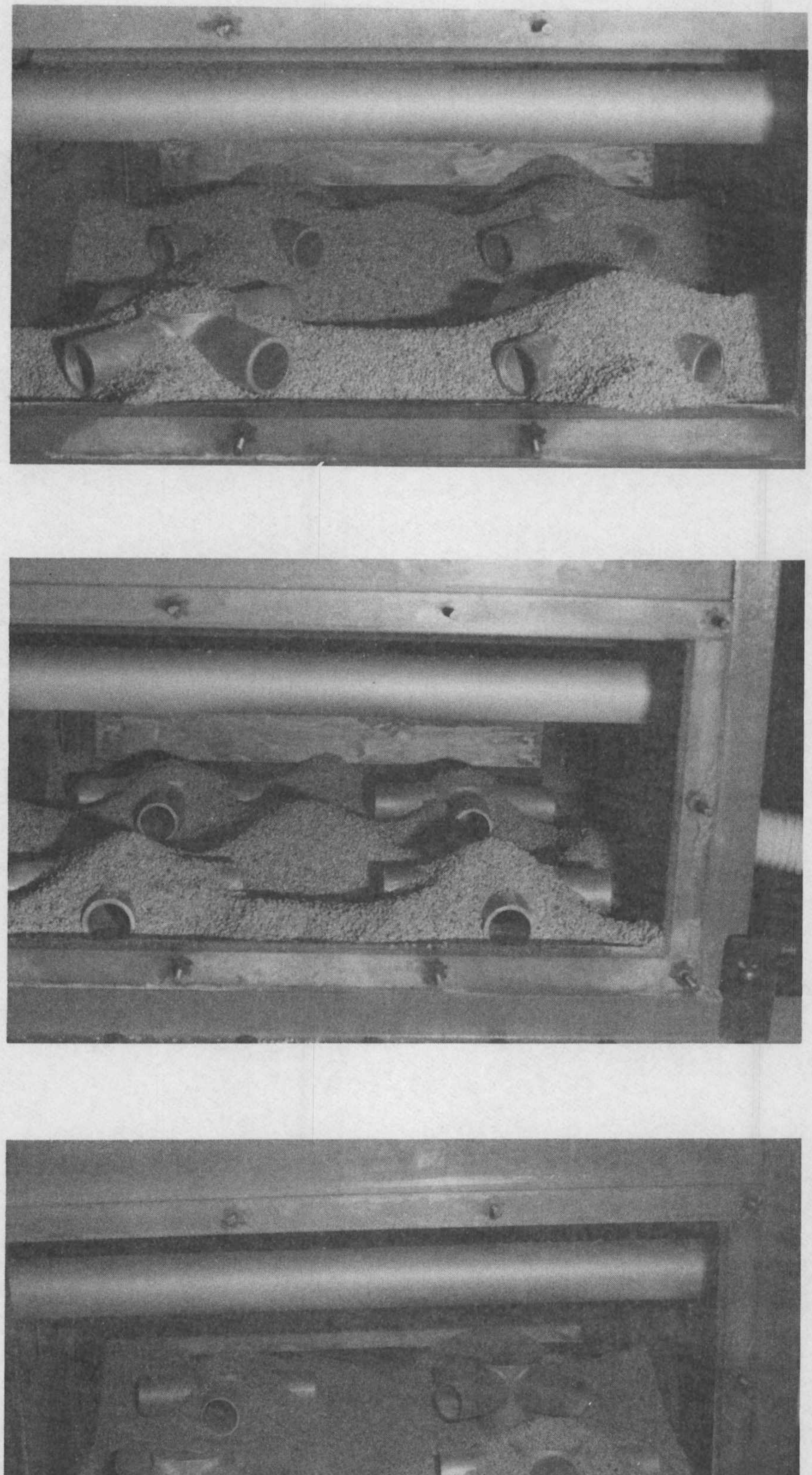

Figure A.6. Cross Limestone Patterns

Top to Bottom Configurations: X, Plus, Mix

TABLE A.1

CROSS PRESSURE LOSS VERSUS SUPERFICIAL
VELOCITY AND ORIENTATION

General Equation: $\Delta P = CV_s^x$
Units: ΔP = in. H_2O, V_s = ft/sec
Conditions: T = 80° F, P = 14.3 psia

Orientation	Arm Diameter (in)	C	x	r^2 [1]
X	1.30	0.46	1.59	0.949
Plus	1.30	0.33	1.94	0.979
Mixed	1.30	0.59	1.67	0.989
Mixed	1.42	0.50	1.60	0.953

[1]Coefficient of determination.

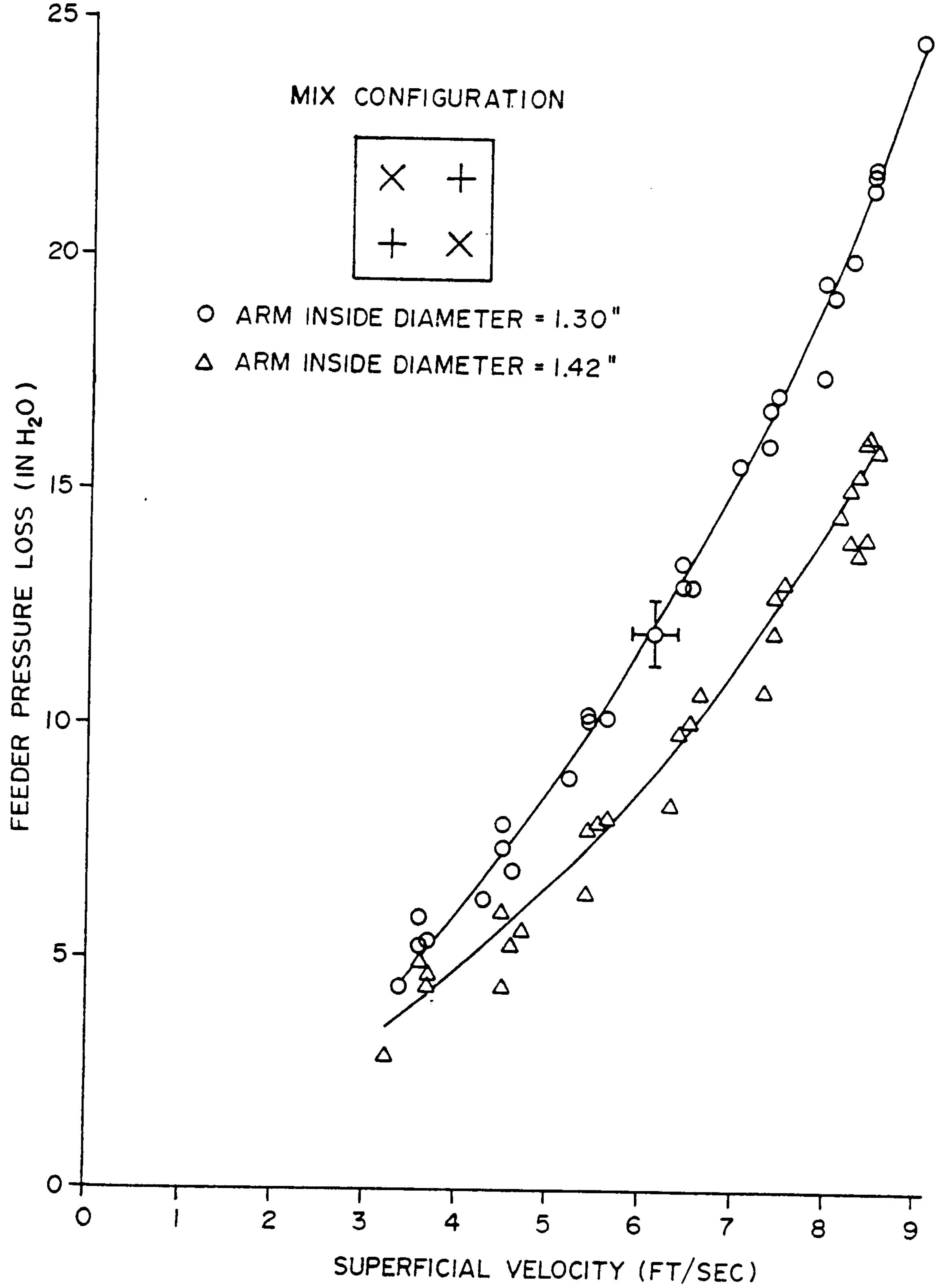

Figure A.7. Pressure Loss Versus Superficial Velocity for Cross Feeder with Two Different Diameters, Mixed Configuration.

The combined system can be quantitatively compared to the systems studied by Knox [11] and Henry [10]. These comparisons are shown in Figures A.8 and A.9. In both cases the observed trends are similar (i.e., Pressure drop increasing with superficial velocity) and the curve shapes are identical. The crosses, however, experienced lower pressure losses than either of the other feed systems with comparable flow areas. The comparable curves and their respective flow areas are shown on both figures. This lower pressure loss would be an advantage in an actual utility fluidized bed because it would allow the use of a lower pressure capacity air system.

Bed expansion

Bed expansion as a function of superficial velocity was calculated for each orientation. The bed expansions versus superficial velocity for all of the orientations are shown in Figure A.10. The band of data are presented because of the scatter of the bed expansion points. Linear regression curve fits [16, p. 87] for each orientation and for all of the orientations combined are presented in Figure A.11. Table A.2 lists the equations for the mixed, plus, x and all orientations combined.

There is very little difference in bed expansion for different orientations. One noteworthy trend is that a combined feed system with a lower pressure loss for a given superficial velocity than another system will also have a lower percent bed expansion than the other system at that particular superficial velocity. Take as an example, the mixed orientation and the all x orientation. At any superficial

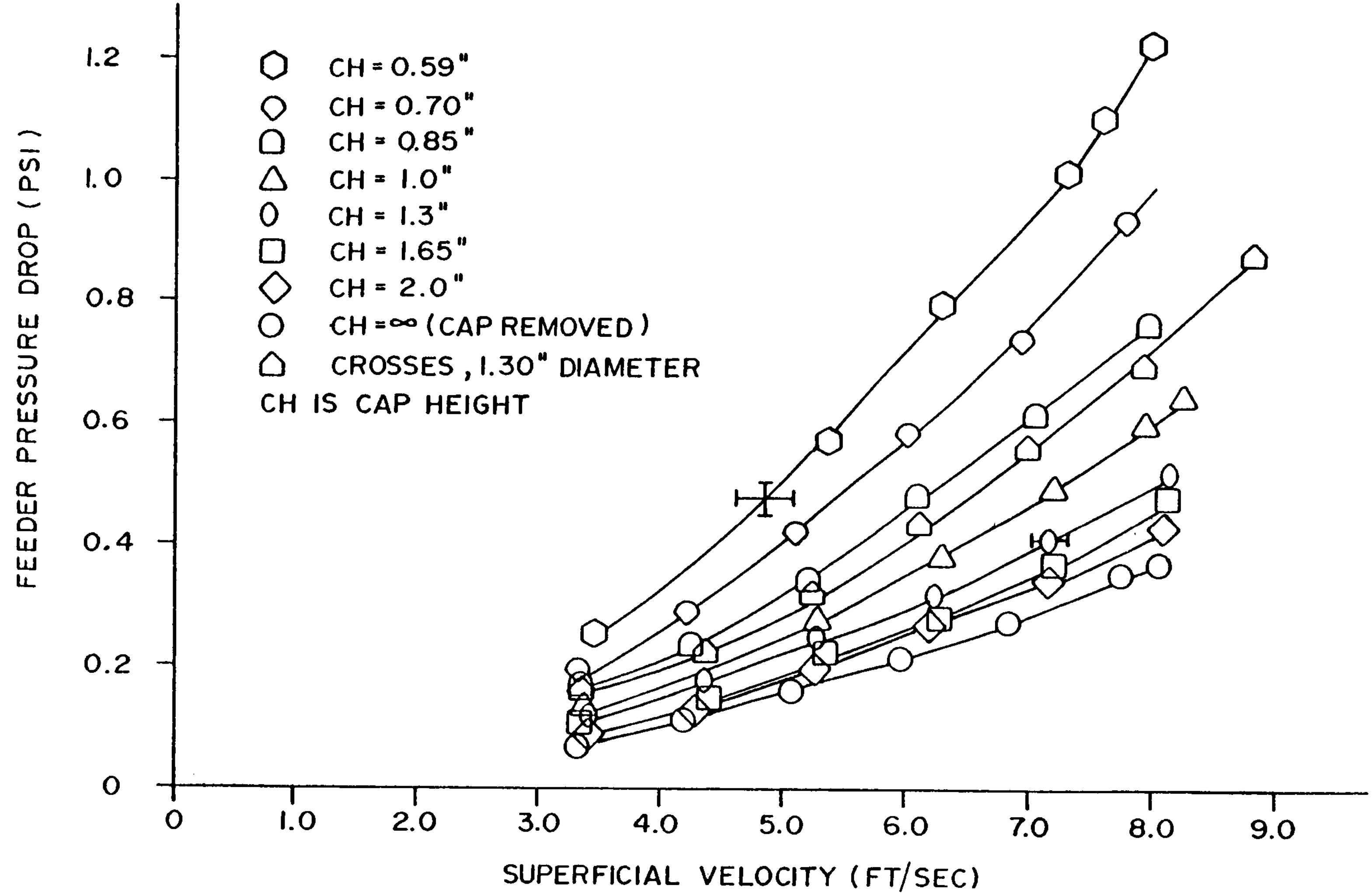

Figure A.8. Pressure Loss Versus Superficial Velocity, Crosses and Floating Cap [10].

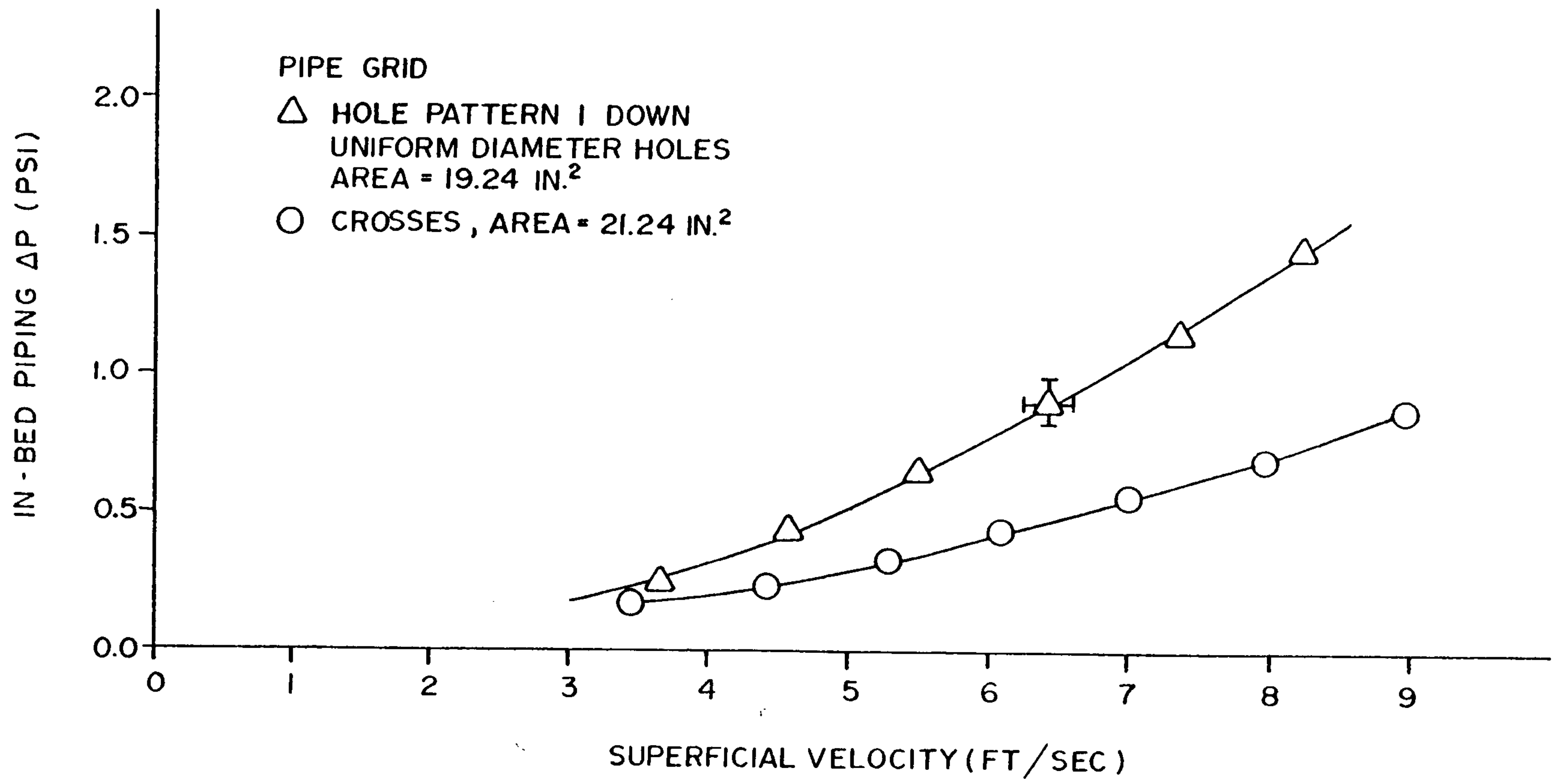

Figure A.9. Pressure Loss Versus Superficial Velocity, Crosses and Pipe Grid [11].

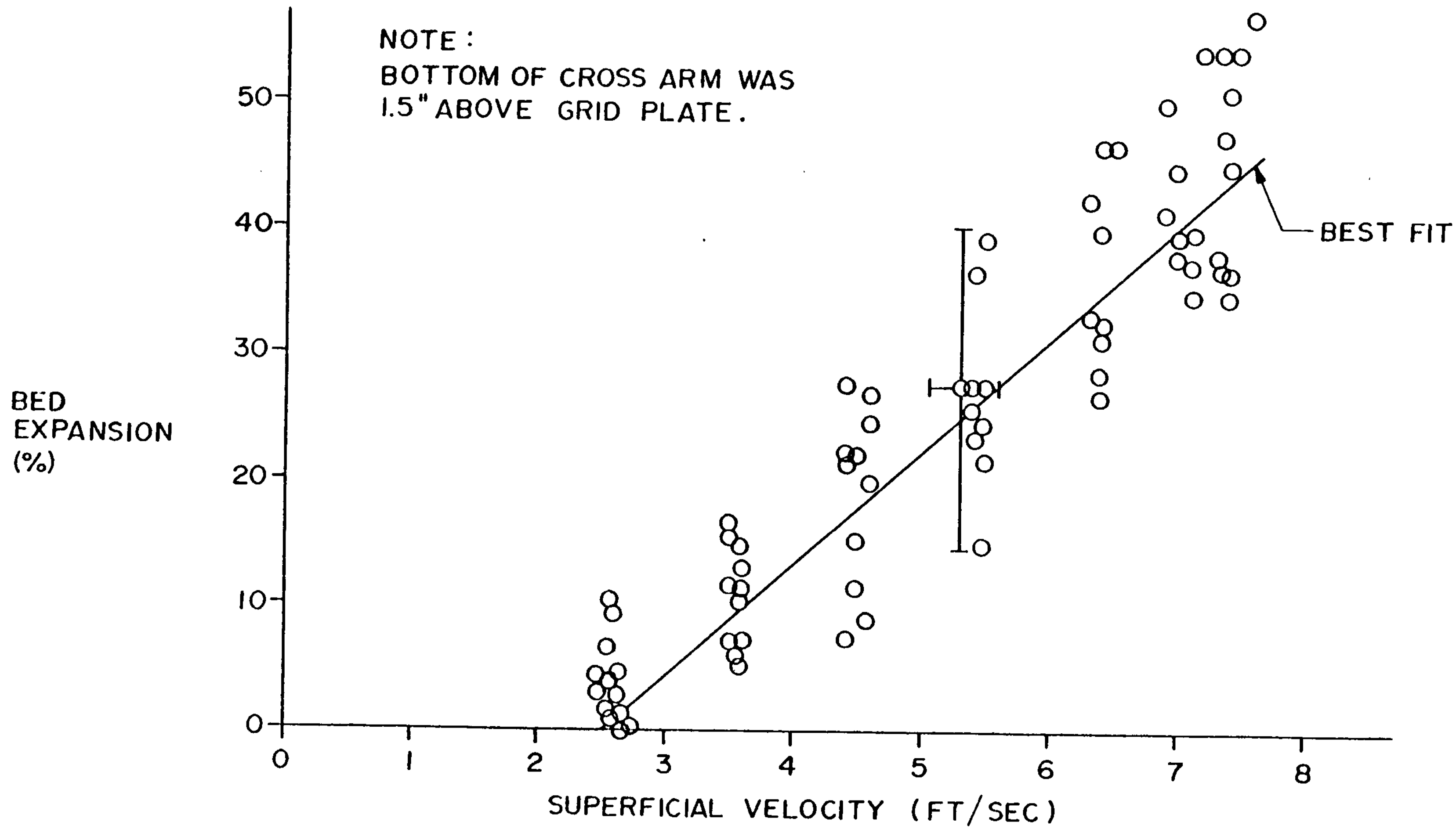

Figure A.10. Percent Bed Expansion Versus Superficial Velocity for the Crosses.

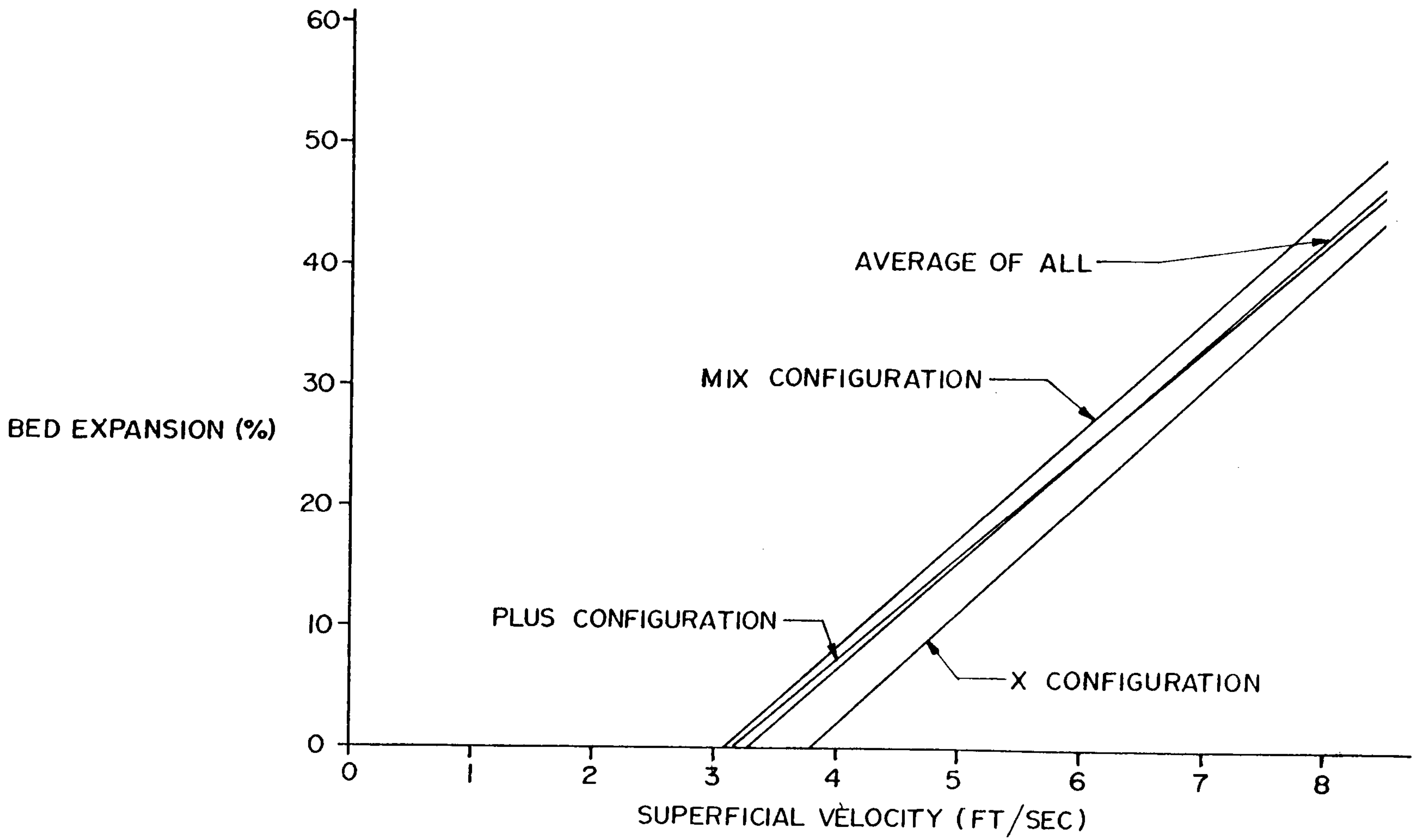

Figure A.11. Percent Bed Expansion Versus Superficial Velocity for Each Cross Orientation and All Orientations Combined.

TABLE A.2

BED EXPANSION[1] VERSUS SUPERFICIAL VELOCITY FOR THE CROSS FEEDER WITH 1.30 INCH DIAMETER ARMS

General Equation: $E = AV_s - B$
Units: E = Percent, V_s = ft/sec
Conditions: T = 80°F, P = 14.3 psia

Orientation	A	B	r^2
X	9.27	34.86	0.893
Plus	8.52	26.32	0.877
Mixed	9.02	27.81	0.860
All Averaged	8.96	29.87	0.856

[1]Bed expansion is corrected for the volume of heat transfer tubes covered. This is explained in Appendix C.

velocity, the all x system has a lower pressure loss (see Figure A.5, page 121) than the mixed system. It also has a lower percent bed expansion than the mixed system at all superficial velocities. This trend is caused by the same mechanism that causes the particular orientation to have a lower pressure loss. For example, the all x configuration had the least bed expansion because most of the air passed through the center of the bed, therefore, the air does not expand the bed as fully as other orientations. Of course, the mixed configuration had the most pressure drop, hence, the least number of main pathways through the bed. Average bed expansion for the crosses is compared to the feeders of Henry [10] and Knox [11] in Figure A.12. The differences are most likely due to the various interpretations of bed depth.

Amplitudes and frequencies of the lower bed pressure

The average amplitudes and the frequencies of the fluctuation of the lower bed pressure are shown in Tables A.3 and A.4 respectively. The average amplitude of the pressure fluctuation tends to decrease with decreasing bed depth and increase with increasing superficial velocity. The larger cross arm diameter seemed to make little difference nor did the particular orientation. The maximum amplitudes for each test are also shown in Table A.3. This pressure pulse is always significantly larger than the average amplitude. This is due to a passing bubble.

The frequency of fluctuation averaged about 2.5 cycles per second for bed depths of 11.5 inches and greater. The most notable characteristic is the doubling of the frequency for lower bed depths. This suggests that at large depths, the frequency is the result of only the

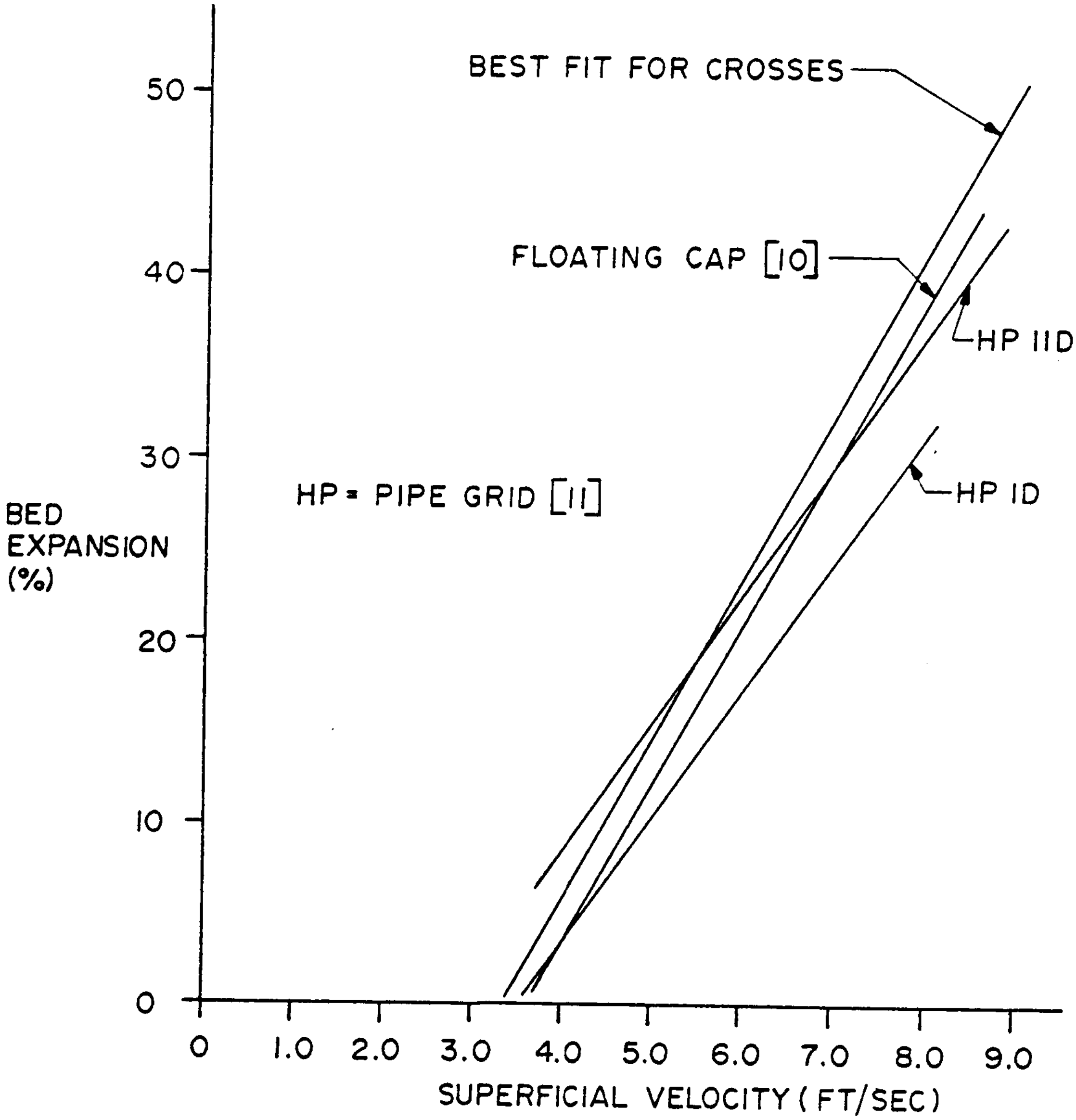

Figure A.12. Percent Bed Expansion Versus Superficial Velocity for Crosses, Floating Cap and Pipe Grid.

TABLE A.3

AVERAGE AMPLITUDES OF THE LOWER BED PRESSURE FLUCTUATIONS FOR THE CROSSES

Configuration	Mix	Mix	Mix	All+	All+	All+	Allx	Allx	Allx	Mix	Mix	Mix
Bed Depth (in)	16.25	12.75	7.0	16.75	11.5	7.0	16.25	11.75	7.0	16.38	12.5	7.5
Superficial Velocity Range (ft/sec)	Amplitudes (± in H_2O)						← Arm Diam. 1.30			Arm Diam. 1.42 → Amplitude (± in H_2O)		
3.6 - 3.7	---	---	---	0.7	0.2	---	---	---	---	---	---	---
4.5 - 4.7	1.0	---	0.2	1.1	0.6	0.3	1.1	0.6	1.0	0.8	0.4	---
5.4 - 5.6	1.5	1.0	0.5	2.5	1.5	1.5	1.3	1.1	1.0	1.2	1.1	1.0
6.3 - 6.6	2.0	2.0	0.7	2.5	1.8	1.5	2.0	1.2	1.0	2.2	1.7	1.2
7.3 - 7.5	3.0	2.5	0.6	3.0	2.0	1.2	2.1	1.7	1.0	3.0	2.5	1.5
7.9 - 8.5	3.0	2.5	0.6	3.5	2.0	1.2	2.5	1.7	1.0	4.0	2.5	1.5
8.2 - 8.6	3.5	3.0	0.6	3.0	2.1	1.5	2.7	2.0	1.0	4.0	2.6	1.5
	Maximum Amplitude (in H_2O)											
	±6.5	±6.0	±0.7	+9.0	+5.0	+3.0	+7.5	+4.0	±2.0	+8.0	+5.7	+3.0

TABLE A.4

FREQUENCIES OF THE LOWER BED PRESSURE FLUCTUATIONS FOR THE CROSSES

Configuration	Mix	Mix	Mix	All+	All+	All+	Allx	Allx	Allx	Mix	Mix	Mix
Bed Depth (in)	16.25	12.75	7.0	16.75	11.5	7.0	16.25	11.75	7.0	16.38	12.5	7.5
Superficial Velocity Range (ft/sec)	Frequencies (Cycles/sec)						← Arm Diam. 1.30			→ Arm Diam. 1.42		
3.6 - 3.7	---	---	---	2.6	---	---	---	---	---	---	---	---
4.5 - 4.7	2.5	---	5.0	2.0	---	4.2	2.5	2.9	6.0	2.7	3.0	---
5.4 - 5.6	2.6	2.4	5.1	2.4	---	6.0	2.8	3.2	5.6	2.9	2.8	4.9
6.3 - 6.6	2.5	2.2	4.9	2.3	2.2	6.0	2.4	3.4	5.6	3.0	2.4	4.8
7.3 - 7.5	2.5	2.4	4.5	2.3	2.5	6.1	2.7	3.6	5.8	2.7	2.5	4.9
7.9 - 8.5	2.0	2.3	4.6	2.0	2.5	5.7	2.5	3.3	5.4	2.1	2.8	4.5
8.2 - 8.6	2.5	2.3	4.5	2.4	2.4	6.0	2.7	3.3	5.4	2.2	2.8	4.6

cross closest to the pressure tap. At lower depths, another cross pressure wave can be detected. The two waves have approximately the same amplitude and frequency, but are out of phase when they reach the pressure tap because of the different distances each must travel. For this to be true, the waves would have to constructively interfere at some times and destructively interfere at other times. This phenomena was experienced and was evidenced by a beat pattern appearing on the strip chart.

The average amplitude data agree with that presented by Knox [11, p. 139] in relative magnitude as well as general trends. The average amplitudes from Henry [10, p. 123] are somewhat larger. The deep bed frequencies (above 10 inches) correspond to those of Knox [11, p. 14] for his deep beds. The shallow bed frequencies for Knox's feeder are also larger and this may suggest the same wave phenomena even though Knox's system was vastly different from the crosses.

The experimentally proven fact that any particular feed system displays a characteristic pressure frequency depending upon feeder configuration, bed depth and superficial velocity suggests that caution be exercised when building a feed system to avoid possible vibration problems that could arise due to resonance. The excessive vibrations that are caused by resonance could potentially damage bed insttrumentation, feeder components or heat recovery equipment.

Conclusions

Combined feeding with the four arm cross designed as shown was not acceptable because of the poor fluidization. The crosses could be used in a fluidized bed if they are modified and sufficiently tested. Modified designs of these crosses could possibly be used as a coal feed system in conjunction with a separate fluidization system.

Modified designs of these crosses could possibly be used as a coal feed system in conjunction with a separate fluidization system.

APPENDIX B

SPHERE CAP AND FLAT PLATE COAL FEED SYSTEMS

Sphere Feeder

Introduction

As an alternative to the floating cap, a feeder with a spherically shaped cap was designed. It consisted of a ball placed in a cage between the feed pipe exit and a flat plate. The flat plate was used in order to aid the ball with radial distribution of the coal. A schematic of the feeder is presented in Figure B.1.

Design

The gap was set by adjusting the plate height h. This is related to flow area in the following manner. The area of flow is a truncated cone of side length ℓ, base radius R and top radius $r\sin\theta$. This area is:

$$A_{Flow} = 2\pi \left(\frac{R+r\sin\theta}{2}\right)\ell \tag{B.1}$$

or simply, $A_F = \pi (R + r\sin\theta)\,\ell$ (B.2)

where r, R, ℓ and θ are defined in Figure B.1. The length ℓ is equal to the length j minus the sphere radius r.

$$\ell = j - r \tag{B.3}$$

The length j is given, using Pythagorean's theorem, by equation B.4.

$$j = [(h-r)^2 + R^2]^{\frac{1}{2}} \tag{B.4}$$

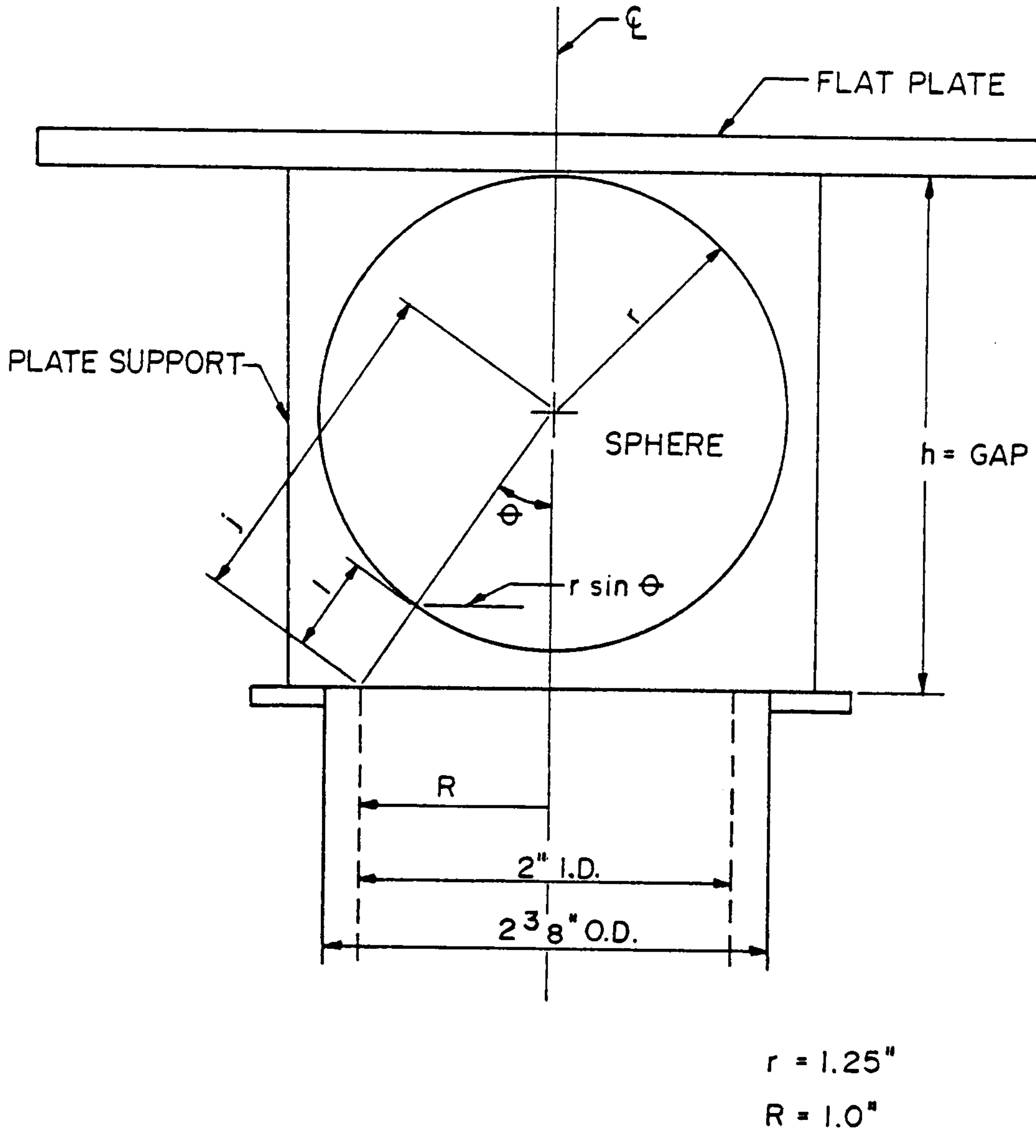

Figure B.1. Sphere Feeder Schematic.

Substituting this into equation B.3 gives the length ℓ in terms of plate height, h, sphere radius, r, and pipe radius, R.

$$\ell = j - r = [(h-r)^2 + R^2]^{\frac{1}{2}} - r \tag{B.5}$$

From Figure B.1, equation B.6 is obtained for the sin θ.

$$\sin\theta = \frac{R}{r+\ell} \tag{B.6}$$

This was substituted into equation B.2 to yield equation B.7.

$$A_F = \pi[R + r\,(\frac{R}{r+\ell})]\,\ell. \tag{B.7}$$

This simplifies to equation B.8.

$$A_F = \pi\,(\frac{2r\,R\ell + R\ell^2}{r+\ell}). \tag{B.8}$$

Equation B.5 was substituted into equation B.8 and through considerable algebraic reduction equation B.9 was obtained.

$$A_f = \frac{\pi(R^3+Rh^2-2rRh)}{[(h-r)^2 + R^2]^{\frac{1}{2}}}\ . \tag{B.9}$$

Data for three separate gaps are given in Figure B.2. The flow area for each gap is given below for a 2.5 inch diameter sphere (mass of 1091.40 grams) and the standard 2.0 inch schedule 40 feed pipe (R = 1.0" and r = 1.25").

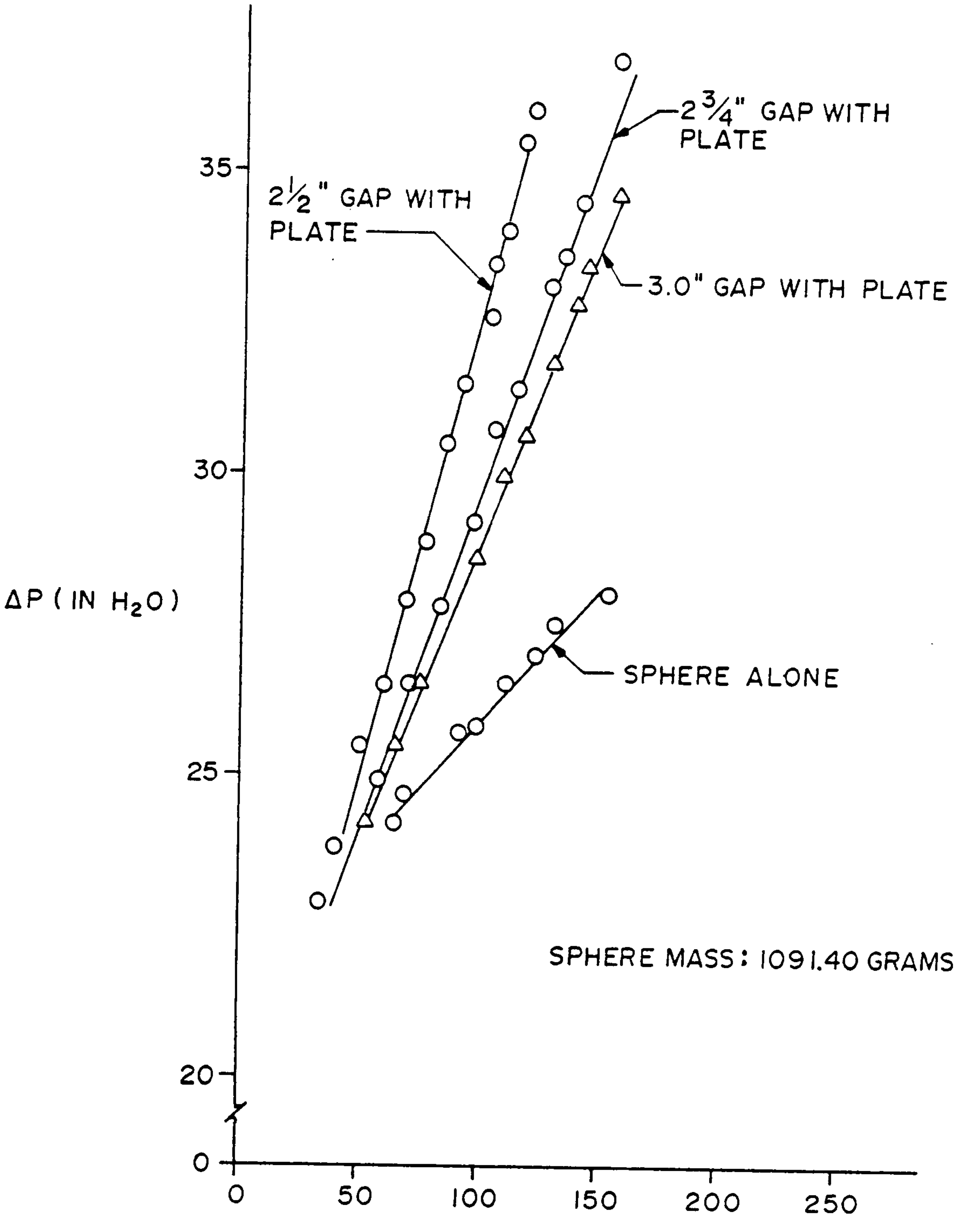

NOTE:
THE ERROR BANDS ARE SMALLER THAN THE SYMBOLS.

Figure B.2. Sphere Pressure Loss Versus Flow Rate, Air Only.

h(in.)	A_F (in.^{2})
2.25	0.97
2.75	2.94
3.00	3.90

Data for a sphere alone are also presented on Figure B.2 for comparison.

Air-only results

The sphere pressure loss versus flow rate relationship is seen to be linear. The sphere was very stable in the flow, in fact, it would stay in the flow without any cage. The larger gap decreases pressure loss as would be expected.

A flat plate was also designed with a two inch diameter hole cut into the top. The results of an air test with one gap are given in Figure B.3. The hole reduces the pressure loss by allowing air to pass through the plate.

Limestone tests

The sphere feeder was tested in a limestone bed. It was cycled several times and hung open once. Very little limestone, 15 pounds, drained down the feed line. The clog was a result of insufficient clearance between the ball and cage. The ball was 2.5 inches in diameter, the cage had a 2.688 inch inside diameter and the largest bed particle was 0.25 inch. Clogging would have been eliminated if the cage inside diameter was 2.813 inches or greater.

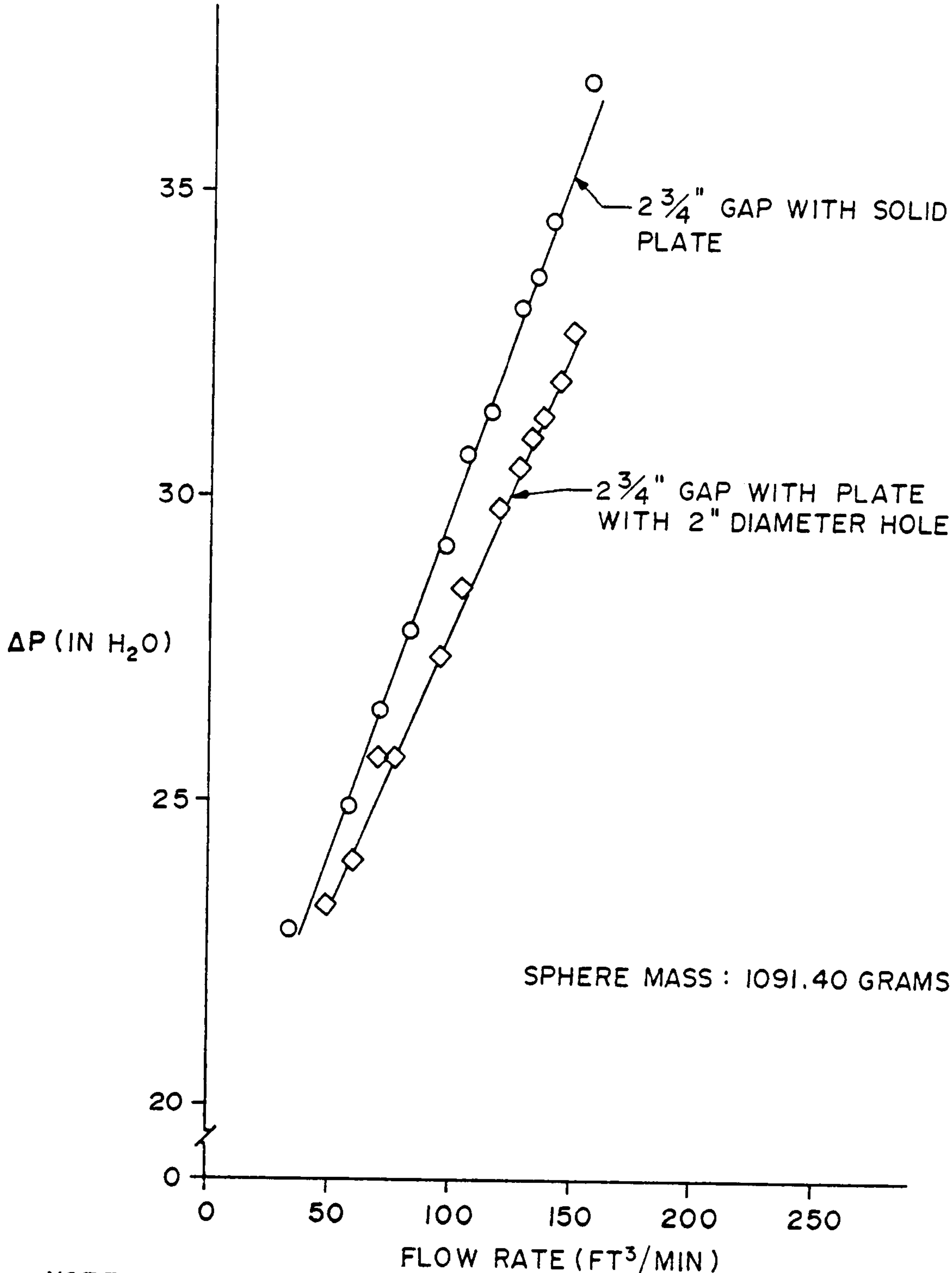

NOTE :
THE ERROR BANDS ARE SMALLER THAN THE SYMBOLS.

Figure B.3. Sphere Pressure Loss Versus Flow Rate, Solid Top and Top with Hole, Air Only.

Conclusions

The sphere feeder is very desirable for three reasons. One, the pressure loss versus flow rate variation is linear. Two, the ball is very aerodynamically stable in the air flow. No tilting or hysteresis was present as with the flat cap. Three, the ball would wear evenly over its entire surface. This also avoids another of the problems encountered in flat cap design. With more study, the sphere feeder could be a very desirable design. Investigation should concentrate in the area of smaller mass spheres and superior cages.

Flat Plate Feeder

Introduction

A flat plate feeder was also examined. A 6.5 inch diameter plate was tested with air only at three heights: 0.25 inch, 0.50 inch and 0.75 inches.

Design

The flat plate was designed to prevent bed drainback by the angle of repose method. This was done by having the angle measured from the horizontal, between the plate and the exit pipe edge (the angle vertex was placed at the pipe edge) to be less than the limestone angle of repose. The angle of repose was defined as the angle, measured from horizontal, which the limestone makes when placed in a free pile. This angle has a value of 30 degrees. The feeder angle, ϕ, was determined from equation B.10.

$$\phi = \tan^{-1} \left[\frac{\text{Plate Radius - Pipe Outside Radius}}{\text{Plate Height}}\right]. \qquad \text{(B.10)}$$

For the 6.5 inch diameter plate, 2.325 inch outside diameter pipe and 0.75 inch maximum height, ϕ was determined to be approximately 20^{o}. This is much less than the angle of repose, so drainback should be prevented for a slumped bed. This method of preventing drainback would probably not be effective because of the interaction between slumped and nonslumped bed sections. Thus, a purge flow of air would be required to keep bed material from entering the feed lines.

Results

Air only test results are presented in Figure B.4. The data match very well with the valve cap results as shown by the projections. This illustrates the fact that valve caps operate as flat plates when fully open and this also shows how little outside diameter affects pressure loss. No limestone or coal feed tests were performed with the flat plate.

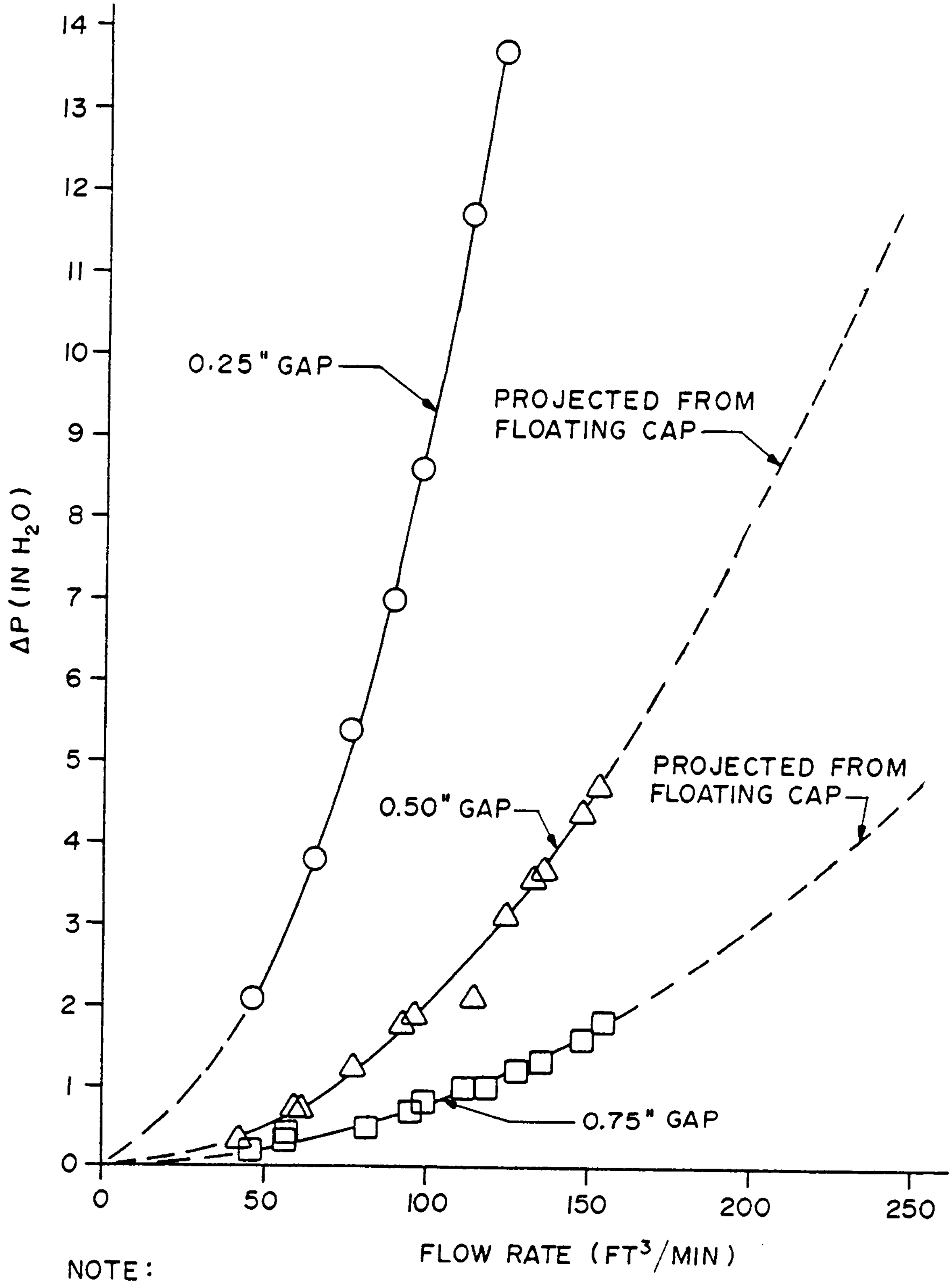

NOTE:
THE ERROR BANDS ARE SMALLER THAN THE SYMBOLS.

Figure B.4. Flat Plate Pressure Loss Versus Flow Rate for Various Plate Gaps, Air Only.

APPENDIX C

DATA REDUCTION AND ERROR ANALYSIS

Data Reduction

Introduction

In order to properly evaluate feed systems, extensive data were taken to allow comparison of the feeders in various aspects. Much of the data taken was in elementary form and had to be reduced to a meaningful parameter. This appendix covers how each of these reductions were effected.

Pressure

Plenum box, lower bed, and upper bed pressures were recorded on a Gould Brush 2400 strip chart recorder. For the valve cap, sphere and flat plate feeders, the pressure just below the coal exit point was also recorded on the strip chart. The average pressure, the average amplitude of fluctuation, and the frequency of fluctuation were taken off traces from this recorder. Average pressure and amplitude of fluctuation were determined by inspection. Frequency of fluctuation was determined by counting the number of pressure cycles in a given increment of time.

Barometric pressure was read from a standard mercury-in-glass barometer and was corrected for temperature and altitude.

Fluidization air flow rate

The fluidization air flow rates was measured using a calibrated orifice designed and tested by Knox [11, pp. 78-83] and Henry [10, pp. 30-36]. The pressure drop across the orifice was measured with a water-in-glass manometer and the corresponding flow rate was taken from an orifice calibration curve. Flow rate was converted to the actual bed conditions by the use of the ideal gas laws for temperature and pressure. This is shown in equation C.1.

$$Q_{FA_B} = Q_{FA_A} \, (T_B/T_A) \, (P_A/P_B). \tag{C.1}$$

Transport air flow rate

The transport air flow rate was measured by the use of a standard orifice meter. The discharge equation for an orifice is

$$Q = K_o A (2g\Delta h)^{\frac{1}{2}}. \tag{C.2}$$

In this equation, K_o is the flow coefficient which depends upon the particular orifice and pipe arrangement and the flow. A is the orifice area, g is the standard gravitational acceleration, and Δh is the change in head across the orifice in units of length of fluid flowing.

To determine Δh in inches of air from a water-in-glass manometer, equation C.3 was used

$$\Delta h = \Delta s \, \frac{\gamma_{H_2O}}{\gamma_{Air}} \, . \tag{C.3}$$

Δs is the manometer deflection in inches of water, γ_{H_2O} is the specific weight of water and γ_{Air} is the specific weight of air. Equation C.3 can be substituted into equation C.2 to obtain equation C.4.

$$Q = K_o \, A \, (2_g \, \Delta s \, \frac{\gamma_{H_2O}}{\gamma_{Air}} \,)^{\frac{1}{2}} \tag{C.4}$$

The orifice was designed with an orifice diameter to pipe diameter ratio (d/D) of 0.6. This will give an orifice flow coefficient, K_0, of 0.65 which remains constant with flows as low as 50 cubic feet per minute. Even at 10 cubic feet per minute, K_0 varies less than 5 percent, therefore, this equation was applied even for very low flows [13, p. 422].

To determine the flow rate at the orifice, the specific weight of air must be evaluated at the orifice conditions in the pipe which will be denoted by the subscript P. From standard conditions, denoted by the subscript 0, the specific weight of air at the pipe conditions is given by equation C.5.

$$\gamma_{Air\ P} = \gamma_{Air\ 0} \left(\frac{T_0}{T_P}\right) \left(\frac{P_P}{P_0}\right). \qquad (C.5)$$

Substituting equation C.5 into equation C.4 and substituting values for $\gamma_{Air\ 0}$, γ_{H_2O} (this is assumed to remain constant over the range of experimental conditions which were assumed to be T_0 = 80°F and P_0 = 14.3 psia), g, A and K_0 gives equation C.6.

$$Q_{TA_P} = 7.664\ (\Delta s\ T_P/P_P)^{\frac{1}{2}} \qquad (C.6)$$

In equation C.6, Q_{TA_P} is given in cubic feet per minute when Δs is in inches of water, T_P is in degrees Rankine and P_P is in absolute pounds per square inch. To evaluate the flow rate at the bed, Q_{TA_B}, use equation C.6 with equation C.7.

$$Q_{TA_B} = Q_{TA_P}\ (T_B/T_P)\ (P_P/P_B) \qquad (C.7)$$

$$Q_{TA_B} = 7.664\,(\Delta s\ P_P/T_P)^{\frac{1}{2}}\ (T_B/P_B) \qquad (C.8)$$

Again, equation C.8 gives Q_{TA_B} in cubic feet per minute when Δs is in inches of water, T_P and T_B in degrees Rankine and P_P and P_B in absolute pounds per square inch.

Bed expansion

Bed expansion is characteristic of a particular fluidizing system. It can be used as a basis of comparison between fluidizing systems. Bed expansion is a function of bed superficial velocity and fluidization system. It was calculated by using the bed depth as read from a tape measure attached to the bed wall. The bed depth was corrected to account for feeder volume and the volume of the heat transfer tubes. The feeder volume divided by bed area was always subtracted from the bed depth, however, the volume of the heat transfer tubes changed as the bed depth changed because various numbers of tubes were covered. This change was accounted for by the use of Table C.1. For bed depths between those listed in the table, a simple linear interpolation was used. Expansion is defined as the bed depth minus the slumped or no fluidization depth divided by the slumped depth times 100.

Coal mass flow rate

Coal was metered into a three inch diameter pneumatic conveying line by a Vibra-screw Volumetric Live-bin Screw Feeder [10, pp. 23 and 24]. The coal mass flow rate ($\dot{m}$) is only a function of the angular speed ($\dot{\theta}$) of the screw. The screw feeder was calibrated by setting an angular speed and measuring the mass of coal that was fed in a particular interval of time. The result from a linear regression of the data [16, p. 87] is given in equation C.9 where $\dot{m}$ is in pounds per minute when $\dot{\theta}$ is in R.P.M.

TABLE C.1

BED DEPTH CORRECTION FOR VARIOUS HEIGHTS
FOR UT TEST FACILITY

Bed Depth (in)	Subtract Volume (ft^3)	Height Correction (in)
8.0	0	0
9.0	0.06545	0.196
10.0	0.13090	0.393
11.0	0.13090	0.393
12.0	0.21817	0.654
13.0	0.30544	0.916
14.0	0.30544	0.916
15.0	0.37088	1.113
16.0	0.43633	1.309
17.0	0.43633	1.309
18.0	0.52360	1.571
19.0	0.61087	1.833
20.0	0.61087	1.833
21.0	0.67632	2.029
22.0	0.74176	2.225
23.0	0.74176	2.225
24.0	0.82903	2.487
25.0	0.91630	2.749
26.0	0.91630	2.749
27.0	0.98175	2.945
28.0	1.04720	3.142
29.0	1.04720	3.142
30.0	1.13446	3.403
31.0	1.22173	3.665
32.0	1.22173	3.665
33.0	1.28718	3.862
34.0	1.35263	4.058
35.0	1.35263	4.058
36.0	1.43990	4.320
37.0	1.52720	4.581

$\dot{m} = 0.3511\ \dot{\theta}$. (C.9)

Angular speed was recorded from a tachometer attached to the screw and was read as data from the control panel.

Coal feed tests

When coal was fed into the bed, samples were taken using the sample probes. The samples contained a mixture of coal and limestone with a typical sample mass of 60 to 90 grams (3.32 cubic inches). The coal was separated from the limestone by passing a hand held magnet over the sample. Once the two constituents were separate, the mass of each was recorded. Because recycling was never 100 percent effective, some coal always remained mixed in the limestone. This was referred to as background coal.

Two separate background tests were performed by filling the bed with limestone from a typical recycle, running the blower to fluidize the bed for the length of time of a normal coal feed test and taking bed samples with the probes. It should be noted that it was extremely important to run the blower because the less dense coal floated to the top of the fluidized bed, therefore reducing the coal concentration at the probes. The background concentration ratio was found to be 0.0026 grams of coal per gram of limestone. This was significant because typical sample ratios were between 0.01 and 0.04 grams of coal per gram of limestone. With the background ratio, the sample could be corrected to show the results of coal feeding only, by subtracting the mass of coal due to background. This was effected by multiplying the sample's limestone mass by the background ratio and subtracting this from the measured coal mass. This difference was the corrected coal mass.

To complete this reduction, the corrected coal mass was divided by the total sample mass to produce a ratio of the mass of coal fed by the distribution system to the total sample mass. All of these ratios (twelve were obtained unless a probe failed to open, then there were nine) were averaged to yield a bed average ratio. Each sample ratio was compared to the bed average ratio as a percent with the bed average ratio used as the basis, i.e., sample ratio minus the bed average ratio divided by the bed average ratio times 100. This percentage comparison would show whether a given location was coal rich or lean compared to the bed average. For any feeder, a random distribution of lean and rich regions is desirable.

Error Analysis

Introduction

In any experiment, the data acquired have some associated uncertainty because of inaccuracies in instrumentation and human error. Because the raw data have uncertainties calculated values also have error. The uncertainty in a calculated term can be determined by the method of Kline and McClintock presented in Holman [18].

Error analysis - Kline and McClintock method [18]

The uncertainty in a calculated result, R, is to be determined. Let R be a function of n independent variables, X_1, X_2, . . . X_n.

$$R = R(X_1, X_2, \ldots, X_n)$$

Let the uncertainty in each of these variables be denoted by w_1, w_2, . . . w_n respectively. Then the uncertainty in R is denoted by w_R and given by equation C.11.

$$w_R = [(\frac{\partial R}{\partial X_1} w_1)^2 + (\frac{\partial R}{\partial X_2} w_2)^2 + \ldots + (\frac{\partial R}{\partial X_3} w_3)^2]^{\frac{1}{2}} \quad (C.11)$$

This equation was used to determine the uncertainties in each of the calculated values.

Experimental apparatus - information

Table C.2 is a listing of all of the equipment utilized in this experiment. It also includes the range, least count and serial numbers of the instruments. The least counts of the instruments can be used to determine the accuracy of their measurements. These accuracies are shown in Table C.3.

Error analysis

Using equation C.11 and the values listed in Table C.3, the uncertainties in all of the calculated parameters were determined and listed in Table C.4. These uncertainties are shown as error bands on some figures displaying these parameters. Some error bands are not shown because they are smaller than the symbols used to construct the figures.

TABLE C.2

INSTRUMENTATION USED IN EXPERIMENT

Instrument	Company	Serial # / Model #	Range	Least Count	Systems Employing Instrument	Measurement
Manometer	Meriam	H37182 33KB35	0-30 inches H_2O	0.1 inches H_2O	Fluidization and Transport Air Flow	Orifice ΔP Pressure
Pressure Gauge	U.S. Gauge	-/18636	0-15 psi	0.05 psi	Transport Air Flow	Air Pressure
Digital Thermocouple Reader	Omega	590018 J2/65A	-328 to 1432°F	0.5°F	Fluidization and Transport Air Flow Bed, Blower and Plexiglas	Inlet and Orifice Temp Temp/Safety
Tachometer	Reliance Electric	GE-18829/-	0-155 RPM	5 RPM	Coal Feed	Vibra-screw Angular Speed
Strip Chart Recorder	Gould	00357/ 2007-4404-00	Variable	Variable	Plenum, Lower and Upper Bed, Coal Feed Transport Air Flow	Pressure and Differential Pressure
Barometer	Mounted by Experiment		25.5-32.7 in Hg	0.01 in Hz	Fluidization and Transport Air	Atmospheric Pressure
Barometer Thermometer	Mounted on Barometer		-10-120°F	2°F	Barometer	Temperature

TABLE C.2 (Cont.)

Instrument	Company	Serial # / Model #	Range	Least Count	Systems Employing Instrument	Measurement
Stopwatch	Hever	-/101	∞	0.2 sec	Blower	Time
Tape Measure	---	---	0-7 ft	0.063 in	Bed	Bed Depth
Balance	Ainsworth	57917/A-4	0-160 g	±0.0001 gram	Bed Sampling	Coal and Limestone Mass
Balance	Ohaus	UT 1257/-	0-2600g	0.1 gram	Flat Cap	Flat Cap Mass

TABLE C.3

EXPERIMENTAL MEASUREMENTS AND ASSOCIATED UNCERTAINTIES

Description of Measurement	Symbol	Experimental Uncertainty (±)
Transport Air Pressure in the Pipe	$P^*_{P_g}$	0.05 psi
Atmospheric Pressure	P_{ATM}	0.0049 psi
Bed Pressure (All tests except flat cap air only)	P_{B_g}	0.5 in H_2O
Bed Pressure (Flat cap air only tests)	P'_{B_g}	0.05 in H_2O
Above Bed Pressure	P_{AB_g}	0.2 in H_2O
Plenum Box Pressure	P_{P_g}	0.5 in H_2O
Dense Phase Coal Feeder Pressure	P_{C_g}	0.05 in H_2O
Blower Inlet Air Temperature	T_A	0.5° F
Bed Temperature	T_B	0.5° F
Transport Air Temperature in the Pipe	T_P	0.5° F
Transport Air Manometer ΔP	h_s	0.05 in H_2O
Fluidization Air Flow Rate [11, p. 82]	Q_{FA_A}	66.7 cfm
Slumped Bed Height	h_s	0.25 in
Operating Bed Height	h	2.0 in
Vibra-screw (Live-bin Feeder) Angular Speed	$\dot{\theta}$	2.5 RPM
Coal Sample Mass	M_C	0.0005 grams
Limestone Sample Mass	M_{LS}	0.0005 grams

TABLE C.4

CALCULATED PARAMETERS AND THEIR UNCERTAINTIES

Description of Parameter	Symbol	Defining Equation	Calculated Uncertainty (±)
Transport Air Pressure in Pipe (Absolute)	P_p	$P_p = P_{p_g} + P_{ATM}$	0.0502 psi
Bed Pressure (Absolute) (Not Flat Cap)	P_B	$P_B = P_{B_g} + P_{ATM}$	0.0187 psia
Bed Pressure (Absolute) (Flat Cap)	P'_B	$P'_B = P'_{B_p} + P_{ATM}$	0.0502 in. H_2O
Pressure Drop Across Limestone Bed	ΔP_B	$\Delta P_B = P_{B_g} - P_{AB_g}$	0.54 in. H_2O
Pressure Drop Across Fluidization System	ΔP_F	$\Delta P_F = P_{p_g} - P_{B_g}$	0.71 in. H_2O
Pressure Drop Across Dense Phase Feed	ΔP	$\Delta P = P_{C_g} - P'_{B_g}$	0.071 in. H_2O
Fluidization Air Flow Rate (Bed Conditions)	Q_{FA_B}	$Q_{FA_B} = Q_{FA_A} \left(\frac{T_B}{T_A}\right)\left(\frac{P_{ATM}}{P_B}\right)$	68.2 cfm
Superficial Velocity	V_s	$V_s = \frac{Q_{FA_B}}{240}$	0.28 ft/sec

TABLE C.4 (Continued)

Description of Parameter	Symbol	Defining Equation	Calculated Uncertainty (±)
Transport Air Flow Rate (Bed Conditions)	Q_{TA_B}	$Q_{TA_B}=7.664(\Delta s \frac{P_p}{T_p})^{\frac{1}{2}}(\frac{T_B}{P_B})$	0.58 cfm
Transport Air Flow Rate (Bed Conditions)	Q'_{TA_B}	$Q'_{TA_B}=7.664(\Delta s \frac{P_p}{T_p})^{\frac{1}{2}}(\frac{T'_B}{P'_B})$	0.51 cfm
Percent Bed Expansion	E	$E=(\frac{h-h_s}{h_s})\ 100$	13.6%
Momentum Correction Factor	K	$K=\frac{\pi d^2 mg}{4\rho Q^2}$	0.044
Coal Mass Flow Rate	$\dot{m}_{Coal}$	$\dot{m}_{Coal}=0.3511\dot{\theta}$	0.88 lbm/min
Corrected Coal Mass	m_{cc}	$m_{cc}=m_c-0.0026m_{LS}$	0.0005 grams
Total Mass	m_T	$m_T=m_c+m_{LS}$	0.0007 grams
Corrected Coal to Total Mass % Ratio	R*	$R=\frac{m_{cc}}{m_T}\ 100$	0.0006
Bed Average R	$\bar{R}$*	$\bar{R}=\frac{1}{n}\Sigma R$	0.0021
Corrected Coal to Limestone Comparison			
Percent Ratio	C*	$C=\frac{R-\bar{R}}{\bar{R}}\ 100$	0.11

APPENDIX D

SMALL DIAMETER VALVE CAP DESIGN

Small Diameter Valve Cap Design

Four bar cage design

The problem was to design the smallest diameter cap that would fit inside a 2.875 inch inside diameter cage and completely cover a 2.0 inch schedule 40 pipe regardless of the cap's location inside the cage. (The 2.875 inch inside diameter was superseded by 3.0 inches later in the program.) For safety, it was decided to design the cap to reach the outside edge of the pipe which is 2.375 inches in diameter. The geometry for a four bar cage is shown in Figure D.1. Four bars were used instead of three because the cap could be made smaller. A purely graphical solution yielded a cap radius of 1.344 inches. The analytic solution is covered next.

Referring to Figure D.1, the three governing equations from purely geometric considerations are:

$$r_s = r_c \cos \alpha + x \cos 45^{\circ} \qquad (D.1)$$

$$x \sin 45^{\circ} = r_c \sin \alpha \qquad (D.2)$$

$$r_c = x + r_o \qquad (D.3)$$

In these equations, r_s is the inside radius of the cage, r_c is the cap radius to be determined and r_o is the pipe outside radius. x and α are both defined as shown.

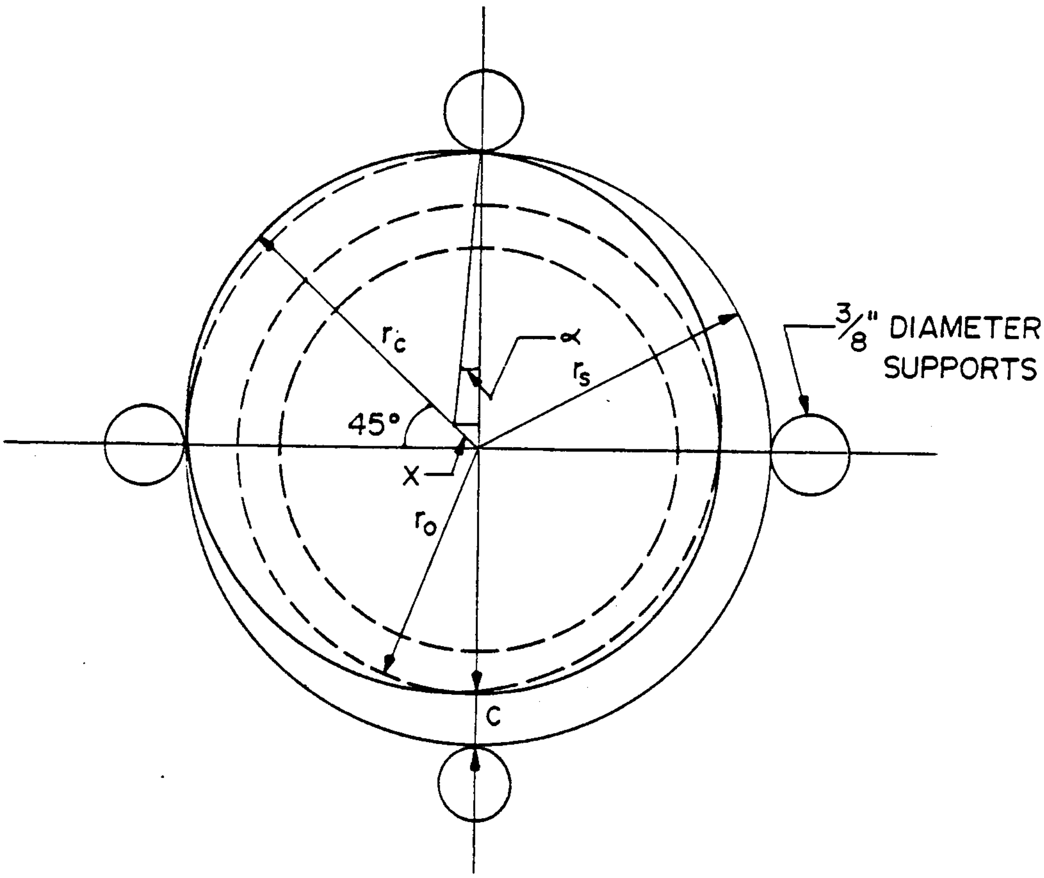

r_c = CAP RADIUS (CALCULATED)

r_o = PIPE OUTSIDE RADIUS (1.188")

r_s = CAGE SUPPORTS INSIDE RADIUS (1.438")

C = OPERATING CLEARANCE

Figure D.1. Small Diameter Valve Cap Four-Bar Geometry.

Using equation D.3, solving for x and substituting this into D.2 one obtains equation D.4

$$(r_c - r_o) \sin 45^o = r_c \sin \alpha . \tag{D.4}$$

Solving for sin α in D.4 yields:

$$\sin \alpha = \frac{1}{r_c} (r_o - r_o) \sin 45^o. \tag{D.5}$$

Again using equation D.3 solving for x and substituting this into D.1 gives equation D.6.

$$r_s = r_c \cos \alpha + (r_c - r_o) \cos 45^o. \tag{D.6}$$

From trigonometry, $\cos \alpha = (1 - \sin^2\alpha)^{\frac{1}{2}}$, thus equation D.6 becomes:

$$r_s = r_c(1 - \sin^2\alpha)^{\frac{1}{2}} + (r_c - r_o) \cos 45^o. \tag{D.7}$$

Substitute equation D.5 into equation D.7 to obtain equation D.8

$$r_s = r_c \left[1 - \frac{1}{r_c^{\,2}} (r_c - r_o)^2 \sin^2 45^o\right]^{\frac{1}{2}} + (r_c - r_o) \cos 45^o. \tag{D.8}$$

Or simply,

$$r_s = \left[r_c^{\,2} - (r_c - r_o)^2 \sin^2 45^o\right]^{\frac{1}{2}} + (r_c - r_o) \cos 45^o. \tag{D.9}$$

This can be easily solved by trial and error when the appropriate values are inserted for r_s and r_o, 1.438 inches and 1.188 inches respectively. The minimum calculated cap radius was found to be 1.3365 inches. This would be a diameter of 2.673 inches. 2.688 inches was the diameter used.

Three bar cage design

To employ the 2.688 inch diameter cap for a three bar cage, the supports must be moved in closer. This is because the cap can sit further back between supports. The basic geometry is shown in Figure D.2.

Referring to the figure, the three basic equations are:

$$r_c \sin \alpha' = r_s' \sin 60^0 \tag{D.10}$$

$$x' + r_c = r_o + r_s' \cos 60^0 \tag{D.11}$$

$$x' = r_c \cos \alpha' \tag{D.12}$$

The parameters in these equations are defined as follows. The new cage inside radius that is to be calculated is r_s'. The primes denote values for the three-bar geometry. The pipe outside radius is r_o and the cap radius is r_c. x' and α' are defined as shown in Figure D.2. This system of equations contained three unknowns: r_s', x', and α'. They were solved in the following manner.

The first step to the solution was to substitute equation D.12 into equation D.11.

$$r_c \cos \alpha' + r_c = r_o + r_s' \cos 60^0. \tag{D.13}$$

Equation D.10 was solved for r_s' and substituted into equation D.13.

$$r_c \cos \alpha' + r_c = r_o + (r_c \frac{\sin\alpha'}{\sin 60^\circ}) \cos 60^0. \tag{D.14}$$

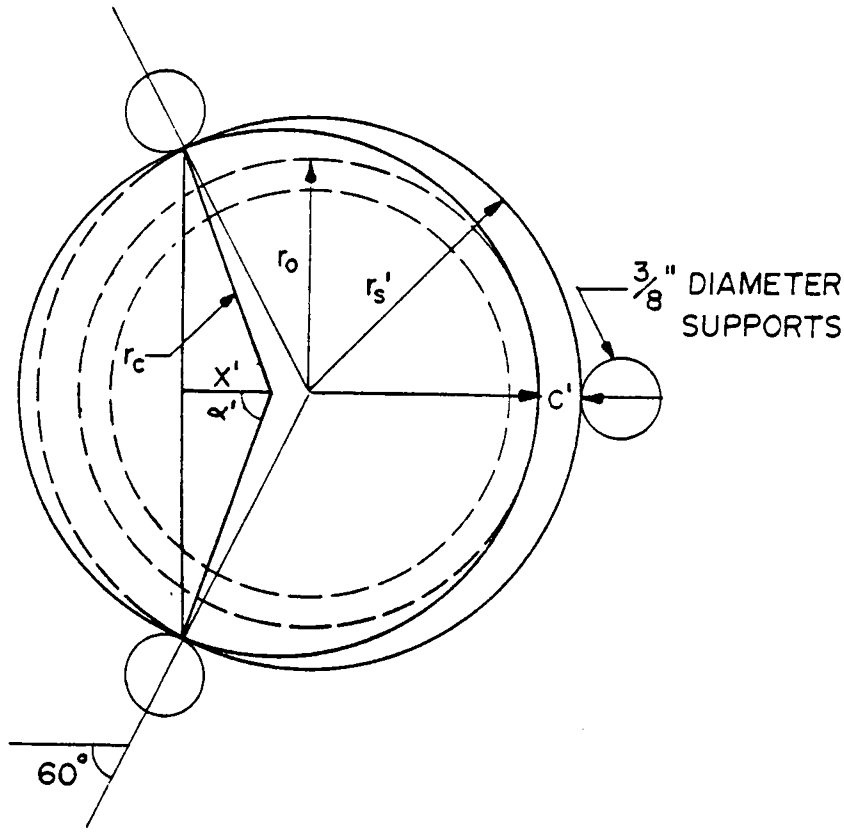

r_c = CAP RADIUS (1.344")

r_o = PIPE OUTSIDE RADIUS (1.188")

r_s' = CAGE SUPPORTS INSIDE RADIUS (CALCULATED)

C' = OPERATING CLEARANCE

Figure D.2. Small Diameter Valve Cap Three-Bar Geometry.

This equation simplifies to equation D.15

$$r_c - r_o = r_c\ (\cot 60^0 \sin \alpha' - \cos \alpha'). \qquad (D.15)$$

This equation was solved by trial and error for a cap radius of 1.344 inches and a pipe outside radius of 1.188. This gave a value of α' of 65.78^0 (1.148 rad). From equation D.10, the cage inside radius is determined to be 1.415 inches. This is a cage inside diameter of 2.830 inches.

Cage clearances

For the four bar cage, the minimum clearance was the difference between the cage inside diameter ($2\ r_s$) and the cap diameter ($2\ r_c$). This was 0.188 inches. The minimum clearance occurs only when the cap rests on one cage support and its diameter lies along the pipe diameter. During operation, the cap does not sit as this, instead it rests as shown in Figure D.1. The clearance, C, in this position is given by equation D.16.

$$C = r_s - (r_c \cos \alpha - x \sin 45^0). \qquad (D.16)$$

Equation D.3 was solved for x and equation D.2 was solved for α. With these values, C was found to be 0.209 inches.

For the three bar cage, the operating clearance, C', is given by equation D.17.

$$C' = r_s' - [r_c - (r_s' \cos 60° - x')]. \qquad (D.17)$$

This simplifies to:

$$C' = r_s' (1 + \cos 60°) - r_c - x'. \qquad (D.18)$$

Equation D.11 was used to obtain x', then equation D.18 was used to solve for C'. The three-bar clearance, C', was found to be 0.227 inches. (Although of no practical concern, the clearance when the cap rests on one bar is 0.108 inches.)

Small diameter valve cap - air only design

The first cap designed was made to remain fully open at the conditions outlined in Chapter 3. Using equations 6.8 and 6.17 for a 0.75 inch gap, K was found to be 1.30 and the weight to be 0.364 pounds. The cap height was calculated via equation D.19 with a steel density, ρ_s, of 0.279 pounds per cubic inch.

$$w = (\text{Volume}) \left(\frac{\rho_s g}{g_c}\right) = \left[\frac{\pi}{4} (d^2)\ h\right] \left(\frac{\rho_s g}{g_c}\right) = 0.364. \qquad (D.19)$$

This equation gave a valve of h equal to 0.230 inches. The actual cap manufactured was less than this height to provide a conservative margin for design. The actual thickness manufactured was 0.20 inches.

Small diameter valve cap - air plus solids design

To initiate the design of the value cap, equation 6.16 was employed. This equation determines the maximum weight which can be supported by given feed conditions. The equation is repeated below as equation D.20.

$$w_{Total} = \frac{\dot{m}_{Air}\ V_{Air}}{g_c}\ (K+JS). \qquad (D.20)$$

As a design basis, the solid mass flux to air mass flux ratio, J, was given a typical value of 2.0. The solid velocity slip ratio, S, was estimated to be about 0.80.

The air flow rate used was 97.3 CFM at 80^{o}F, 14.7 psia. A 0.75 inch gap giving a value of K equal to 1.30 was also employed. These conditions yield a cap weight of 368.6 grams (0.812 pounds) from equation D.20. The corresponding cap height for steel with density of 0.279 pounds per cubic inch was 0.513 inches. Again, a smaller height was used to provide a conservative margin for design. The actual height employed was 0.45 inches.

Standard valve cap

A 0.75 inch thick cap was also made to use as a standard to compare with the largest 3.5 inch diameter cap which had been previously investigated.

APPENDIX E

MODELLING OF FLUIDIZING AIR BUBBLE CAPS

Introduction

The pressure loss across the bubble cap fluidization device can be predicted by a simple incompressible analysis. This technique can be used to alter the performance of these devices to meet design specifications.

Model

The initial step in the model is to examine the schematic of one of the 24 bubble caps shown in Figure E.1. The air passes from the plenum area, through the large section, bends approximately 110° and exits through 16 small passageways.

The air passing through the bubble cap experiences several losses which are: an entrance loss, a loss through pipe one, a bend loss, a constriction loss, a loss through pipe two and exit loss. Mathematically, these losses are expressed as follows.

The entrance loss (h_{Le}) is given by equation E.1, where K_e is the entrance loss coefficient defined on p. 305 of Roberson and Crowe [13], V_1 is the air velocity in pipe one, the large pipe, and g is the acceleration due to gravity.

$$h_{Le} = K_e \frac{V_1^2}{2g} . \qquad \text{(E.1)}$$

PIPE 2:
$L_2 = 0.688"$
$D_2 = 0.128"$ (DIAMETER - TYPICAL 16 HOLES)

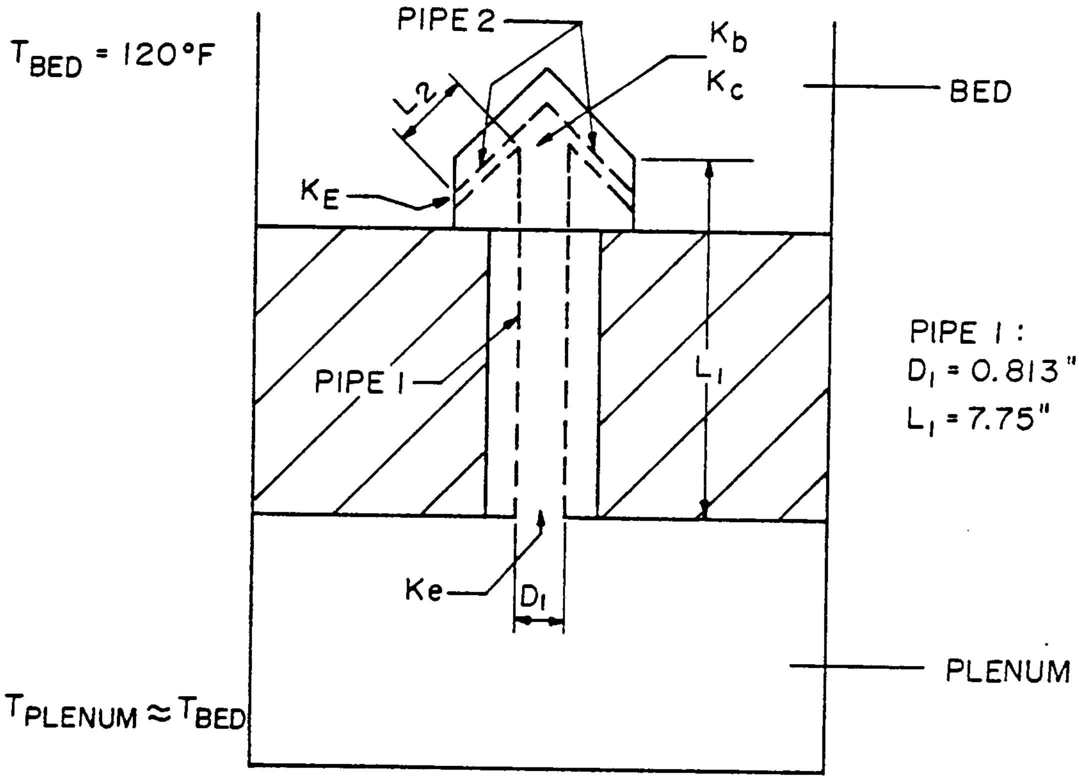

K_e = ENTRANCE LOSS COEFFICIENT
K_b = BEND LOSS COEFFICIENT
K_c = CONTRACTION LOSS COEFFICIENT
K_E = EXIT LOSS COEFFICIENT

Figure E.1. Schematic Bubble Cap System.

The loss in pipe one (h_{L1}) is given by equation E.2, where f_2 is the friction factor of pipe one [13, p. 298], L_1 is the pipe length, D_1 the diameter, V_1 the air velocity in pipe one and g is the acceleration due to gravity.

$$h_{L1} = \frac{f_1 L_1}{D_1} \frac{{V_1}^2}{2g} . \tag{E.2}$$

The bend loss (h_{LB}) is described by equation E.3 for a 90 degree bend. The bubble cap bend was not 90 degrees, it was about 110 degrees, however, it was assumed that this would make little difference. In this equation, K_b is the bend loss coefficient [13, p. 305], V_1 is the air velocity in pipe one and g is the acceleration due to gravity.

$$h_{LB} = K_b \frac{{V_1}^2}{2g} . \tag{E.3}$$

The constriction loss (h_{Lc}) is shown in equation E.4. This equation contains K_c, the constriction loss coefficient [13, p. 305], the air velocity in pipe two, V_2, and the acceleration of gravity, g.

$$h_{Lc} = K_c \frac{{V_2}^2}{2g} . \tag{E.4}$$

The loss in pipe two (h_{L2}) is presented in equation E.5, where f_2 is the friction factor in pipe two [13, P. 298], L_2 is the length of pipe two, D_2 the diameter, V_2 the air velocity in pipe two and g the acceleration of gravity.

$$h_{L2} = \frac{f_2 L_2}{D_2} \frac{{V_2}^2}{2g} . \tag{E.5}$$

Finally, the exit loss, h_{LE}, actually a free expansion, is given by equation E.6. Here, K_E is the exit loss coefficient [13, p. 205], V_2 the velocity of the air in pipe two and g is the acceleration due to gravity.

$$h_{LE} = K_E \frac{V_2^{\,2}}{2g} . \qquad (E.6)$$

The sum of these losses is the total head loss through the device in inches of air (h_L).

$$\Sigma\, h_L = (K_e + \frac{f_1 L_1}{D_1} + K_b) \frac{V_1^{\,2}}{2g} + (K_c + \frac{f_2 L_2}{D_2} + K_E) \frac{V_2^{\,2}}{2g} . \qquad (E.7)$$

Equation E.7 is a theoretical prediction, but to see if it holds it must be compared to the actual bubble cap performance.

An initial point from one test was chosen. The conditions were: air temperature of $120^{o}F$, air pressure of approximately atmospheric, air flow rate of 1203 cubic feet per minute and bed area of four square feet.

From Roberson and Crowe, [13, p. 305] K_e = 0.50 and K_b = 1.1. Also from the same reference for D_2/D_{Exit} = 0.0, K_E = 1.00.

The velocity in pipe one is the flow rate (1/24 x 1203 cubic feet per minute) divided by the area, a circular cross section of 0.813 inches in diameter.

$$V_1 = \frac{Q_1}{A_1} = 232 \text{ ft/sec.} \qquad (E.8)$$

The velocity in pipe two is the flow rate (1/16 x 1/24 x 1203 cubic feet per minute) divided by the cross sectional area, a circular cross section of 0.128 inches in diameter.

$$V_2 = \frac{Q_2}{A_2} = 584 \text{ ft/sec.} \tag{E.9}$$

To determine if the incompressible analysis was valid, the Mach number (Ma) in each pipe was checked. According to White [19, p. 216] a flow is incompressible if Ma $\leq$ 0.3. The Mach number is the ratio of the air velocity in the pipe to the speed of sound (c) at the pipe conditions.

$$Ma = \frac{V}{c} . \tag{E.10}$$

The speed of sound (c) is given by equation E.11 where k is the specific heat ratio of air, T is the temperature in degrees Rankine and R is the gas constant for air.

$$c = \sqrt{kRT} \tag{E.11}$$

Using R = 1,716 ft-lbf/slug - °R, k = 1.40, and T = 120°F (580 °R) the speed of sound is 1,180 feet per second. Thus from equation E.10:

$$Ma_1 = \frac{V_1}{c_1} = \frac{232}{1180} = 0.20,$$

and $$Ma_2 = \frac{V_2}{c_2} = \frac{584}{1180} = 0.49.$$

The incompressible assumption for pipe one is fine, however, pipe two is above the limit. This will introduce some error, but it will be neglected. If much larger flow rates were being considered an analysis that included compressibility effects would be required.

With the velocity in pipe one, the Reynolds number in pipe one (Re_1) was determined and the friction factor in pipe one (f_1) was taken from Figure 10.8 in Robertson and Crowe [13, p. 298]. Reynolds number (Re) is given by equation E.12 where V is the velocity, D is the pipe diameter and ν is the kinematic viscosity.

$$Re = \frac{VD}{\nu} . \tag{E.12}$$

From E.12, $Re_1 = 83{,}121$ and from Roberson and Crowe [13, p. 298], $f_1 = 0.0186$.

The same analysis was done for pipe two yielding: $Re_2 = 32{,}976$ and $f_2 = 0.0228$. Note that 120^oF and 14.7 psia were used for the property values.

Since all of the parameters in equation E.7 are known, the head loss across the bubble cap was determined.

Σh_L = 9,994 feet of air at 120^oF.

The pressure loss (ΔP) across the bubble cap is given by equation E.13,

$$\Delta P = \Sigma h_L \gamma_{Air} \tag{E.13}$$

where γ_{Air} is the specific weight of the air at the temperature of the bubble caps. Substituting values gives:

$$\Delta P = (9{,}994 \text{ ft}) \, (0.0684 \frac{\text{lbf}}{\text{ft}^3}) \, (\frac{\text{ft}^2}{144 \text{ in}^2}) \tag{E.14}$$

$$\Delta P = 4.75 \frac{\text{lbf}}{\text{in}^2} . \tag{E.15}$$

For water at $80^{o}F$, this pressure loss is 132 inches of water. From the experiment, the pressure loss was 140 inches of water, therefore, the prediction was 5.7 percent off.

To be certain, another point from a completely different test was tried. These conditions were a flow rate of 759 cubic feet per minute at $112^{o}F$. The calculated pressure loss was 54 inches of water and the experimental pressure loss was 63 inches of water. This was 14.3 percent off.

Discussion

The theoretical prediction has some error involved. The main sources being the incompressible assumption, the loss coefficients and reading the friction factors from a graph. However, this method does offer a quick and simple procedure to analyze the bubble cap's performance to meet desired specifications. The holes can be changed in diameter, pipes lengthened or shortened and the entrance improved as quick ways to alter the pressure loss characteristics. Other methods could include adding or removing caps or changing their basic design such as having more or less exit ports per cap. The bubble caps are an extremely adaptable system.

VITA

Reid L. Kress was born on August 3, 1958, in Meriden, Connecticut. His family moved to Oak Ridge in 1959 where Reid attended local elementary schools and graduated from Oak Ridge High School in 1976. While in high school, Reid played on the soccer team and was president of the National Honor Society.

In 1976, Reid entered The University of Tennessee at Knoxville. He received his Bachelor of Science degree in Mechanical Engineering in June of 1980. During summers, Reid worked as a lifeguard for the Oak Ridge Recreation Department and as an engineering assistant at Technology for Energy Corporation located in Knoxville. During his senior year, Reid served as president of the Tennessee Alpha chapter of Tau Beta Pi and as vice-chairman of the UT student chapter of the American Society of Mechanical Engineers.

Reid entered the Graduate School of The University of Tennessee in June 1980 under a National Alumni Graduate Fellowship and as a research assistant for the Mechanical and Aerospace Engineering Department. He received his Master of Science degree in Mechanical Engineering in June 1982.

The author is a member of the American Society of Mechanical Engineers, Tau Beta Pi, Pi Tau Sigma, Phi Kappa Phi and several other honor societies. He is employed by Technolgy for Energy Corporation of Knoxville.

Reid is the son of Dr. Tom S. Kress and Ms. Dee M. Kress of Oak Ridge, Tennessee. He is very happily married to the former Ann Denman of Oak Ridge, Tennessee.